Topic 2 – Analytical methods for determination of stable operation of IBRs in a future power system

2022 CSIRO GPST Research

Commonwealth Scientific and Industrial Research Organisation

1 May 2023

Team: Sudipta Dutta, Weihua Zhou, Nabil Mohammed, Behrooz Bahrani, Mobolaji Bello, Deepak Ramasubramanian

Contents

List of figures

List of tables

Executive Summary

With growing penetration of renewable energy resources which are power electronics based, there is a need to change how we plan and operate the power system. To enable safe and reliable power delivery in future power systems with significant contribution from inverter-based-resources (IBRs), development of methods for determining stability and stability margins around different system operating conditions is important. This topic was identified as a critical topic in the CSIRO *Australian Research Planning for Global Power Systems Transformation* research roadmap around Stability Tools and Methods

In a conventional synchronous machine system, since most models are standardized, it is relatively easier for a transmission planner/operator to evaluate the stability of the network, especially from an analytical perspective. However, with IBRs, knowledge of the IBR control details is generally not accessible/visible to the transmission planner/operator due to intellectual property (IP) management of the original equipment manufacturer (OEM). This can result in an inability to analytically evaluate the stability of the network and rather, the only resort left is to carry out numerous time domain simulations. Analytical evaluation of stability is usually achieved without running a time domain simulation, but instead stability is evaluated by obtaining the closed loop solution of mathematical equations.

These time domain simulations are computationally demanding despite application of high performance computing hardware, and can many hours to run and thus at present are not ideal for near real time evaluation of stability of a network with large percentage of inverter based resources. It is acknowledged that there are few initiatives across the industry that are tackling this challenge, but they are still in initial stages of development. Further, as IBRs are current limited devices, their operating point has a larger impact on their stability, as compared to the impact of operating point on the stability of traditional inverter resources.

To help address this dual challenge, this project has two main objectives: (i) Development of a framework to assess multiple operating points over which the IBR can be expected to operate, and (ii) Develop an algorithm to assess control stability of IBRs over the determined multiple operating points using black box models. To achieve the first objective of assessment of operating point, a process has been developed that utilizes grid strength assessment (to identify potential weak locations in the grid), voltage control areas (to identify clusters of buses for reactive power control), and frequency response-based unit commitment and dispatch evaluations. Achieving the second objective has been through preliminary work to develop both an analytical and a data driven prediction algorithm that can estimate the impedance characteristics of a device at any arbitrary operating point, by using only few operating points as inputs to develop a set of training data.

The results show the use of metrics such as remaining available MVA to identify locations that can have potential stability issues at different operating points. Further, the application of the training algorithm on different IBR control structures has been showcased. Using the obtained estimated impedance characteristics, a system planner and operator can make a determination if a particular operating point (after running the described screening analysis) is going to be small signal stable or not. Based on the result, the operating point can be changed to help move the network towards a more stable operating point. The assumption here is that this starting operating point is not N-1 secure, or may be N-1 secure from a powerflow perspective, but not secure from a stability perspective.

In relation to the 2021 Topic 2 Research Roadmap, the work done in this project address the topics listed below and advances the work by the respective percentage amount:

- Stability margin evaluation (Critical topic) – 30%
- Small signal stability screening methods (Critical topic) – 30%
- Voltage and reactive power management (High priority topic) – 25%

Acknowledgement

The research presented in this report was funded by CSIRO, Australia's national science agency, and carried out as part of CSIRO's contribution to the initiatives of the Global Power System Transformation (GPST) Consortium. This research supports Australia's transition to a stable, secure and affordable power system and contributes to critical research identified by the Consortium required to accelerate the decarbonisation of our electricity grid. More details can be found at **https://www.csiro.au/en/research/technology-space/energy/G-PST-Research-Roadmap**

1. Introduction

With growing penetration of renewable energy resources which are power electronics based, there is a need to change how we plan and operate the power system.. To enable safe and reliable power delivery in future power systems with significant contribution from inverter-based-resources (IBRs), development of methods for determining stability and stability margins around different system operating conditions is important. This topic was identified as a critical topic in the CSIRO *Australian Research Planning for Global Power Systems Transformation* research roadmap around Stability Tools and Methods [1]

Traditionally, a stability evaluation of a power network is carried out using a small signal analysis technique. This technique is based upon the method of linearizing the equations describing the dynamics of the network and subsequently evaluating the system stability. Since the linearized equations hold valid only in a small region around the point of linearization, the method is known as small signal analysis. An interested reader is referred to [2] (among many other available literature) for more background information on this topic. This kind of analysis is useful, as it can help identify natural characteristics of the network that would otherwise not be easy to identify if only time domain simulations were used.

In a conventional synchronous machine system, since most models are standardized, it is relatively easier for a transmission planner/operator to evaluate the stability of the network, especially from an analytical perspective. However, with IBRs, knowledge of the IBR control details is generally not available to the transmission planner/operator due to intellectual property (IP) management of the original equipment manufacturer (OEM). This can result in an inability to analytically evaluate the stability of the network and rather, the only resort left is to carry out numerous time domain simulations. During the preparation of the Topic 2 research roadmap [1] when all transmission network service providers (TNSPs) in Australia where asked "*What is the existing process used to analyse and evaluate stability of the network with IBR percentages? Is it purely simulation based?",* all responses were unanimous with both positive sequence and electromagnetic time (EMT) domain simulation software being the workhorses to evaluate system stability [1]. EMT and positive sequence software are used for planning studies (mid-to-long term) but only positive sequence software are used for operational studies (near real time). Here, it was ascertained that desktop time domain simulation techniques that involve numerically integrating a set of differential algebraic equations over the simulation period is the primary technique. Positive sequence simulation software is used primarily for traditional studies such as frequency response, while studies related to system strength and voltage events are carried out in EMT domain. Very little focus is presently given to the use of analytical methods such as small signal analysis with presence of IBRs. Although small signal analysis is widely used by the TNSPs in evaluation of system modes and tuning of power system stabilizers/power oscillation dampers, the present analysis methods/techniques/software rely on having visibility of the block diagrams of the various equipment. This model-based technique however brings up challenges with the reduction in the synchronous machine fleet. This is largely due to the "black box" nature of proprietary IBR control systems, which presently makes it difficult to carry out analytical evaluation of their performance.

It is not that one cannot undertake analytical stability evaluation of black box OEM models. One of the most effective methods that has been used and continues to evolve in the industry are methods based on impedance-based frequency scans [3]. These methods provide a detailed impedance seen into power system equipment and/or the network, such that resonant conditions or low damping conditions can be identified. The methods can often be run with both positive sequence tools as well as EMT tools and allow the investigation of several network topological conditions as well as operating conditions with a relatively low computational burden. There are two major methods involved to generate these scans: (i) injection of a perturbation signal at various frequencies into a simulation model or hardware setup followed by application of signal processing techniques on the output of the model or hardware [4], and (ii) injection of various random inputs into the simulation model or hardware setup followed by processing of both the input and output using system identification algorithms [5] [6] [7]. Irrespective of the method used, if the resultant frequency domain information is to be used for a system wide stability analysis, there are limited options available. The accuracy of the model obtained from an impedance scan can be verified by time domain studies around the critical resonant modes that have been identified.

One option is to treat the entire network as two subsystems connected in series with each other, followed by a scan of each subsystem. Using the resultant two scans, a determination of stability can be obtained [8] [9]. When obtaining the scan of an inverter model, it is typically carried out by connecting the model to an infinite bus followed by the injection of perturbations. As a result, the characteristics of other devices are not captured. A second option is to attempt to generate a state space formulation through curve fitting of the frequency domain data using a process known as vector fit [10]. An example of the result of fitting frequency domain data is shown in Figure 1 for a simple IBR simulation model. Once a state space representation has been obtained for each black box model through the process of vector fit, it could then potentially be applied in the small signal stability analysis of an entire network to obtain results as shown by the example in Figure 2. In this example, the voltage controller gain of an IBR was to be tuned in order to improve the stability of the network. It should be noted that the use of these methods are limited to the small signal analysis. If a controller is already at its saturation limit (such as sustained operating at a current limit), then this analysis would be able to pick up the impact of this scenario. However, the analysis based on the development of transfer functions would usually not be able to pick up the impact of a controller going into saturation as a result of a disturbance such as a fault.

While the above process might seem ideal, there are numerous practical challenges. Evaluation of the impedance-based frequency scan by itself has numerous challenges. Few challenges are highlighted in [11] [12]. For this phase of the project, it is assumed that the impedance-based scan can be successfully obtained. However, like any small signal stability technique, the obtained scan is only valuable at the power system operating point at which it has been evaluated. Small changes in the operating point in relation to bus angle, voltage magnitude, active or reactive power output can lead to differences in the overall impedance characteristic, which can subsequently result in potential differences in stability. An example of variation of the impedance-based characteristic of an IBR is shown in Figure 3 for a 2.5 MVA inverter with variation in active power reference from 0.1 to 2.0 MW and variation in voltage reference from 0.9pu to 1.1pu. When connected to a network of finite strength, the variation in small signal stability for this same variation in operating point is shown in Figure 4. Although all operating points are stable in this example, the evaluation of stability across the entire range of operating points is not a trivial task. While it is technically not impossible to evaluate stability of the system at every practical system operating condition including contingencies, power dispatch levels etc, it can be cumbersome and also computationally expensive. Further, when the power system transitions from one operating condition to another, the stability of the system can also evolve.

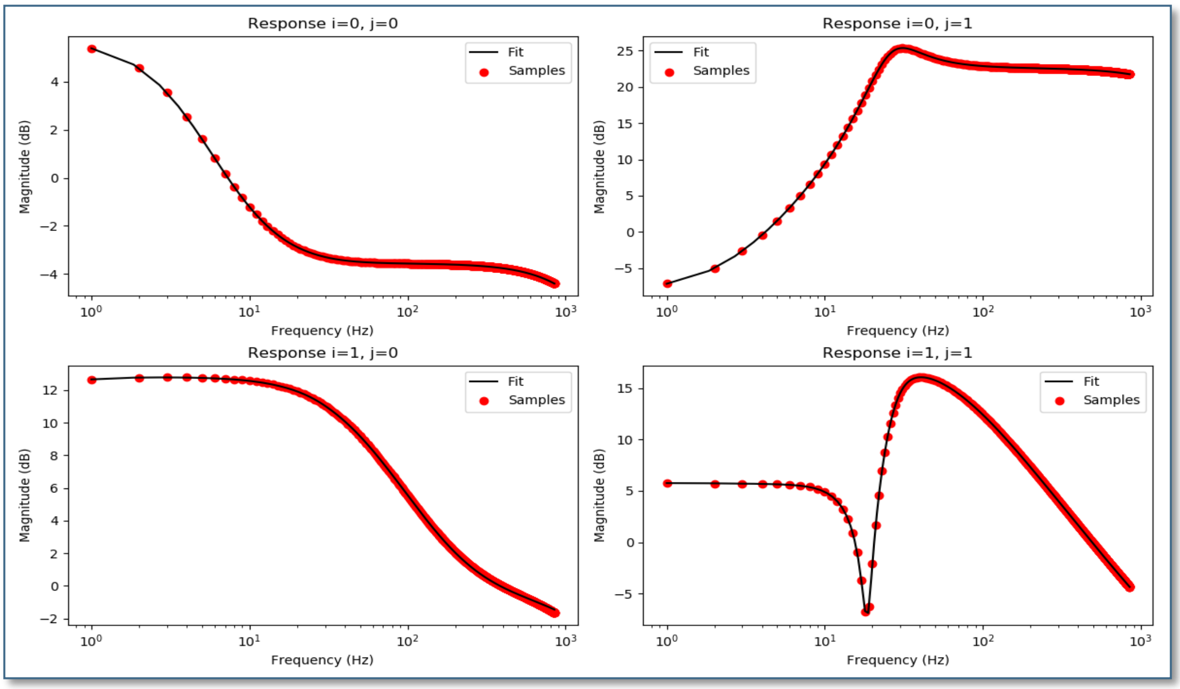

Figure 1: Example result of using the process of vector fit to curve fit frequency domain data to generate a state space formulation

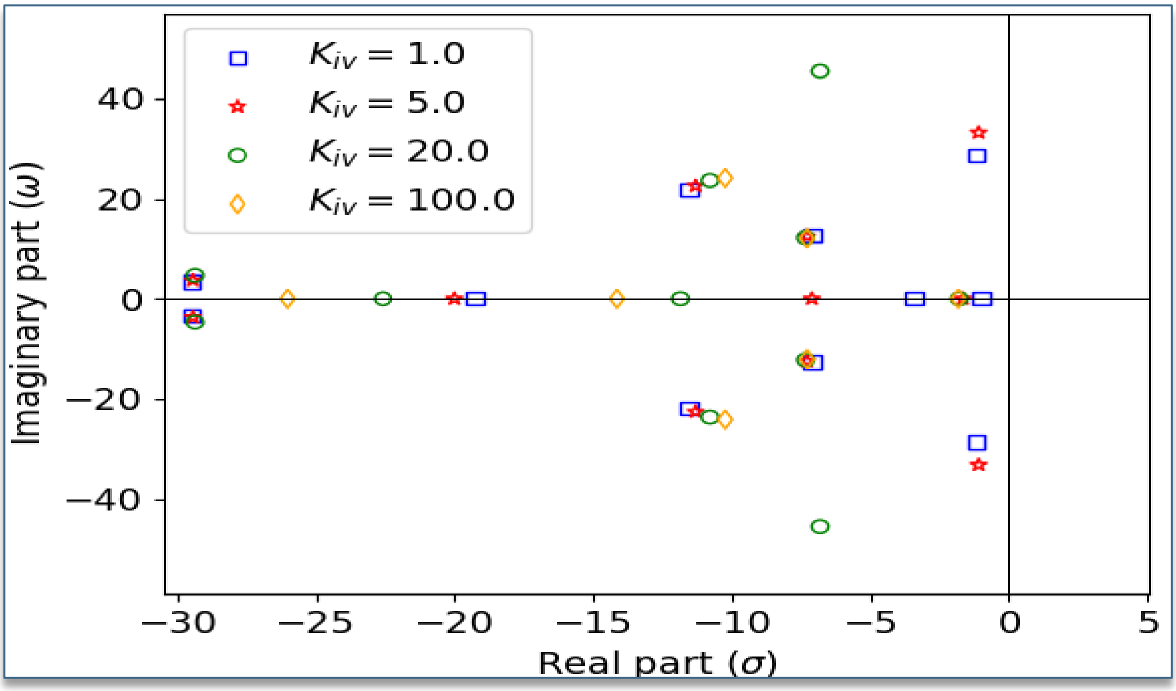

Figure 2: Example results of using state space realization to carry out stability analysis in an IBR-rich system

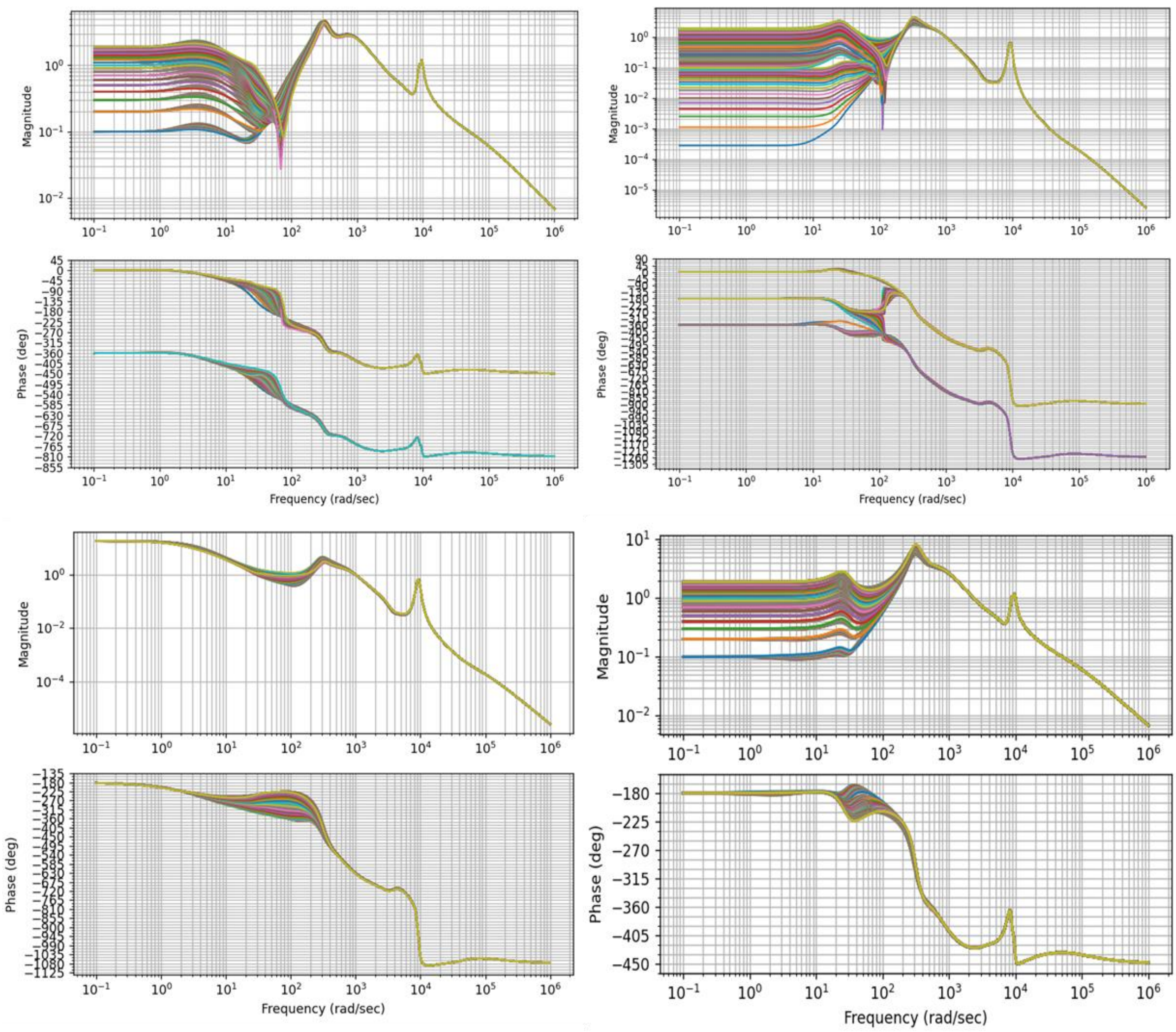

Figure 3: Example showcasing the variation of impedance of an IBR with operating point

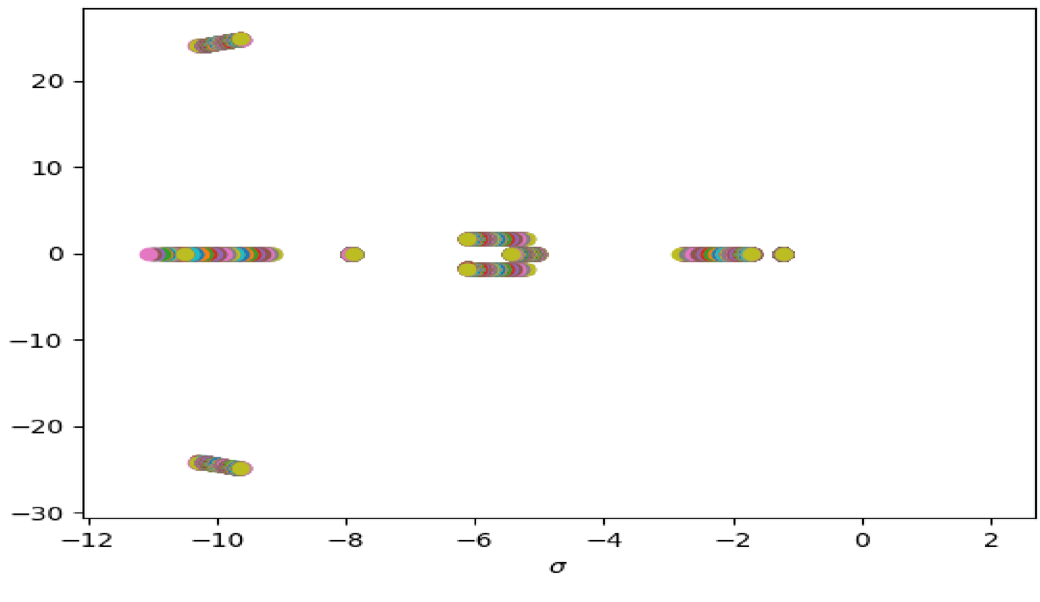

Figure 4: Example showcasing the variation in system stability with variation in operating point

In such a scenario, it is important for transmission planners and operators to be able to identify risks to system stability with changes in power flow and voltage across the network. Although AEMO's Power System Model Guidelines [13] prohibits the use of a small signal model that is only valid at a single operating point, the black box nature of IBRs can cause challenges in formulation of a suitable small signal model that can be valid over multiple operating points.

A solution to this challenge can be to understand the trajectory of these evolution paths. If these trajectories can be understood, then, it can eliminate the need of evaluating the stability of the network at every single operating point, significantly reducing the computational burden and providing many new insights into how a system moves and its effect on its stability margin. Now, the stability of the various devices in the network need only to be evaluated at a few select operating points, and the stability at any subsequent operating point can be evaluated using the knowledge of the trajectory evolution. Such a concept, if successful, can even help system operators in real-time to anticipate excursions into unstable conditions and allow time to take corrective actions. In this research work, analytical methods will be developed to evaluate the impact of operating point on stability of a system with high amounts of IBR plants. Further, the objective is to develop a process/analytical function that allows for ease in evaluating the stability at each operating point, based on information of other operating points in the capability curve. This research work has two parallel approaches. The first to determine an example evolution of operating points in a large network over a single day. The second is the development of analytical methods/processes to evaluate, in a computationally efficient manner, the change in stability of the network as the operating point changes.

1.1 Relation to Research Roadmap

The research work carried out in this project is related to the following open questions from the Topic 2 research roadmap [1]:

- Is it possible to evaluate non-linear stability margins using blackbox IBR models? Here, non-linear refers to the large signal behavior of the IBR. Blackbox models should be good enough if the model reflects actual device behavior under different conditions, e.g. limits modeled properly, controller saturation modeled properly, internal device protection modeled properly etc. The blackbox model should also possibly capture the dynamics of an IBR over a specified frequency range. However, research would need to be done to evaluate whether a non-simulation based analytical process can be used to evaluate the stability margins under varying network behavior.
- Would there be an approach to construct piecewise impedance scans at different operation points to obtain a large signal picture?
- How would stability properties of other sources in the network be represented when designing an IBR plant?
- Would it be possible to efficiently evaluate small signal modes and stability profile with black box models?
- Development of a multi-operating point small signal model (either impedance based or linearised state space). Here again, there should be close synergy with Topic 1 to develop a multi-operating point model that can also be easily interfaced with existing small signal stability tools used by TNSPs in Australia

Specifically in relation to the topics of the research roadmap, this project has progressed work related to:

- Stability margin evaluation (Critical topic)
- Small signal stability screening methods (Critical topic)
- Voltage and reactive power management (High priority topic)

For each of these topics, the percentages of the research plan task that have been progressed are:

- Stability margin evaluation (Critical topic) – 30%
- Small signal stability screening methods (Critical topic) – 30%
- Voltage and reactive power management (High priority topic) – 25%

1.2 Preliminary background work

Prior to this project, EPRI had carried out preliminary work in the area of identifying analytical functions that can span various operating points and deliver a frequency scan evaluation at a user defined operating point [12]. In this section of the report, an overview of this preliminary work is provided. First, the impedance/admittance of an IBR was evaluated at one particular operating point and a state space model representation was realized using the vector fit process. Subsequently, before trying to extend the model developed for a single operating point to multiple operating points, it was tested for different operating conditions to ensure that the approach leads to accurate estimation of the admittance in a wide range of operation. While selecting different operating points, three variables are selected to characterize an operating point: the inverter active power reference, the inverter reactive power reference, and the point of common coupling (PCC) voltage in per unit. For the different operating points, since the purpose is to study the inverter characteristics, for different values of active and reactive power references, different values of grid impedance and grid voltage magnitude were used, to ensure correct voltage at the PCC. For example, the grid impedance and voltage magnitude which results in 1.01 p.u. voltage at PCC when the inverter injects 200 MW, 40 MVAr were different from the grid impedance and voltage magnitude which results in 1.01 p.u. voltage at PCC when the inverter injects 180 MW.

For each selected operating point, the following procedure was followed:

- Using the active and reactive power and PCC voltage magnitude references, select suitable grid impedance and voltage magnitude.
- Achieve a steady state in the simulation model at the selected operating point and subsequently, inject disturbances of various frequencies in the voltage or current and conduct the frequency scan.
- Estimate the admittance of the IBR model and develop a state space model corresponding to the admittance by following the vector fit process.

To verify the accuracy of the estimated admittance and evaluated state space model, the short circuit ratio (SCR) value at which an instability is observed was identified. The values of active power reference, the reactive power reference and the inverter terminal voltage as well as the comparison of the SCR values at which the system goes unstable for these operating points is tabulated in Table 1. It is seen that the model estimated through a vector fit closely follows the EMT simulation model. Further, it is to be noted that the estimation process is computationally more efficient that running the EMT simulation. Note that the X/R ratio for the grid impedance was kept at 6.0 for all these operating points. It can also be seen that the value of SCR at which the system becomes unstable changes depending on the reactive power and the terminal voltage, while for unity power factor operation, this value does not seem to change with a change in the active power injection.

Table 1: Operating point at which instability manifest in an example to establish sufficiency of state space model for an example IBR

			SCR at which instability occurs	
Pref	**Qref**	**Vref**	**Vector fit evaluated model**	**EMT simulation model**
200	0	1.01	1.6	1.7
190	60	1.01	1.4	1.4
180	85	1.01	1.3	1.4
190	-60	1.01	2.0	2.0
180	-85	1.01	2.2	2.2
190	0	1.01	1.6	1.7
180	0	1.01	1.6	1.7
150	0	1.01	1.6	1.7
195	40	1.0	1.5	1.5
195	40	0.95	1.6	1.6
195	40	1.05	1.4	1.4

Once it is established that the state space model evaluated from the vector fit technique is valid for a wide range of operating points (characterized by different values of active power, reactive power and voltage reference), the models at these different operating points can be combined to form a single "polytopic" model. The basic assumption behind the polytopic model can be explained as follows: consider that we choose different operating points $(P_i, Q_i, V_i), i \in [1,2, \dots n]$ to obtain the measurement based admittance model $Y_i(s)$. Consider the admittance model developed for one such point, (P_r, Q_r, V_r). Now, an admittance model developed for r^{th} operating point (P_r, Q_r, V_r) will only be valid in a small region around that point. Similarly, at different points $1,2, \dots n$, it can be inferred that:

$Y_1(s)$ is valid near (P_1, Q_1, V_1)
$Y_2(s)$ is valid near (P_2, Q_2, V_2)
.
.
.
$Y_i(s)$ is valid near (P_i, Q_i, V_i)
.
.
.
$Y_n(s)$ is valid near (P_n, Q_n, V_n)

Hence, $Y_r(s)$ will not be valid at $(P_{r+1}, Q_{r+1}, V_{r+1})$ sufficiently far away, and $Y_{r+1}(s)$ will need to be constructed by following the measurement-based approach at that point. However, if the transfer functions involved are smooth enough, the admittances at point (P_k, Q_k, V_k) between (P_r, Q_r, V_r) and $(P_{r+1}, Q_{r+1}, V_{r+1})$ could be estimated using a weighted combination of $Y_r(s)$ and $Y_{r+1}(s)$, written as,

$$Y_k(s) \approx w_r Y_r(s) + w_{r+1} Y_{r+1}(s)$$

Where $w_r + w_{r+1} = 1$
This concept can be extended over a larger region using more than two points as a polytopic model. Note that the weights w_r and w_{r+1} will depend on the operating point (P_k, Q_k, V_k), so if the point *k* is very close to the point *r*, then w_r will be close to 1 and w_{r+1} will be close to zero, or if the point *k* is closer to the point *r+1*, then w_{r+1} will likely be chosen to be larger. A more rigorous introduction and analysis of polytopic methods can be found in [14] [15]. As shown in [16], a general equation for this process can be developed across a range of operating points. Usually, the weight functions w_i can be chosen to be triangular, trapezoid, Gaussian, double sigmoid etc. In the preliminary work done, a double sigmoid weight function had been selected, because it allows different parameters for the function on different sides without requiring extra normalization steps.

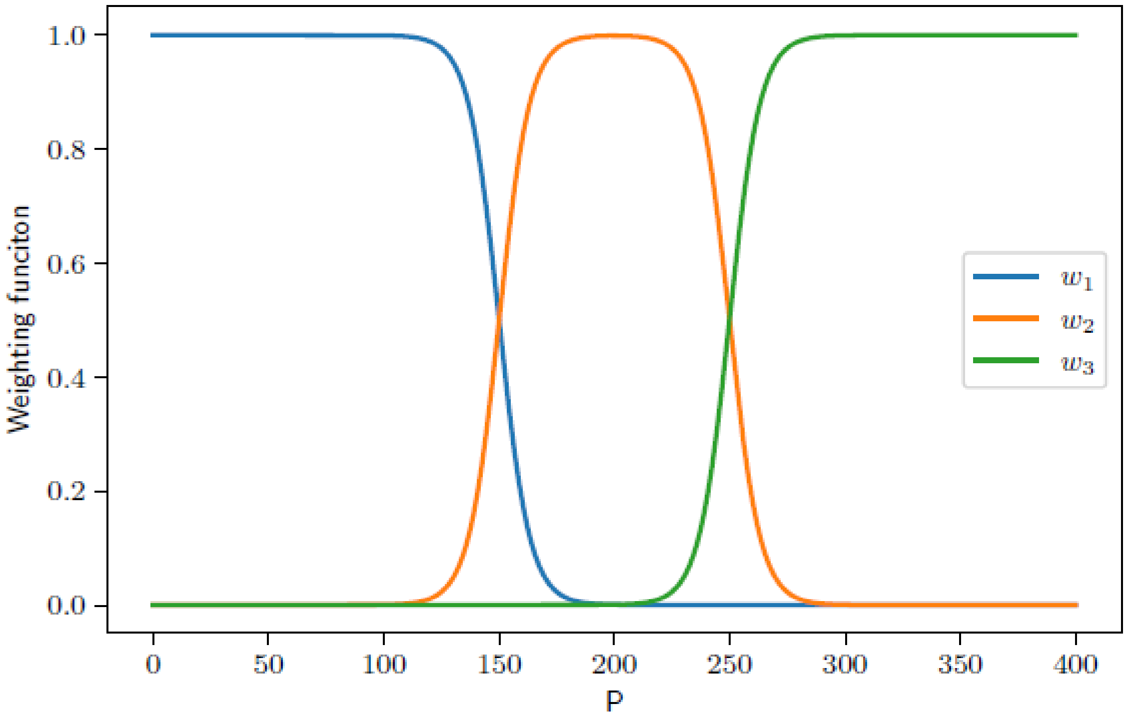

Figure 5: Example of weighting functions that can be used to develop the polytopic model

The weight functions with three points selected at $P = 100$, $P = 200$, and $P = 300$ are shown in Figure 5. The centres and slopes between two adjacent points are set to be the midpoint of the two points and the inverse of the distance between the two points. An example to showcase the applicability of such a polytopic model is described below. The initial points are selected to be $P_1 = 200\ MW, Q_1 = 40\ Mvar, V_1 = 1.01pu$ and $P_2 = 100\ MW, Q_2 = 40\ Mvar, V_2 = 1.01pu$ respectively. It is found that even with these two initial points, the admittance at the midpoint $(P = 150)$, and the two points one third along the distance between point 1 and point 2 from each end $(P = 133.33$, and $P = 166.67)$ is well approximated by the polytopic model. Figure 6 shows the comparison between the admittances obtained based on a measurement from a simulation model and that obtained from the polytopic model provided for $P_{ref} = 150\ MW, Q_{ref} = 40\ Mvar, V_{ref} = 1.01pu$.

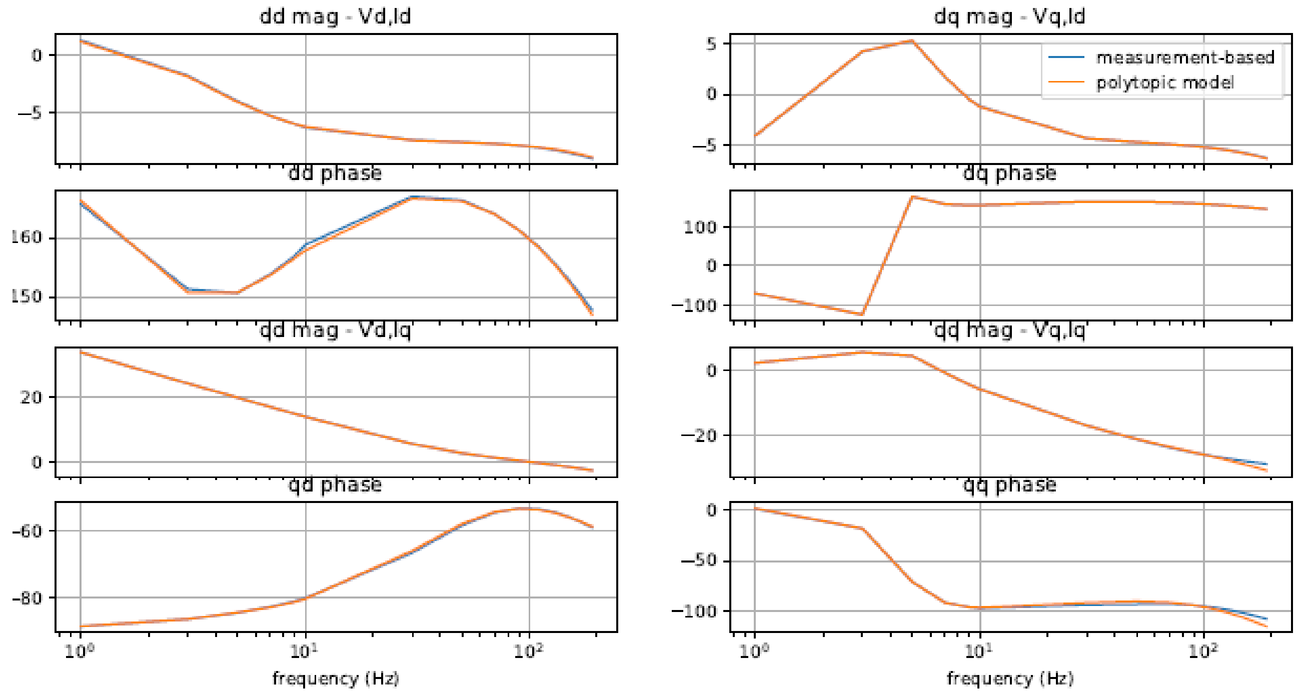

Figure 6: Example comparing the admittance obtained from the polytopic model with that from a measurement-based approach

Through this preliminary work, it was identified that it can be possible to evaluate the impedance/admittance characteristics of an IBR at any operating point, given that these characteristics are known at a particular set of operation points. However, this work also identified the challenges involved in determining an analytical function such as a polytopic model, especially the dimensionality of the project. It was determined that the procedure should be extended to include multiple directions (a change in multiple variables such as P_{ref}, Q_{ref} which determine the operating point of an inverter should be supported).

1.3 Summary of work effort proposed in this project

Since a majority of stability analysis research work is limited to either a single machine infinite bus representation or a particular operating point, this project aims to extend the stability analysis of black box models over multiple operating points, while also identifying the operating points at which inverters are expected to operate. This proposal thus has two main objectives:

1. Development of a framework to assess multiple operating points over which the IBR can be expected to operate
2. Develop an algorithm to assess control stability of IBRs over the determined multiple operating points using black box models

To achieve the first objective of assessment of operating points, grid strength assessment (to identify potential weak locations in the grid), voltage control areas (to identify clusters of buses for reactive power control), and frequency response based unit commitment and dispatch are to be carried out. Due to various techno-economic reasons and due to not knowing the needs of the future power system, legacy/conventional IBRs interconnected to the network today primarily operate in a constant active power (P) and constant reactive power (Q) operation mode wherein, in the few seconds upon the occurrence of an event, the control objective will try to maintain pre-disturbance injection of P and Q, irrespective of whether the system requires those pre-disturbance values to be maintained. Some IBR plants do have a slower supervisory plant control that may provide frequency and voltage regulation, but the time to deliver this service can be tens of seconds, which does not help with system stability and security. Operation of the inverters in a constant P and Q mode upon the occurrence of a disturbance is not suitable as the percentage of IBRs in the system increases. As a result, in a future power system, an IBR may be asked to operate at different points along its capability curve to provide a variety of services to the system.

For the National Electricity Market (NEM), the Energy Security Board and the Australian Energy Market Commission have been deliberating on defining and procuring system services (such as frequency, system strength, and inertia) which IBRs may subsequently be called on to provide such services. However, inverters are current limited devices and as such, they must prioritize the delivery of various services as it has a direct impact on evaluation of whether the IBR will be able to operate in a stable manner as shown in the preliminary work carried out. The prioritization of delivery of these services can thus have an impact on the inverter resource being able to operate in a stable manner. Further, it is acknowledged that in the NEM, and other regions around the world, IBRs already should have the capability to provide system support services such as automatic voltage control and primary frequency response. However, conventionally, these sources are present in the plant controller which can be of much slower time frame and can have deadbands in them to limit the rate and frequency of movement of controls. As a result, around an operating point, with the deadband present in the plant controller, it can be expected that there can be many small signal disturbances which are only impacted by the inverter control level. As the grid moves to a greater percentage of IBRs, it might be required to move these functionality down to the inverter level to improve the stability of the network [17].

As inverters are programmable devices, the dynamic characteristics and stability that are exhibited by the resources are completely dependent on the control architecture used within the inverter, implementation method of the control architecture, parameterization of the control variables, initial operating point of the resource, and nature of the system in which the resource is connected. The challenge that arises here is that the first three factors that impact the dynamic characteristics and stability can be considered as proprietary knowledge protected under intellectual property rights of equipment manufacturers. As a result, from a system planner/operator perspective, the behaviour of the IBR can be a black box with only an input-output characterization. In such a situation, the ability of system planner/operator to understand and ascertain the stability of the IBR, while operating at the designated operating point, is severely limited. In the present state-of-the-art, very few analytical methods are capable of being used to obtain a picture of the stability of system, and instead, numerous computationally intensive and time-consuming simulations are to be carried out. Therefore, efficient small-signal modelling, margin evaluation, and enhancement methods are desired, which can locate the weak operating points that have insufficient stability margins so that damping strategies (e.g., controller parameters re-tuning and installation of grid-forming inverters) can be implemented accordingly. This project aims to address this challenge by developing a process that could allow for application of black box identification methods over a wide range of operating points.

2. Methodology followed in the project

The operation of the IBR at required operating points can be conflicting when viewed from the lens of the IBR control algorithm. For example, operating points that are associated for frequency response are generally dominated by active current injection in phase with the voltage vector while operating points associated with voltage response/control are generally dominated by reactive current in quadrature with the voltage vector. At the same time, there can be an interdependency: for active power to be delivered to control/maintain frequency, control of voltage is critical.

If adequate energy and current headroom are available, an IBR can usually operate in a stable manner. However, IBRs are current limited devices, and oversizing an IBR can come at an additional cost (which could be justified if determined to be necessary). As a result, to determine stability of the IBR system, it can be important to identify the operating point at which IBRs are expected to operate, along with the functional response that is expected from the IBRs. This methodology followed in this project thus has two main components:

- Use of a framework to identify the multiple operating points over which an IBR can be expected to operate in a system with high percentage of IBRs
- Development of an algorithm to assess control stability of the IBRs over the determined operating points, while reducing the need to evaluate the stability characteristics of each individual IBR at each individual operating point. It is envisioned that such an algorithm can subsequently be used in real time operations to evaluate the small signal stability at any operating point, in a fast manner. This however does depend on an accurate model of the network that can represent the topology of the network at that present time, in real time. It is important to understand that to evaluate stability of the network, in addition to the accurate model of the IBR device, accurate representation of the network elements (lines, transformers) and their status (in or out of service) is also important.

The framework to assess the various operating points is expected to utilize a prioritization scheme using the following approach:

- Determine a baseline power flow case that can represent the evolution of a network over successive periods such as 24 hour period
- Evaluate system strength across the entire region to identify locations that have reduced capability to host IBRs. The characterization of this system strength will be a combination of small signal steady state metrics such as short circuit ratio and remaining MVA available.
- Identify the voltage control areas of the region to outline need and magnitude of reactive power reserves. This analysis will allow for rating of reactive resource adequacy in each portion of the system.
- Develop a unit commitment and dispatch profile to help evaluate the active power output of the IBRs in the network over the successive periods
- Evaluate if there would be any prioritization issues of reactive power versus active power delivery of the IBRs
- Preliminary time domain simulation exercises are to be carried out to identify if any stability issues arise as the operating point changes.

In parallel to this effort, the stability characteristics evaluation of an individual IBR device is undertaken considering that it has a capability curve in the active power (P) – reactive power (Q) plane. Now this IBR can operate anywhere in this PQ plane (assuming a battery). However, since the frequency scan for the IBR may have to be re-calculated for every change in operating point, (not only P-Q but also V-theta too), the objective is to understand if it is possible to develop a method (either a continuous function or other advanced method) that can predict the frequency domain characteristics at a new operating point. Further, to maintain computational efficiency, in order to predict the frequency domain characteristics at the new operating point, a minimum number of 'training' or 'input' operating points is to be utilized. To help meet this objective, the following sub-tasks were identified:

- In a single machine infinite bus (SMIB) setup, the theoretical relationship between impedance characteristics (or frequency domain characteristics) and operating point is to be evaluated. To achieve this, a white box model of an IBR will be assumed, and the detailed transfer functions will be derived.

Following this, the behaviour/dependence of transfer functions on operating point can be determined. Such an analytical function representation of the transfer function could give an insight into how much the operating point can impact the impedance characteristics of the IBR.

- Following this, in the same SMIB setup, a black box model of an IBR will be assumed and the impedance characteristic at select operating points (M) will be determined using measurement techniques. Once this done, a method is expected to be derived that can use these M measurement points to derive the impedance characteristic at any of the N operating points within the capability curve (here N >> M). The method used to derive this impedance characteristic at any operating point can be verified using the results from the previous sub-task.
- Using a simple multi-IBR network, the applicability of the method from the previous sub-task will be evaluated, while using a prioritization of operating points identified from the other parallel effort. If successful on the simple multi-IBR network, then application on a larger network can be explored.

In carrying out such a parallel approach, the evaluation of the operating point at which the network can operate and the determination of the characteristics of each individual device of the network are decoupled from each other. This decoupling is necessary to develop the proof of concept. It is expected that as more is learnt and understood regarding the applicability of the method, there will be opportunities to merge the two parallel tracks in a feedback loop.

This project aims to build critical capability for efficient planning that ensures stable and secure operation of the Australian power system. The expected outputs of this method are:

- A list of buses/nodes in a network where it can be beneficial to increase voltage control and reactive power reserves to improve the interconnection of IBR.
- A unit commitment and dispatch profile to showcase the delivery of frequency response from IBRs without conflicting objectives from reactive power delivery.
- A preliminary method to analytically evaluate stability of the IBRs that is required for further development of planning and operational procedures suitable for a high-IBR system.

The following sections will describe the technical details of the work carried out.

3. Establishing the test case for development of operating points

A synthetic power system which represents the Australian mainland power grid was sourced to be used as the test case for this research. This system has ~2300 buses and ~265 generators and was converted from a HyperSim model to PowerFactory to PSSE for further modifications and preparations for the research scope [18]. An approximate (not to scale or to physical location) overlay of the buses in the network over the Australian mainland outline is shown in Figure 7. Here, the blue dots denote all the buses while the yellow dots denote the locations of the generators in the network. Since this is a synthetic network, exact geo coordinates are not available and hence approximations have been made in order to generate a plot.

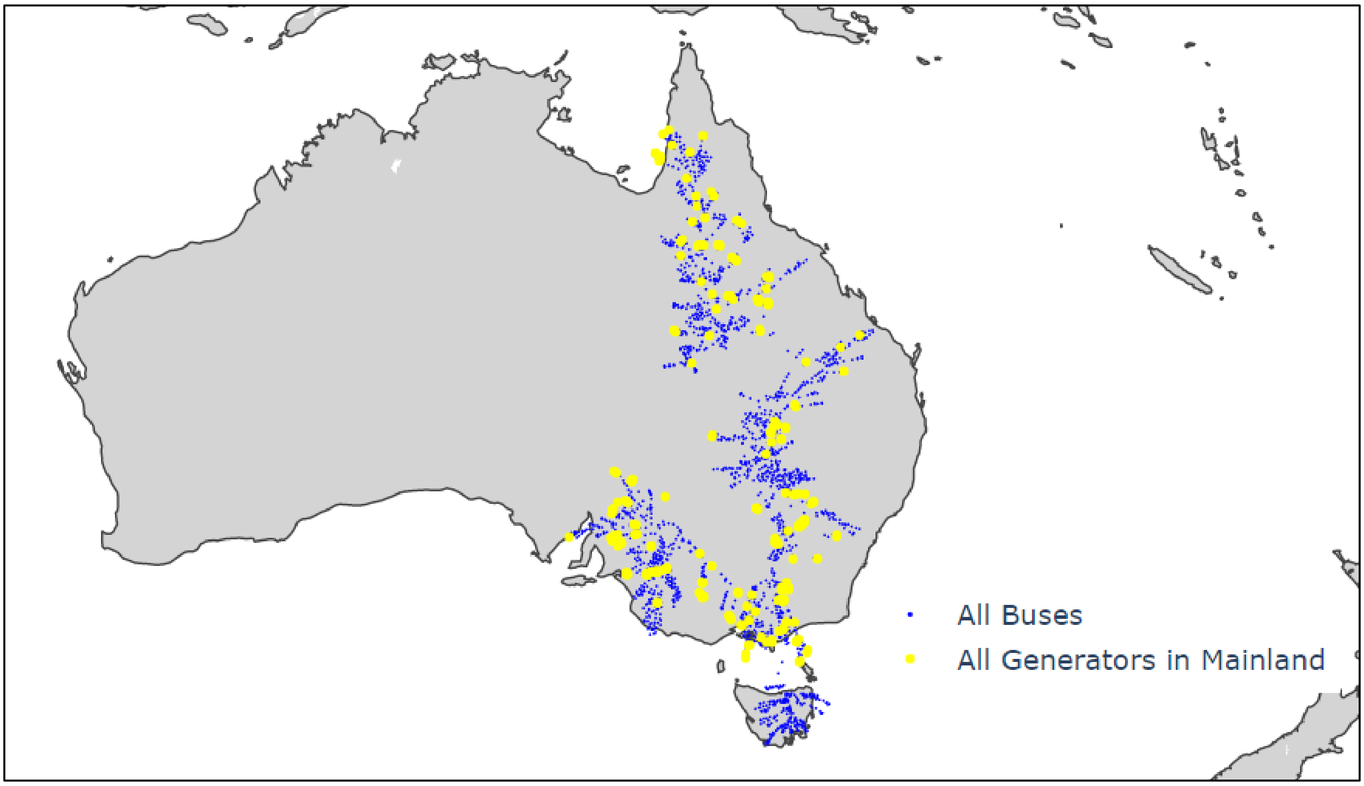

Figure 7: Map of buses in the synthetic system showing an approximate overlay over the Australian mainland

The synthetic power flow case is setup so that the generation, load, and area interchanges match closely to the real grid, although recent transmission upgrades are not considered. Table 2 shows the generation, load, interchanges.

Table 2: Generation, load, area interchanges of synthetic Australian grid

Area name	Generation		Load		Area Interchanges									
					New South Wales		Victoria		Queensland		South Australia		Tasmania	
	MW	MVAR	MW	MVAR	MW	MVAR	MW	MVAR	MW	MVAR	MW	MVAR	MW	MVAR
New South Wales	11269.6	293.7	12278.3	2643.2			-413.5	81.5	-1038.4	116.2				
Victoria	7286.2	-277.8	7717.1	1966	413.5	-81.5					-609.6	245.8	-410.9	-149.3
Queensland	9071.2	518.5	7717.5	2130.7	1038.4	-116.2								
South Australia	2005.7	26.4	1286.2	459.8			609.6	-245.8						

Tasmania	1484.4	-312.9	1033.3	263.5			410.9	149.3						
Total =	31117.1	248	30032.4	7462.3										

As a first step the sequential operating points of the system are determined. Since the objective is to showcase a proof of concept, certain assumptions are made in determining the evolution of the operating point. For example, generation resources in the area assumed to be South Australia have been assumed to be IBRs. Further, 90% generators (by MVA rating) in the areas assumed to be New South Wales and Victoria were assumed to be IBRs. Finally, 60% generators (by MVA rating) in the area assumed to be Queensland were assumed to be IBRs. Although the actual generation source mix is not important for this stage of the study, its importance will be showcased in the time domain simulations. An average diurnal demand was used to generate sequential system demand. The projected 2030 average diurnal demand variation from AEMO (Figure 24 from [19]) was used to modify the existing synthetic power-flow case and create 24 hourly cases with scaled loads and generation. The average hourly loads for the whole system are shown in Figure 8. While the scaling function in PSSE is used to scale all the generation and loads in the system appropriately to match the hourly total system load at each of the 24 hours, a python script was used to ensure that the Pmax of each generator is greater than or equal to the generation. Also, if it was found that the MVA of a generator is less than its Pgen, then the python script was used to change it such that MVA of the generator was the square root of sum of squares of real and reactive power generation at that generator.

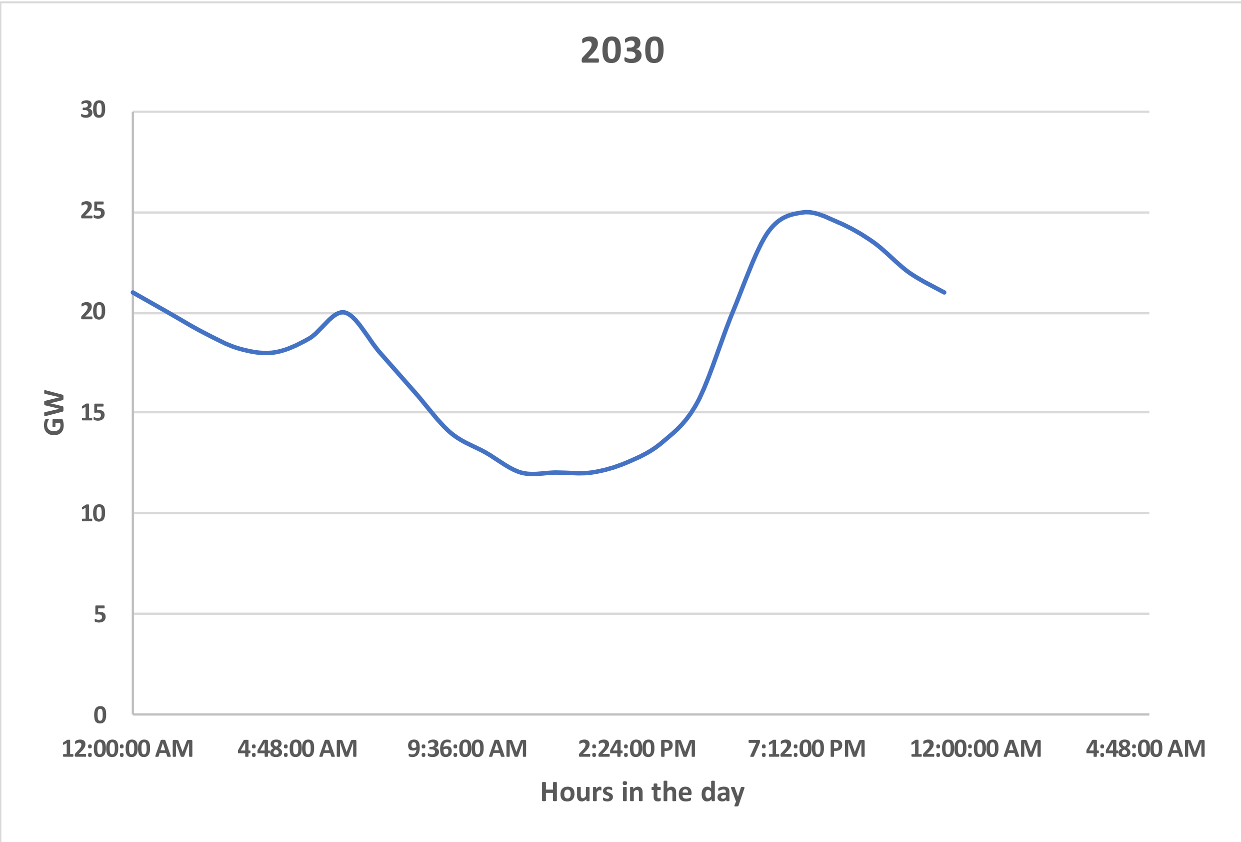

Figure 8: Synthetic load profile generated to mimic a 24-hour average diurnal demand in 2030 (based on [19])

Since inverter-based resources are current limited devices, there is a prioritization of active vs reactive current that they can inject into the network to meet this 24-hour load profile. There are several factors to consider for computing the prioritization of current output which in turn impacts the operating points of the network. Examples of these factors which are used in this study are system strength, reactive power loss minimization, and active power reserves. Each of these factors have been addressed in the subsequent sections.

3.1 System strength evaluation

Short circuit level is an important identifier of strength for the power system. An increase in the percentage of inverter-based generation in large power systems causes a reduction in the available fault current, resulting in a reduction of traditional system strength. The reduction in fault current is due to the displacement of synchronous generation and introduction of current limited inverter-based resources. In addition to this, both planned and unplanned outages would result in a change in network topology and possibly online generation which may further reduce system strength. This new reduced value of system strength could be at a value for which the controls of inverter-based generation have not been designed to operate and thus, it may cause inverter controller instabilities. Knowledge of the short circuit strength of the local grid is hence essential to achieving a safe and stable system with increased percentage of inverter-based resources. It is even more imperative that observability of the reduction in short circuit strength be obtained in both long term and operational planning system studies. A tool developed by EPRI called the Grid Strength Assessment Tool (GSAT) [20] calculates various system strength metrics from a steady state analysis of the network model.

A low SCR value evaluated with traditional steady state calculations (such as simple short circuit ratio (SCR) or weighted short circuit ratio (WSCR)) may not necessarily imply converter control instability as the controllers may have already been designed and tuned appropriately. Similarly, a high SCR may not indicate a stable system as the controllers may have not been designed and tuned appropriately. EPRI's GSAT introduces two new metrics, one metric to evaluate remaining SCC MVA [21] and one new advanced short circuit strength metric [22] for evaluating the potential for inverter controller instability. Without running a dynamic solution, this advanced metric uses dynamic data (controller gains, time constants) of inverter-based resources to identify potential inverter instability. GSAT can also determine these metrics during outage scenarios thereby providing a system planner with a comprehensive overview of system strength.

SCR screening is also a quick way to study the impact of sequential operating points on evolution of grid strength. Buses with poor strength and hence vulnerable to instability can be revealed. In this analysis, it has been assumed that to meet the 24-hour load profile, no change in generation commitment status has occurred. It is recognized that this assumption may not hold true, especially with solar resources assumed to be part of the generation fleet. However, implementing this assumption allows for a preliminary system strength scan to be evaluated.

Since no change in generator topology has occurred, it can be assumed that there is minimal change in system strength across the network (evaluated only at the generator locations) when evaluating system strength based on the rated MVA capacity of the generation source. This is seen in Figure 9. Further, for ease of observing the variations across buses, the plot only shows locations that have a short circuit ratio lower than approximately 50.

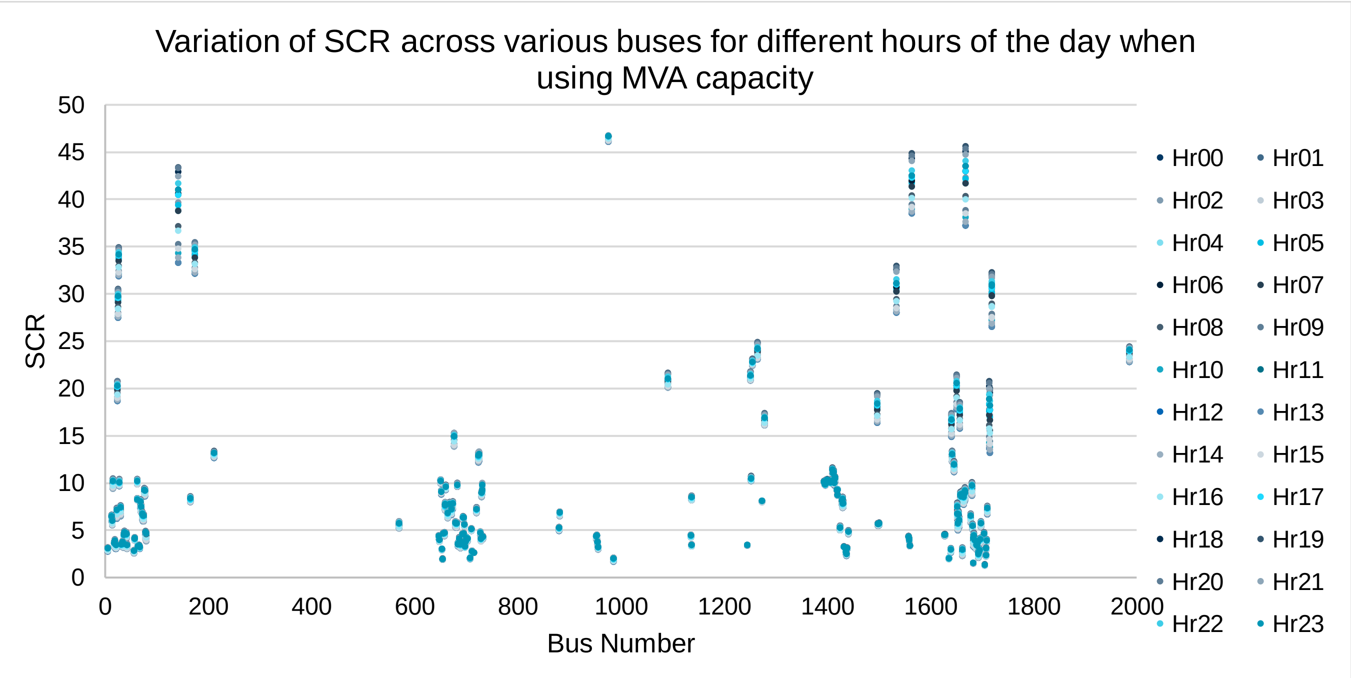

Figure 9: Change in short circuit ratio (plot limited to SCR of approximately 50) over 24 hours when using generation MVA capacity

While system strength has a minimal change at each bus with loading level when using rated MVA capacity of the generation resources, it can change when using the actual active power output of the generation source as shown in Figure 10. `

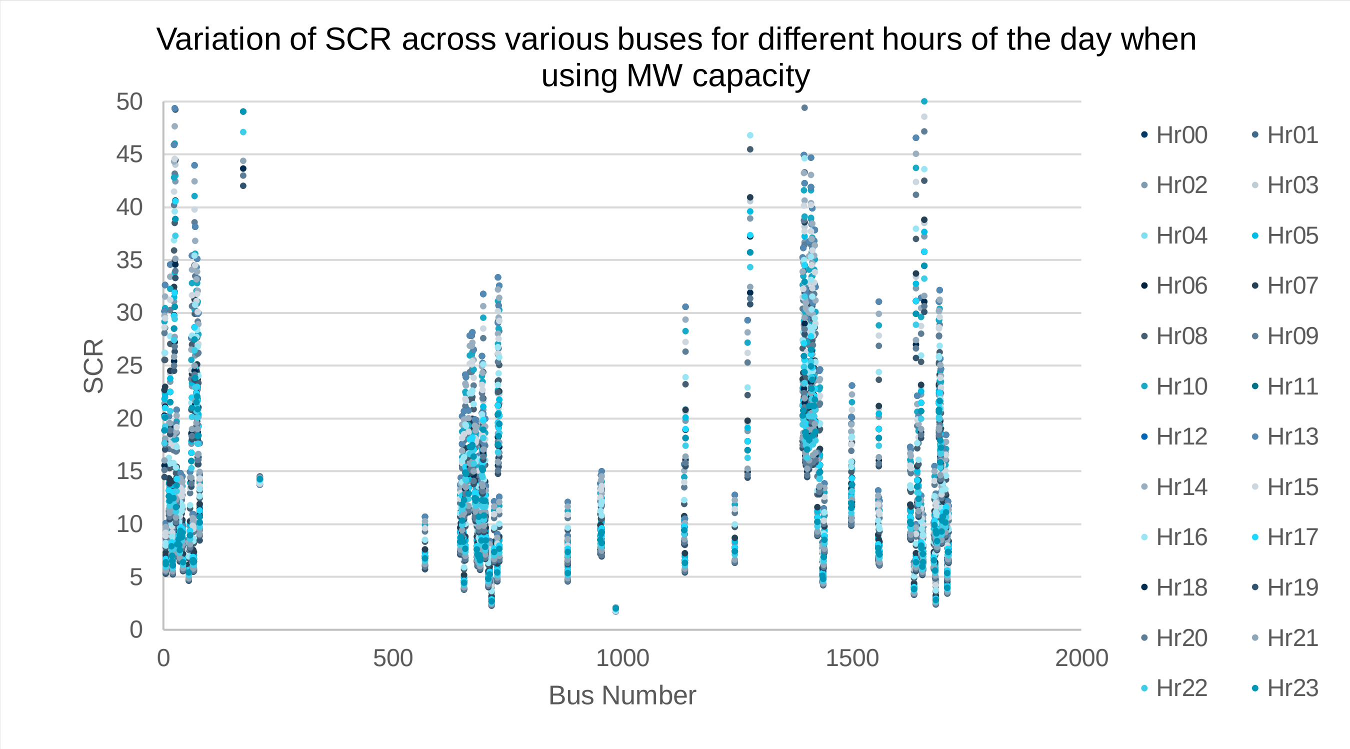

Figure 10: Change in short circuit ratio (plot limited to SCR of approximately 50) over 24 hours when using generation MW capacity

It has been seen in preliminary work that the stability of an IBR resource can be related to its active power output level [23] [24]. As the active power output of the IBRs increase, there can be an increased probability of instability that can occur. This is partly due to the transfer of increased active current through a weaker portion of the network and partly due to the reduced IBR current capacity for reactive current. As the active current increases, within the finite current capacity of the IBR, there is a reduction in the available reactive current that can be supported by the device. As a result, with reduced reactive current support, a particular inverter location can experience instability.

An example is shown in Figure 11 where the short circuit ratio between Hour-11 (light load of 12 GW) and Hour 19 (peak load of 25 GW) is compared. When the actual active power output of the generation source is used, there can be more locations of instability that can exist. This factor can be used to determine the operating point of a resource with regard to stability of the network.

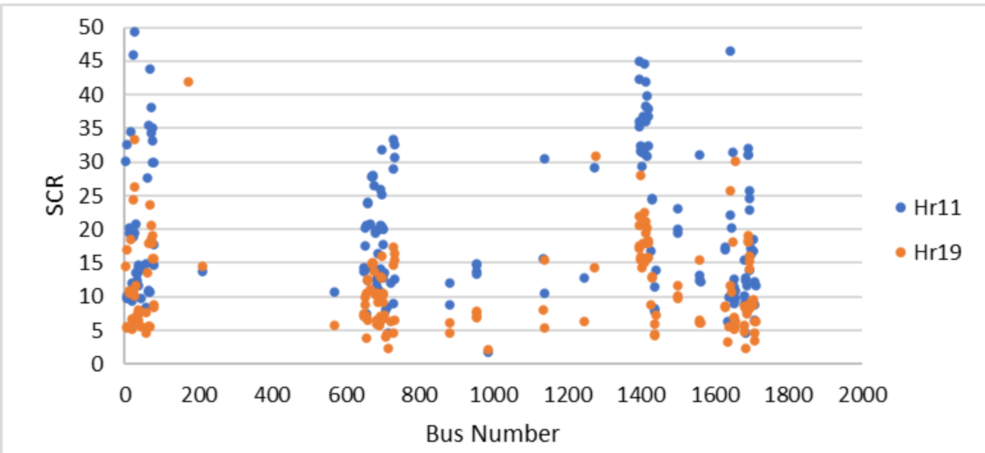

Figure 11: Comparison of short circuit ratio (plot limited to SCR of 50) between light load and peak load conditions when using generation MW output

The figures below show using heat maps the SCR at the various generator locations at two hours of the day corresponding to Hour-11 (light load of 12 GW) and Hour 19 (peak load of 25 GW). Lower the SCR, depicted by more yellow, greater is the risk of instability. Comparing Figure 12 and Figure 13, it can be noted that there are more purple spots corresponding to more generators with higher SCR during the hour with lighter load conditions (Figure 12) compared to hour with peak load (Figure 13).

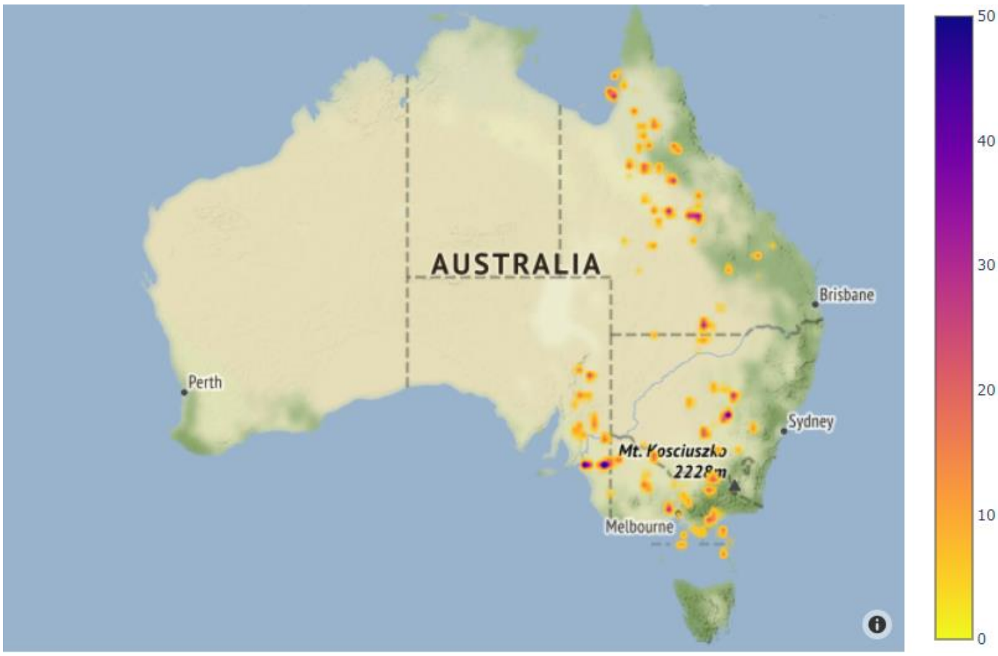

Figure 12: SCR evaluated at light load hour using generator's MW capacity

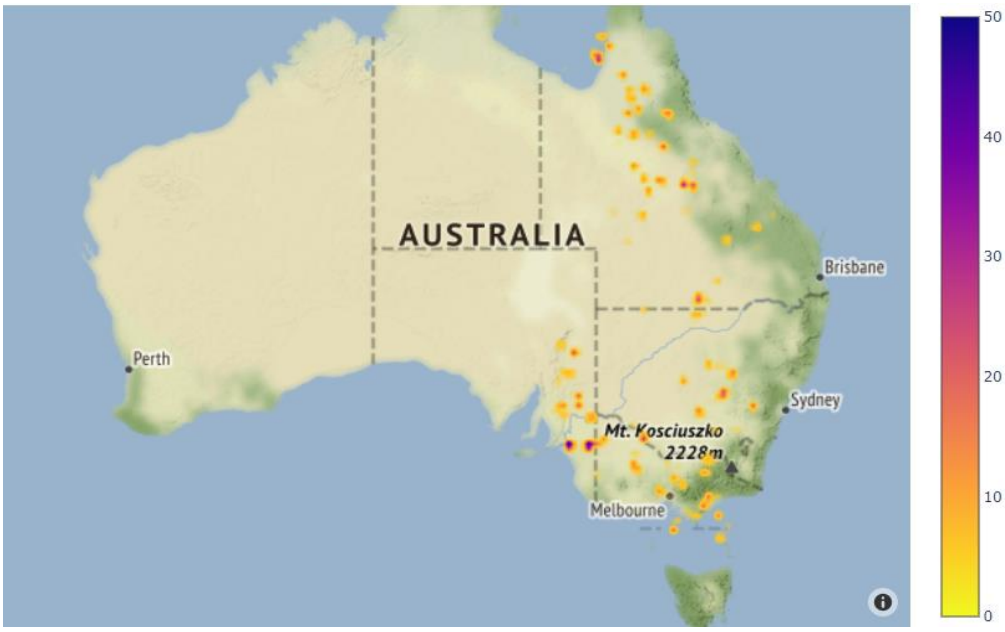

Figure 13: SCR evaluated at peak load hour using generator MW capacity

Figure 14 and Figure 15 show the same comparison for the two hours but using generator MVA capacity which is why the differentiation with more or fewer purple spots is not easily distinguishable.

Figure 14: SCR evaluated at light load hour using generator MVA capacity

Figure 15: SCR evaluated at peak load hour using generator MVA capacity

In addition to evaluating the short circuit ratio, another metric known as MVA availability [21] is evaluated. This metric can also be used to identify locations in the network where instability may arise. The advantages that this metric offers, can be showcased later in the report. Figure 16 shows the heatmap of generators with different available MVAs with minimum SCR threshold of 2.5. The higher the available MVA (hence greener the colour of the generator, the less is the risk of it being unstable. However, the smaller the available MVA, for example generators with negative MVA available, shown with dark pink have a higher risk of instability. It should be noted that these dark pink generators tend to surround generators greener in colour which is because the generators electrically well connected and hence in the central locations have higher current support and hence more stable. The dark pink coloured generators indicate problem generators and flagged down with these analyses. Also note that the negative MVA regions have a correlation with the low SCR regions observed by comparing Figure 16 and the previous heat maps showing SCR.

Figure 16: Generators with available MVA<=50MVA

3.2 Reactive power loss minimization

In addition to just evaluation of system strength, EPRI's Voltage Control and VAR management (VCA) tool [25] [26] was applied to optimize generator voltage setpoints from Volt-Var distribution perspective over the sequential operating points. EPRI's Voltage Control Areas (VCA) Studio is a software application for determining and analyzing voltage control areas of power systems and the optimal schedule of var resources. VCA partitions power systems into voltage control areas using clustering techniques. Each partition contains buses that are similar or near each other in terms of electrical distance, accounting for network properties such as voltage coupling and sensitivity with respect to reactive power perturbations. It solves Multi-Period Optimal Reactive Power Dispatch (MP-ORPD) optimization problem to find the optimal schedule of reactive power resources (var). This schedule includes voltage set-points of regulated buses, switching shunts' status, and transformer taps' status. The analysis process implemented by the VCA Studio software consists of the following: For a power network, or subnetwork, a user selects a range for the number of network partition areas, or clusters, to consider. The tool then uses clustering techniques for determining partition solutions having several areas within the given range and provides information regarding their internal voltage coupling with respect to reactive power perturbations. Based on this information and optional visual verification of the partition solutions, a user can select an adequate partition size. The VCA Studio tool can then be used to perform a detailed reactive reserve analysis for the areas of the selected partition. This analysis determines critical buses and contingencies for each partition area and provides area-specific measures of reactive reserves for both voltage stability and control. For scheduling var resources for the next day, consensus VCA is performed. The consensus VCA is determined based on the similarities of the clustering obtained from each scenario. In this case, different scenarios with different loading levels are the input. The VCA software will perform the above analysis for each scenario. It then computes critical buses and critical contingencies for each cluster for each scenario. The optimization tool of the VCA software schedules the var resources in the system to maximize the dynamic reactive power reserve. The output from the optimization tool is the voltage set-points of the regulated buses, the shunt schedule, and the transformer taps schedule. Critical contingency and critical buses at each time period are included in the optimization problem. Reactive power margin at the critical buses is improved if there are enough reactive power resources near the critical buses. Reactive power deficiency near the critical buses is reported for further investigations.

The importance of minimizing reactive power losses across the network and bringing the voltages across the network closer to 1pu has the effect of reducing the burden on the IBRs to provide large amounts of reactive current. With a reduction of this burden, the stability of the resources can be improved, as shown by the preliminary work done on evaluating impact of operating points on stability of the network.

The VCA tool maximizes the dynamic reserve, which means minimizing the reactive power support from the generators by optimizing the shunts, voltage setpoints, and transformer taps. This tool also allows for maximizing current capability in IBRs for active power. An example of application of the VCA tool to find optimal voltage setpoints and value of shunts for the Synthetic NEM is now discussed. Figure 17 (a)-(x) shows the voltage distribution across different buses of the system before and after optimization for 24 hours. The orange area shows that voltages are initially higher and towards a value of 1.1pu and spread out. However, after optimization, the voltages shown in the blue area are closer to 1 pu resulting in lower reactive power losses and an improved voltage profile. Better utilization of reactive power from each generation source is observed from Figure 19 wherein the reactive power burden is spread across the various sources rather than being concentrated over few select resources. Figure 18 shows the comparison of voltage distribution during light load condition (corresponding to Hr 11) and peak load condition (corresponding to Hr 19). At light load conditions, there are more buses with voltages lower than 1.0pu compared to peak load conditions as expected.

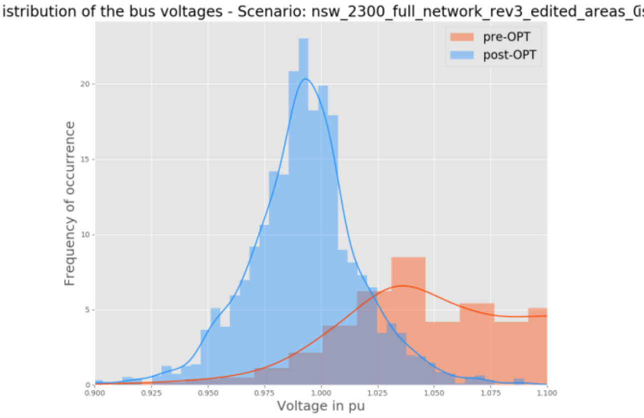

(a) Hour 00

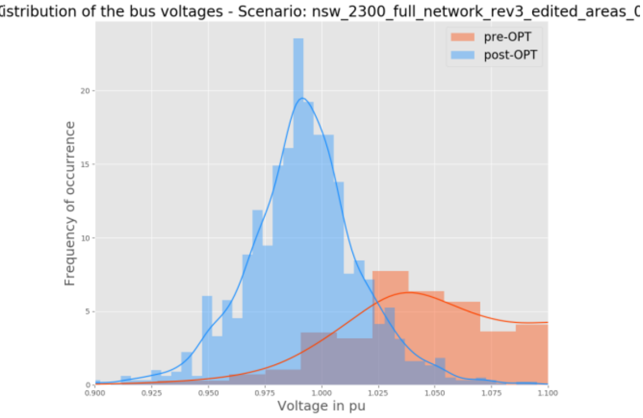

(b) Hour 01

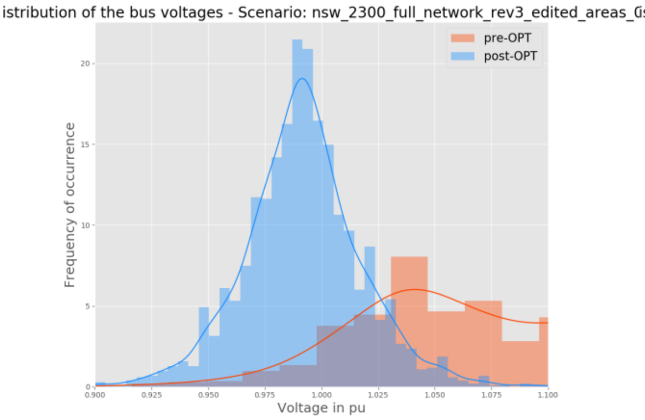

(c) Hour 02

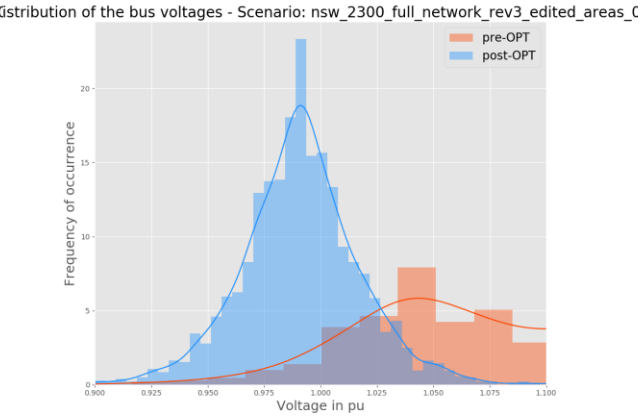

(d) Hour 03

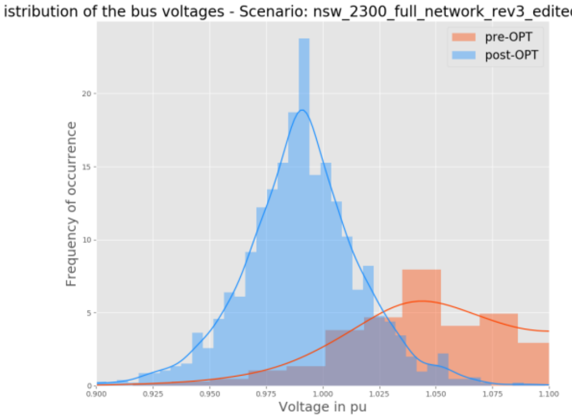

(e) Hour 04

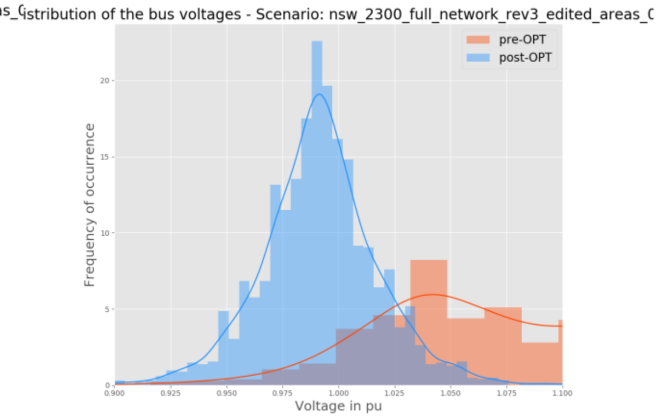

(f) Hour 05

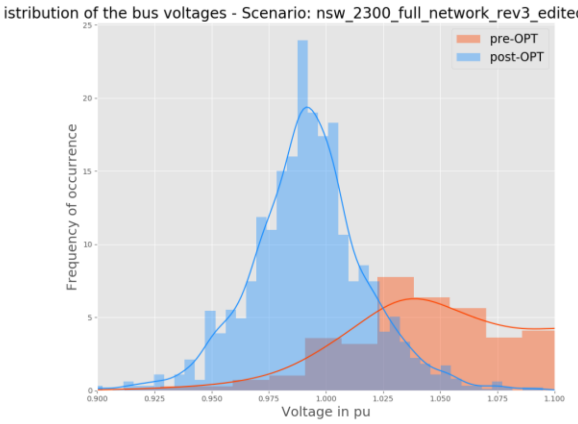

(g) Hour 06

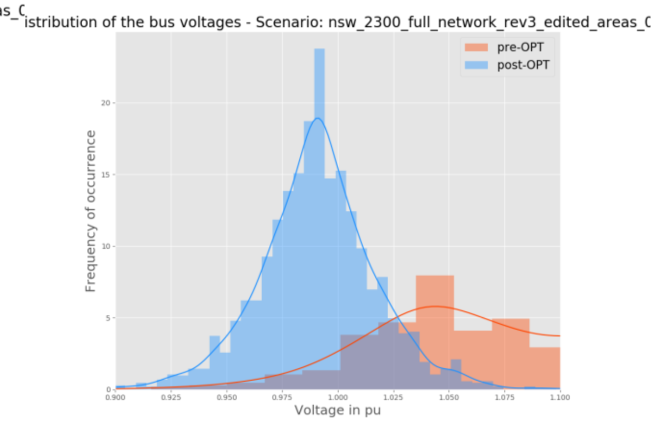

(h) Hour 07

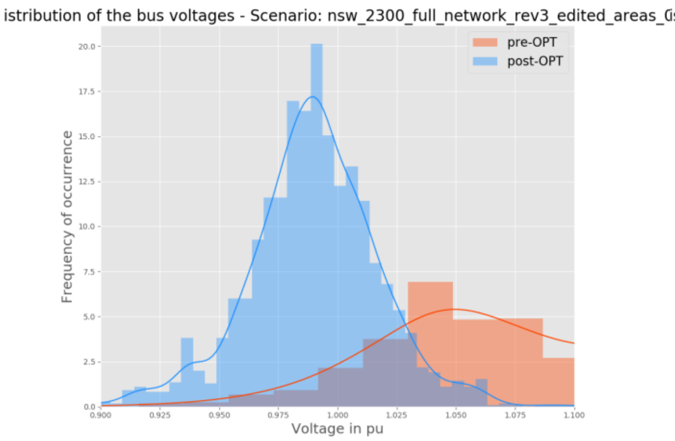

(i) Hour 08

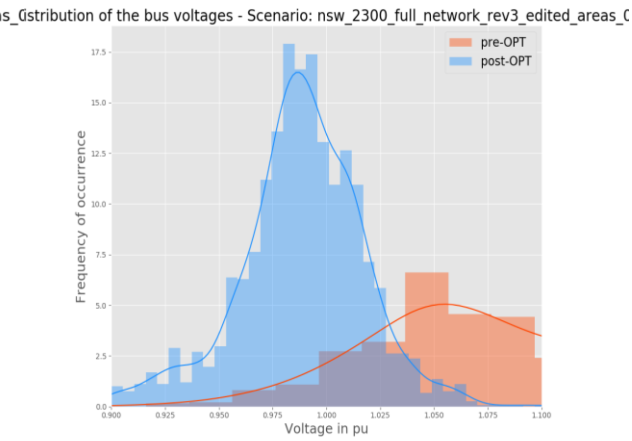

(j) Hour 09

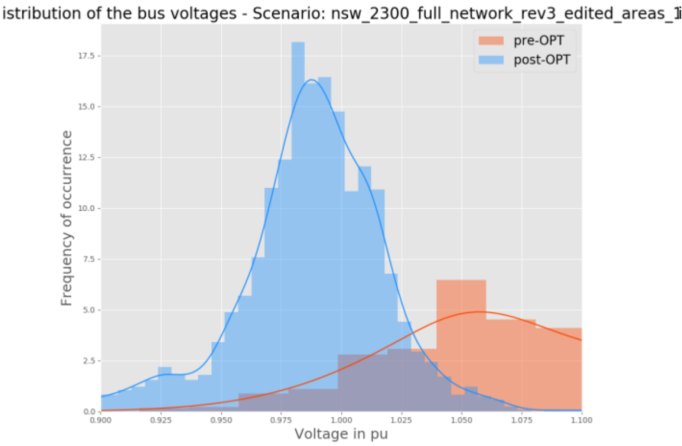

(k) Hour 10

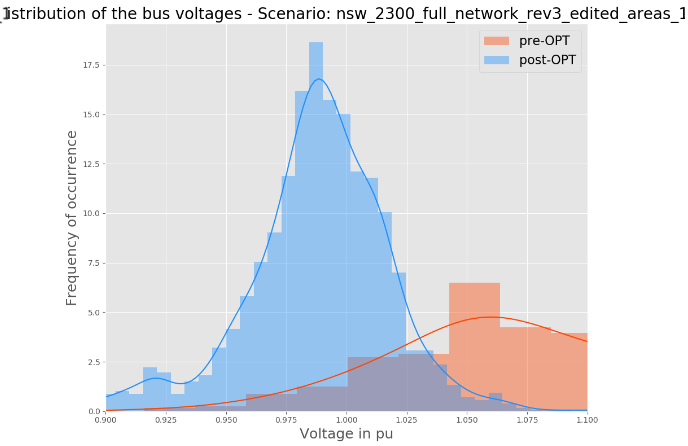

(l) Hour 11

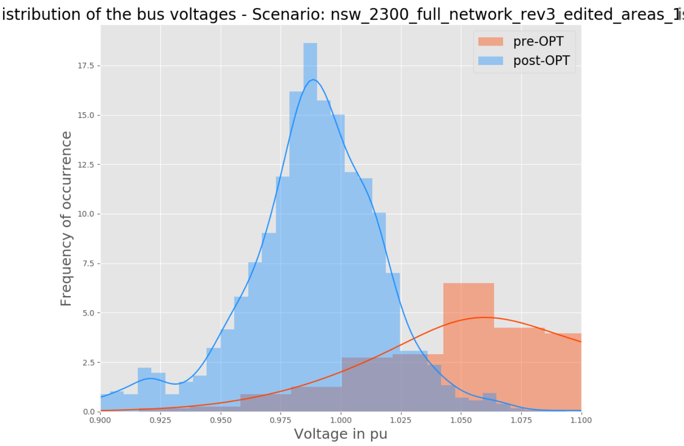

(m) Hour 12

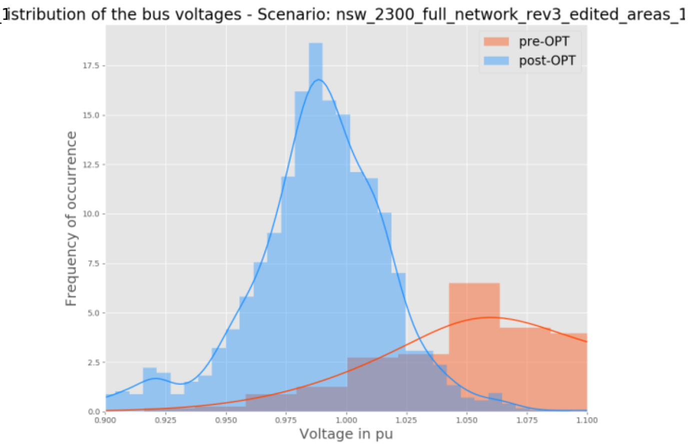

(n) Hour 13

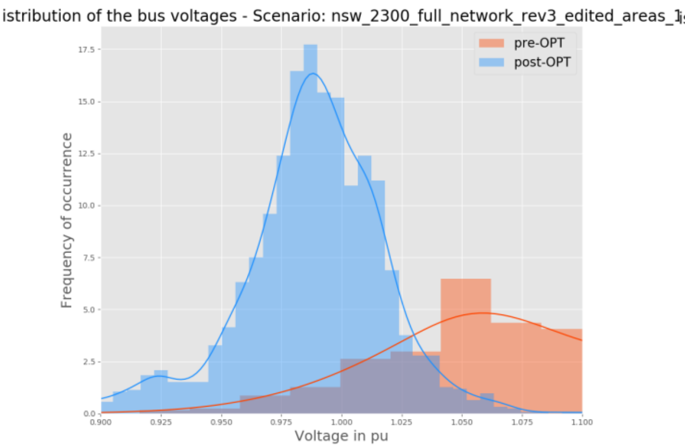

(o) Hour 14

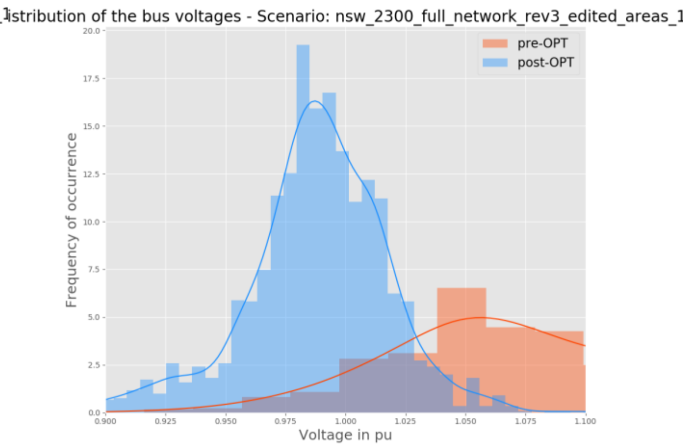

(p) Hour 15

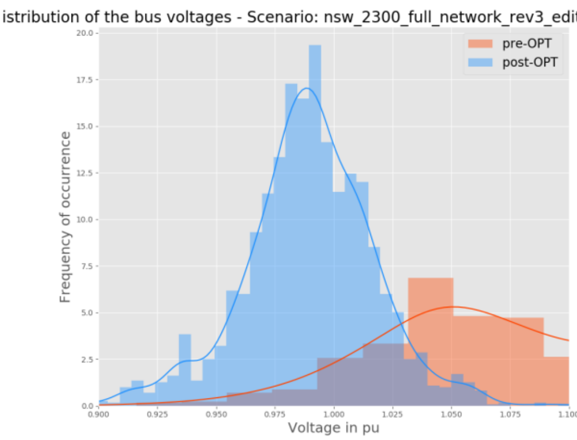

(q) Hour 16

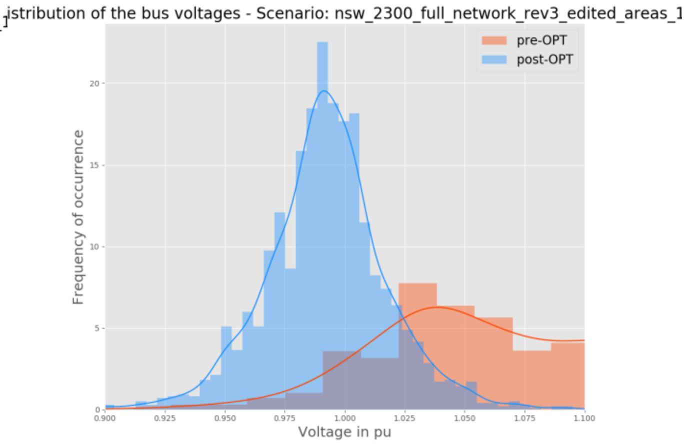

(r) Hour 17

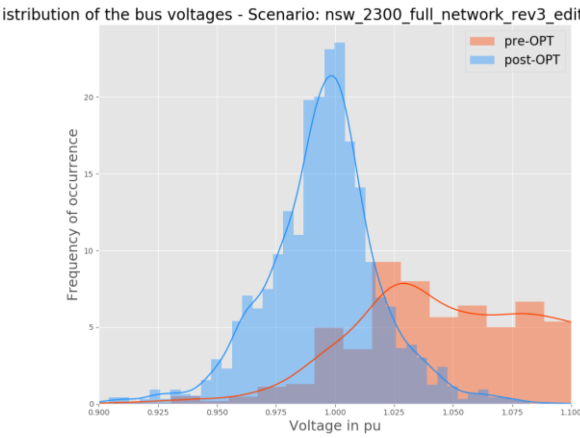

(s) Hour 18

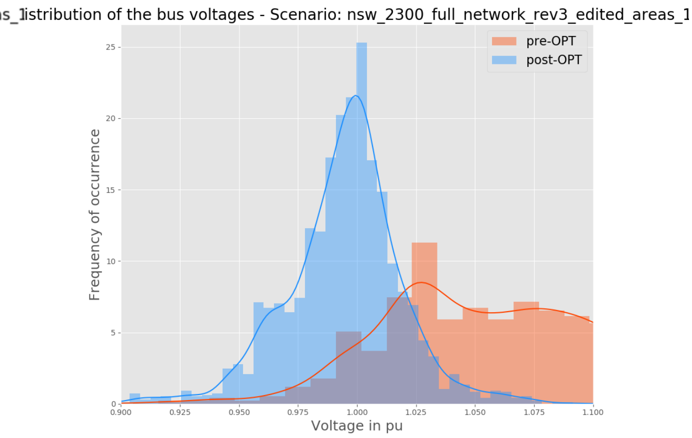

(t) Hour 19

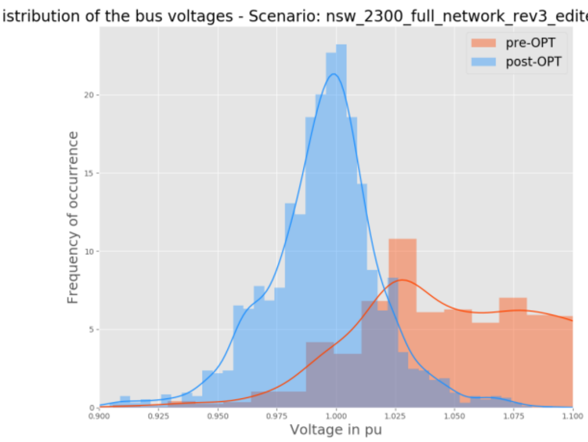

(u) Hour 20

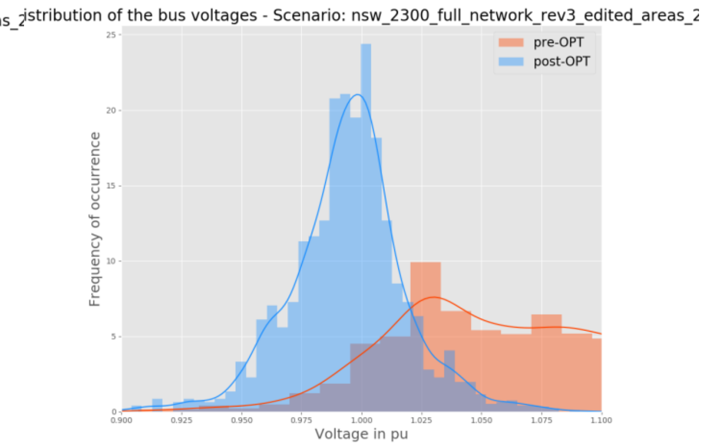

(v) Hour 21

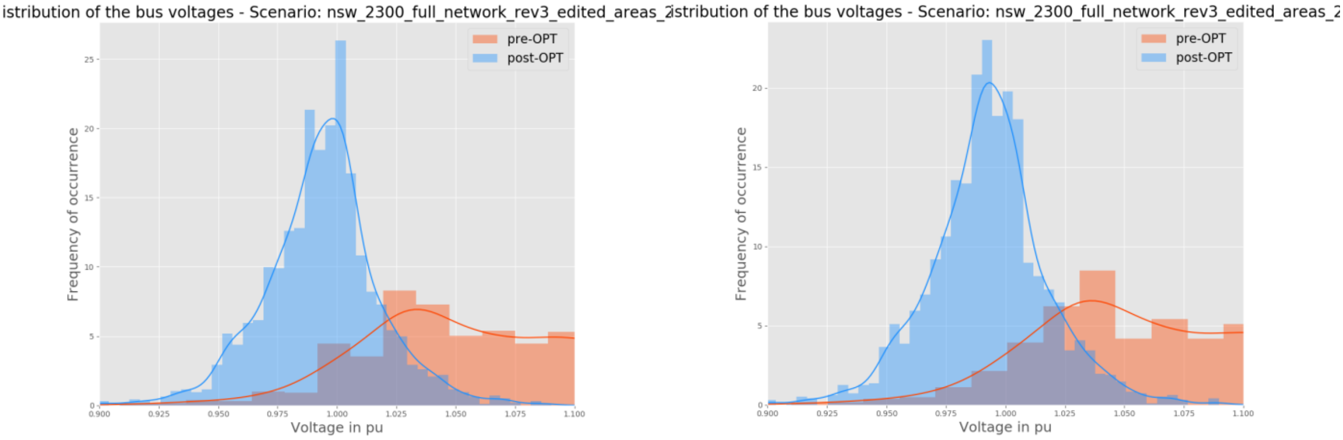

(w) Hour 22 (x) Hour 23

Figure 17: Voltage profile across the network for consecutive hours before and after optimization

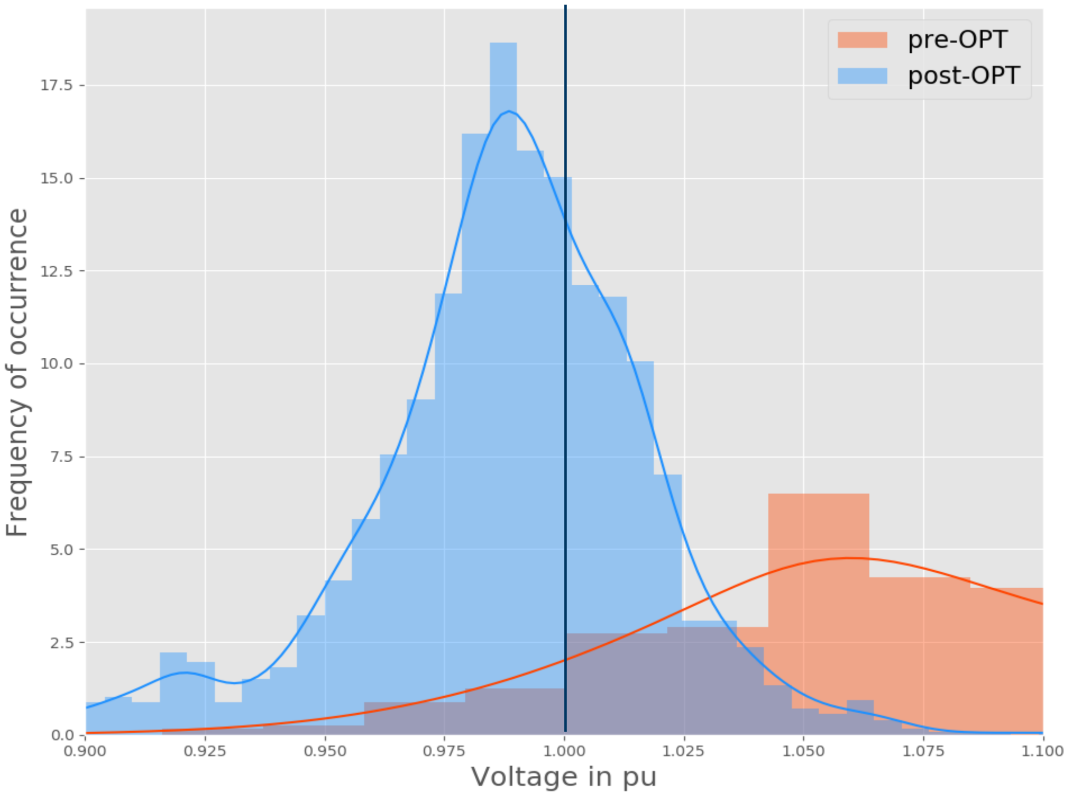

(a)

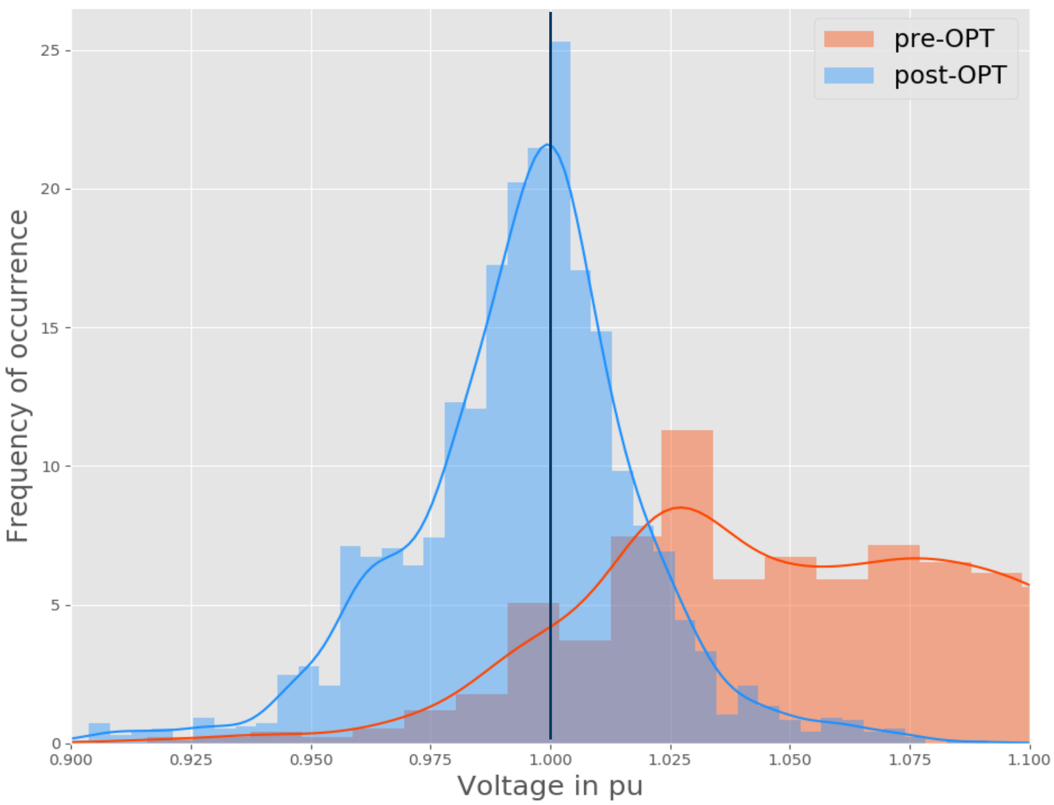

(b)

Figure 18: Voltage distribution for (a) light load (Hr 11) and (b) peak load (Hr 19)

A uniform reactive power profile is not possible at every loading level. Figure 19 (a)-(x) shows the reactive power generation at different generators at different hours of the day pre and post optimization by the VCA tool. A preliminary evaluation across a 24 hour loading period reveals the individual generator reactive power outputs as shown in Figure 20. As loading on the network reduces (light load condition is Hour_11) generator absorb large amounts of reactive power. This operating condition wherein large reactive power absorption is needed could have an impact on the stability of the network [27]. There are a few outlier buses with low voltage in the network which do not impact the stability solution, but do need to be addressed if this work progresses to the next stage.

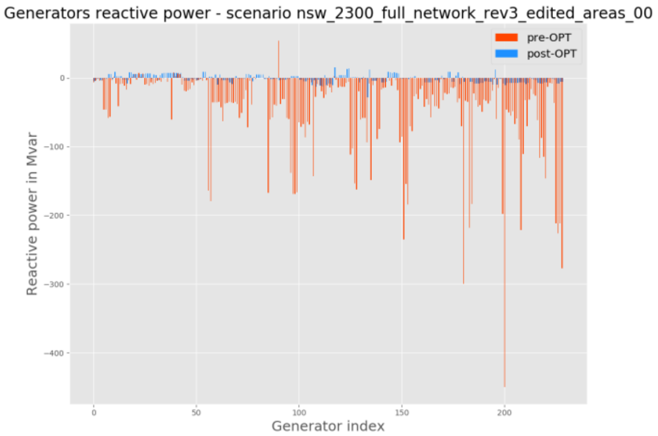

(a) Hour 00

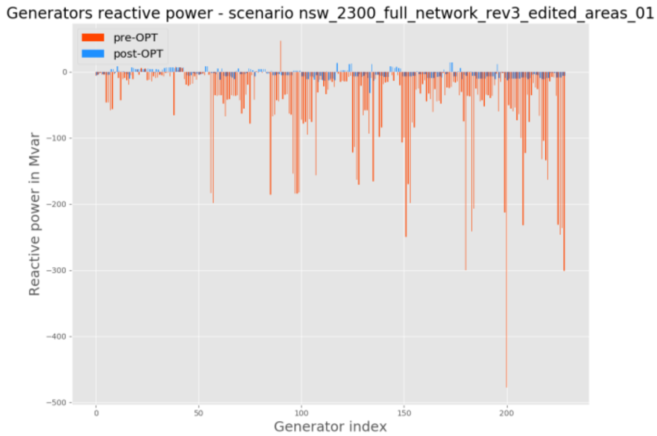

(b) Hour 01

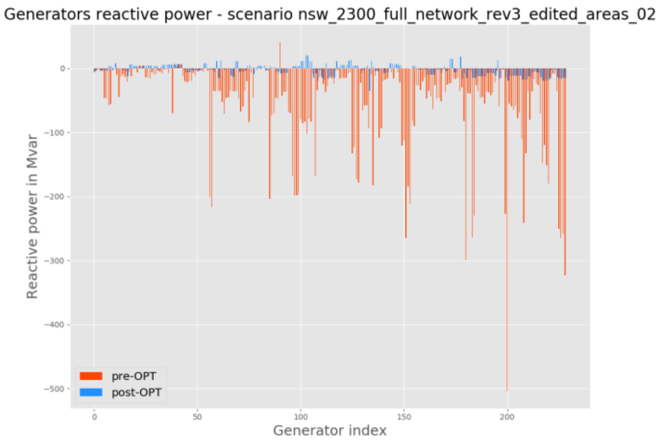

(c) Hour 02

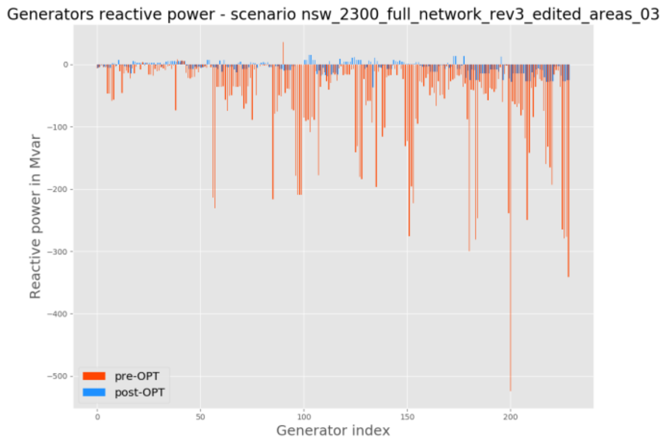

(d) Hour 03

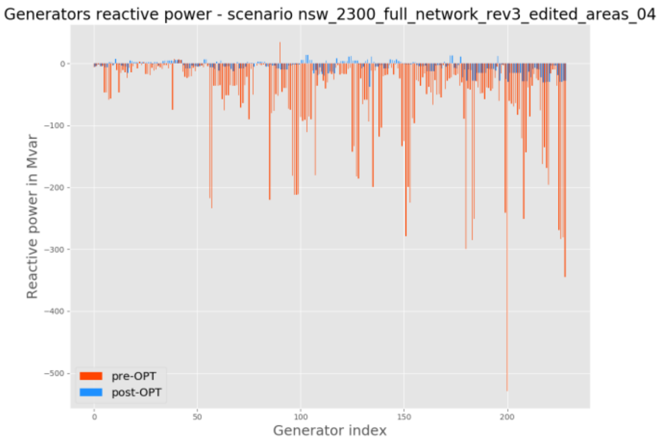

(e) Hour 04

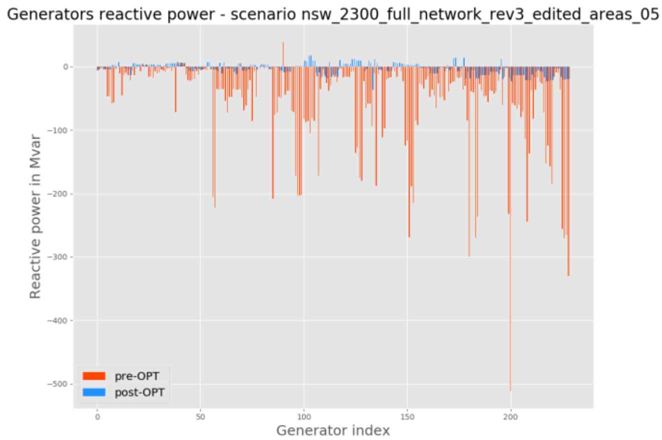

(f) Hour 05

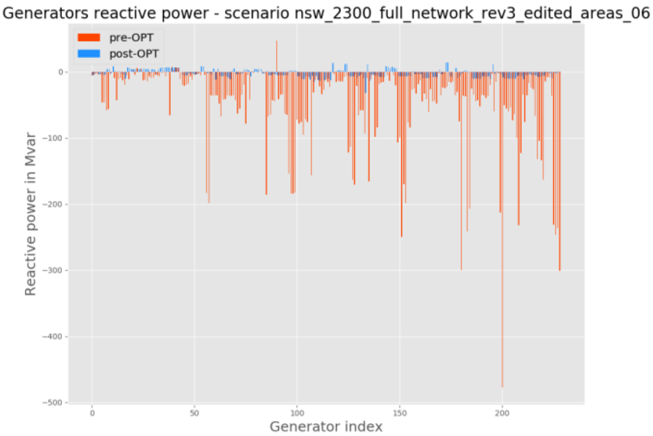

(g) Hour 06

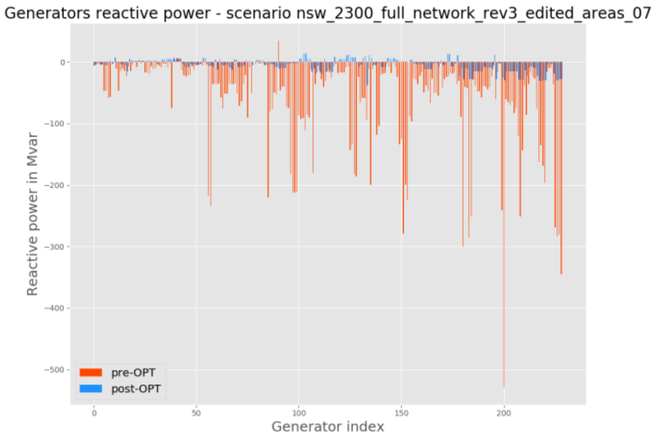

(h) Hour 07

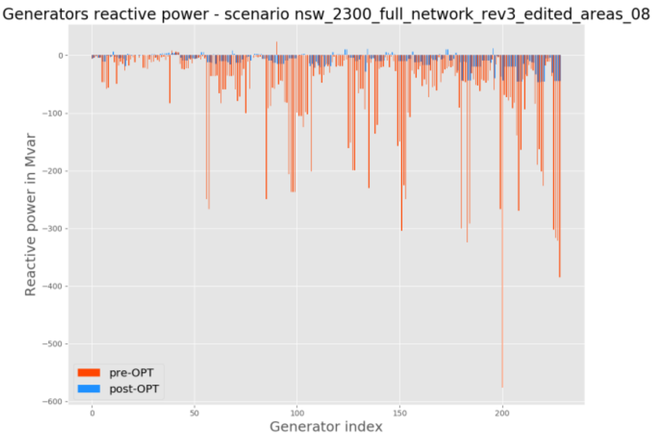

(i) Hour 08

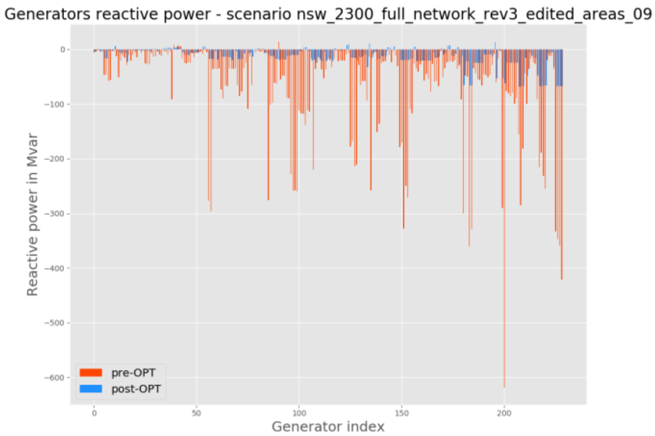

(j) Hour 09

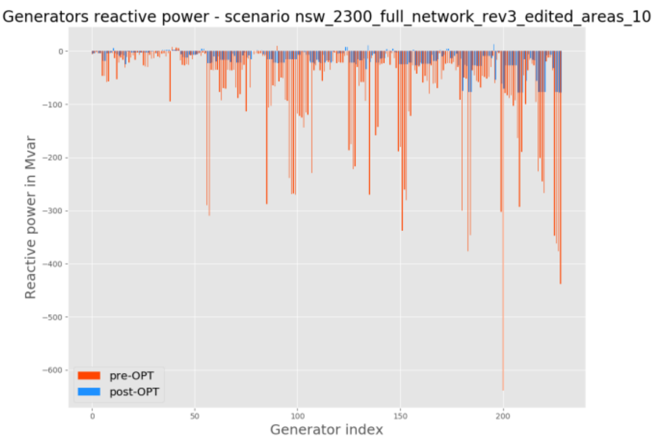

(k) Hour 10

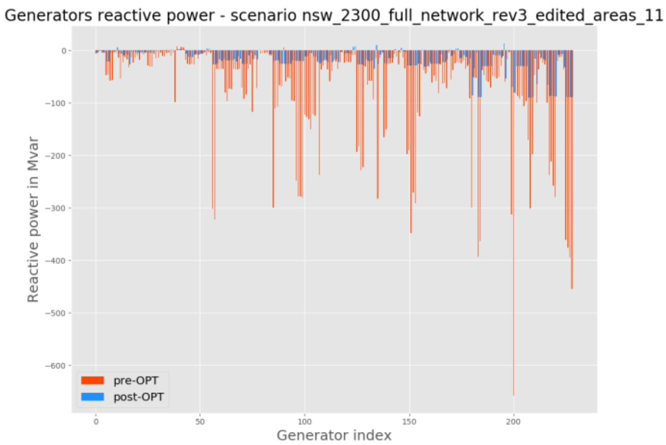

(l) Hour 11

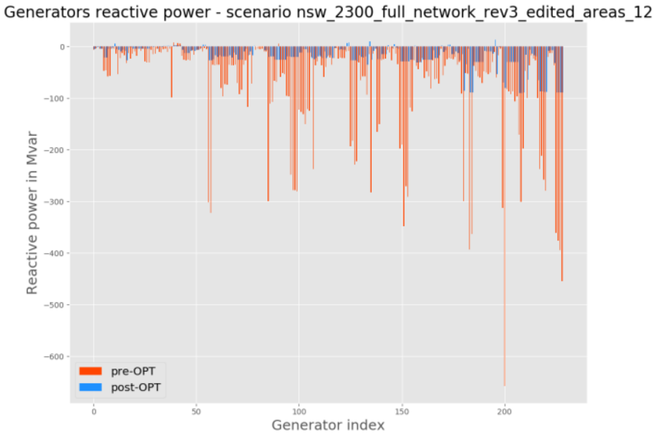

(m) Hour 12

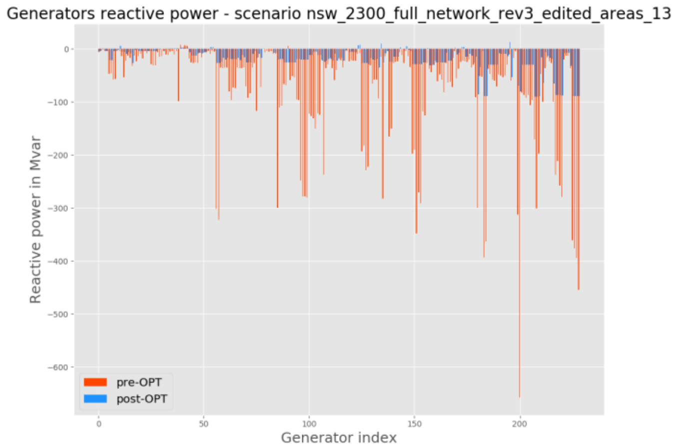

(n) Hour 13

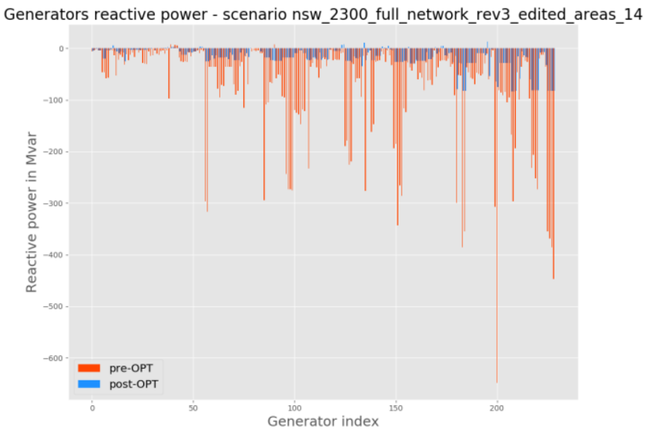

(o) Hour 14

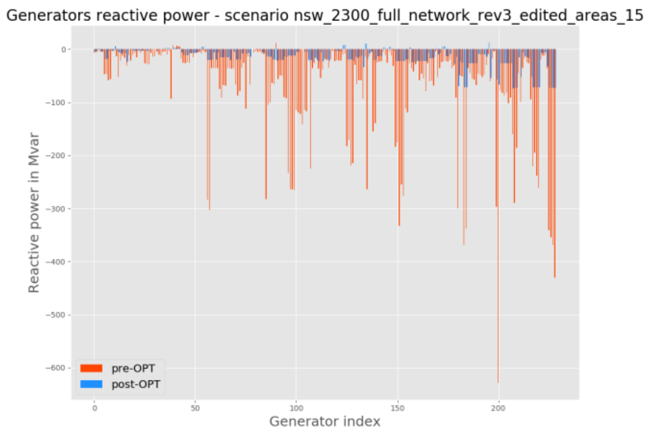

(p) Hour 15

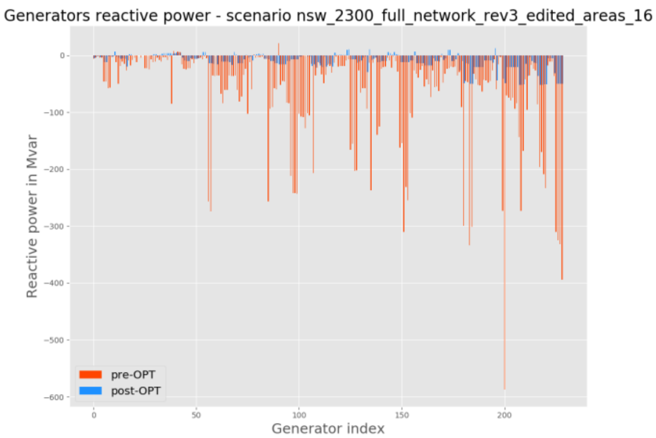

(q) Hour 16

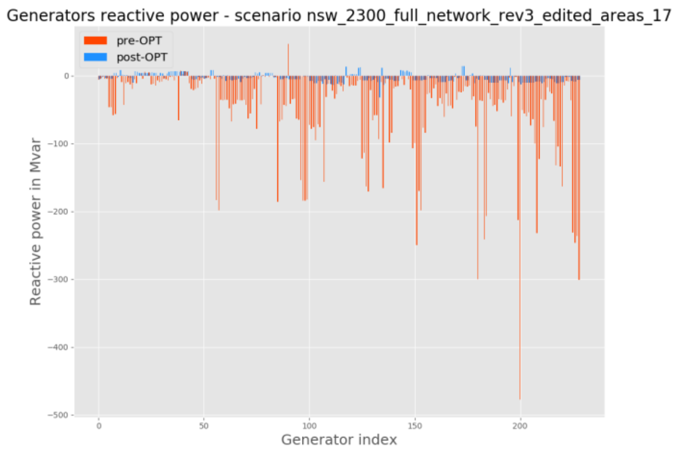

(r) Hour 17

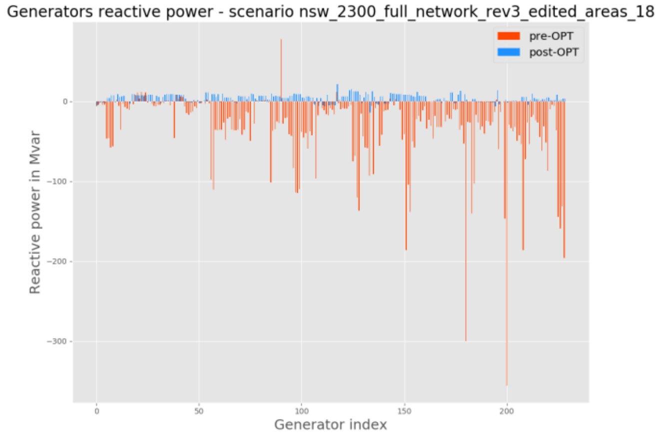

(s) Hour 18

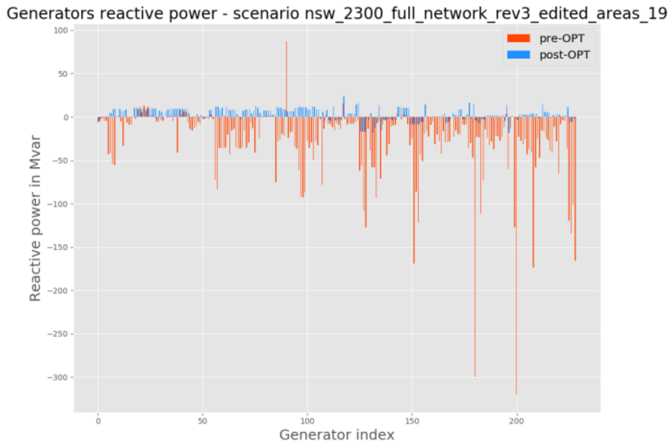

(t) Hour 19

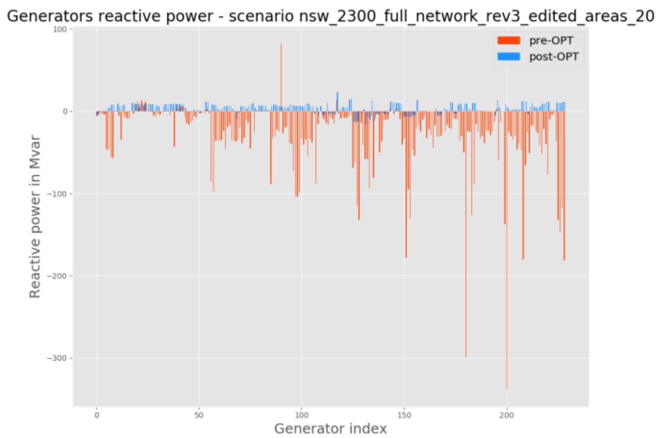

(u) Hour 20

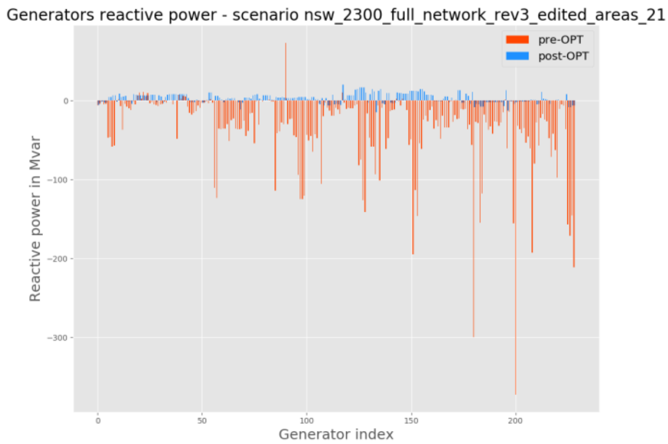

(v) Hour 21

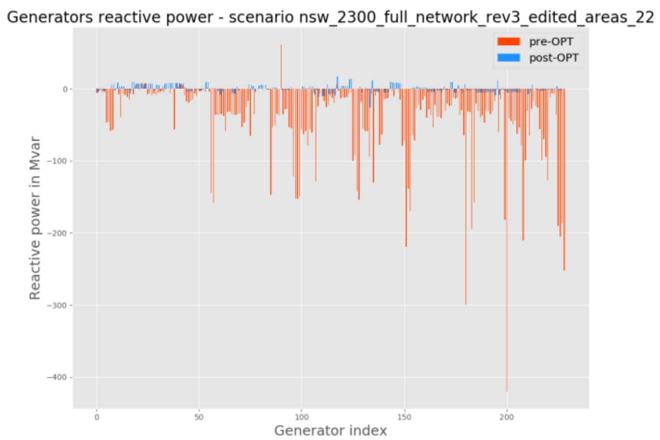

(w) Hour 22

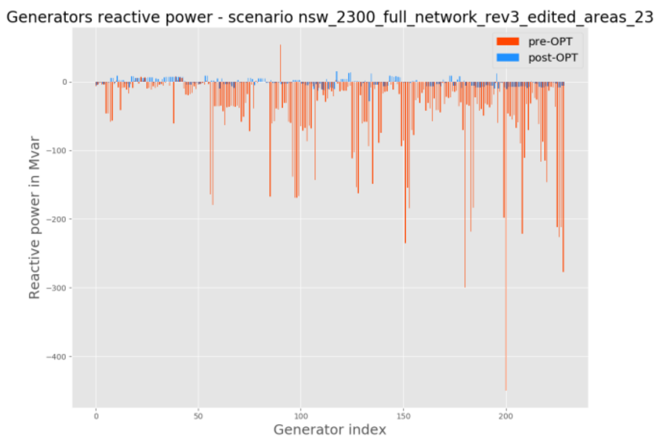

(x) Hour 23

Figure 19: Reactive power at generation sources before and after optimization over consecutive hours

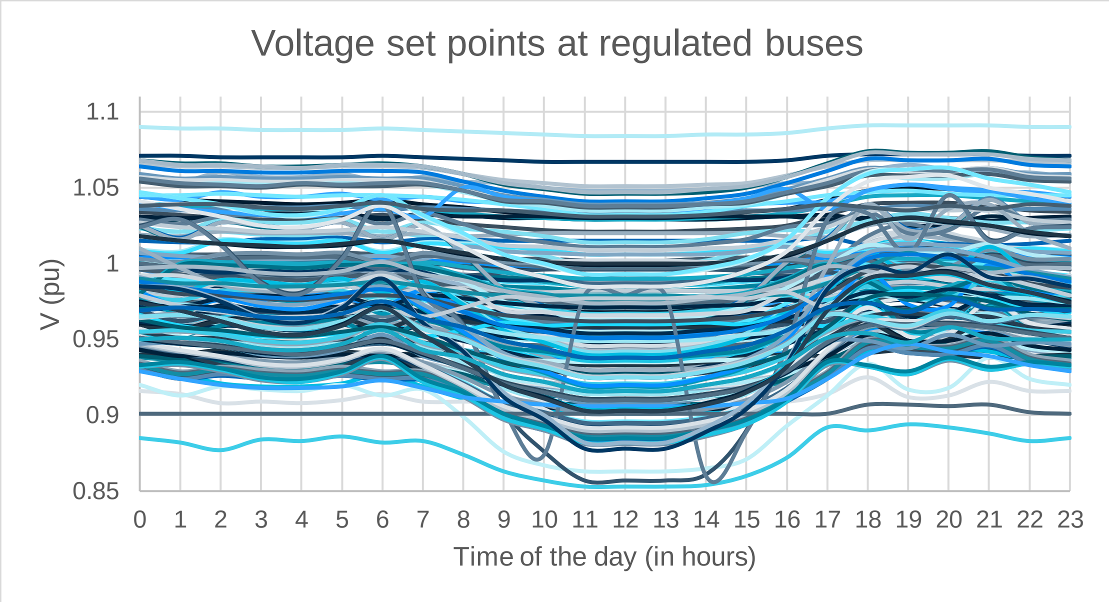

(a)

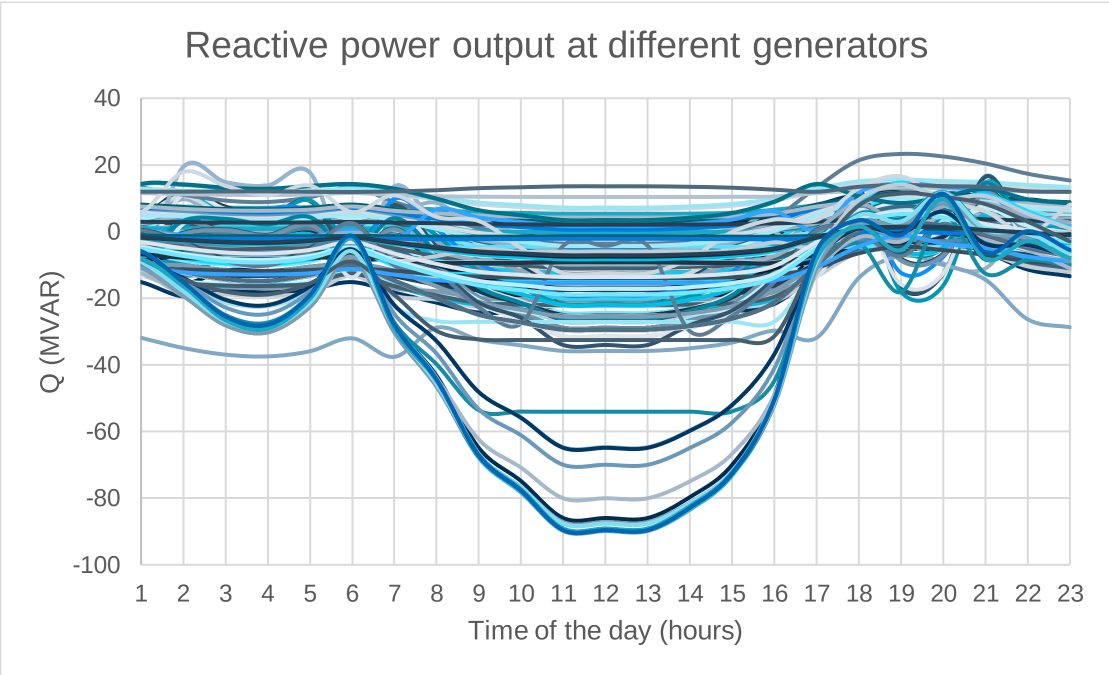

(b)

Figure 20: (a) Progression of optimal voltage set points at regulated buses over 24 consecutive hours, (b) Progression of optimal reactive power output from IBR generators over 24 consecutive hours

3.3 Determination of active power reserves

The purpose of this section is to describe how to create a commitment and dispatch using a day-ahead production cost model (PCM) and the process of taking those results and producing feasible steady-state cases. This process is important to define the active power operating point of each resource, which in-turn can impact its stability, given the restricted current headroom that is available in an inverter. Feasible means that the case converges with steady-state AC power flow, particularly using the Newton-Raphson method as the solution technique. A simple overview of the process is shown in Figure 21. The tools used will be described next, followed by the particular approach taken for this study, then results, and finally a summary of the findings and suggestions for future improvements needed.

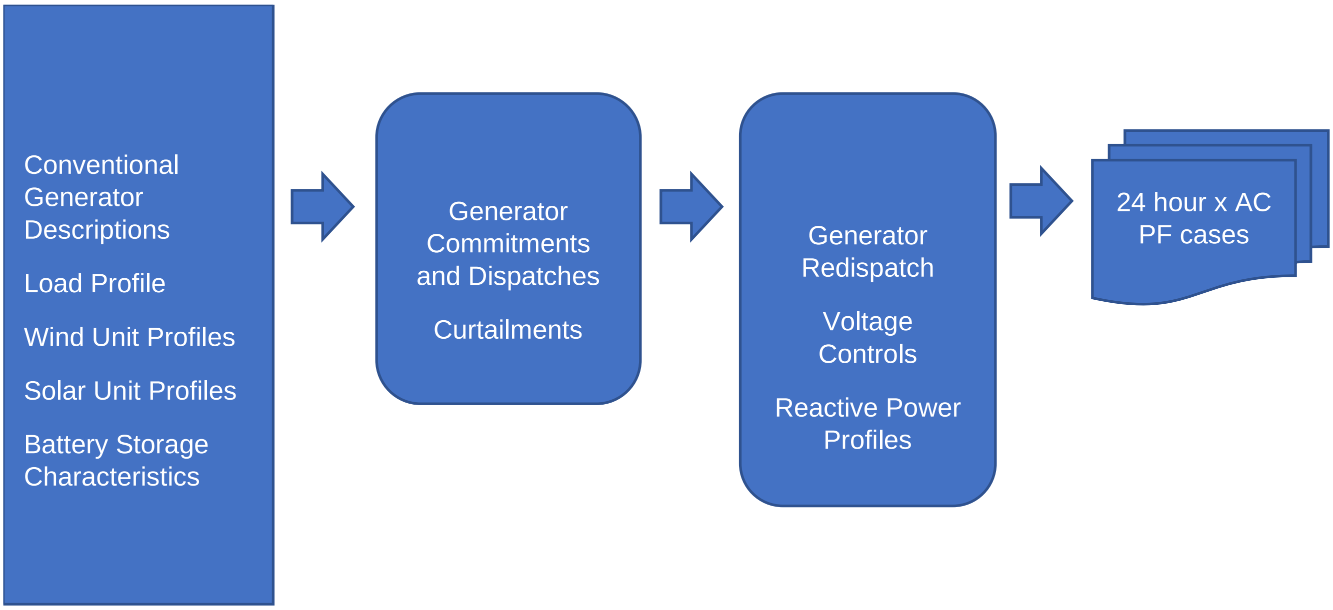

Figure 21: Overview of process used to develop ac-feasible power flow cases based on load pattern

3.3.1 About the PCM Tool

The Unit Commitment and Economic Dispatch (UCED) model is a DC optimal power flow model that provides cost-minimizing unit-commitment and economic dispatch decisions subject to technical constraints. Data interfaces are realized within Python, whereas the mathematical formulation of the problem is implemented in Julia. The optimization model is based on the software tool FESTIV DA [28]. The input file format relies on the PSO format (**https://psopt.com**). The minimization problem of UCED is subject to technical constraints, such as DC-OPF, capacity constraints, minimum operating points, minimum up- and downtimes, storage equations, time varying availability of resources, etc. Ramping constraints are available but where not used for this case study. Cost terms include operational costs, such as fuel costs, start-up costs, and load curtailment costs. The optimization problem can be optimized in a rolling horizon approach to reduce computational complexity (e.g., one day per iteration). The result of this optimization, i.e., the optimal economic dispatch decisions are exported as .csv files, and further postprocessed for input in the GAT tool.

3.3.2 About the GAT and AOC tools

The Grid Analysis Toolkit (GAT) is a suite of software tools for performing steady-state transmission analyses that is used in much of the research in the Transmission Operations Planning area. GAT primarily provides efficient network modelling and the ability to define flexible optimization modelling needs for running steady-state analyses (DCPF, DCOPF, ACPF and ACOPF). One of the applications of GAT is the Automatic Outage Coordinator (AOC) application that one of the stated benefits is to automate the case building process to save engineering time and simplify the management of the outage study process. The current version 1.0 of the tool is still an early beta version that provides much of the core functionality of the process. The tool can define and manage Outage Requests for study under various forecasts and generation schedules to perform Contingency Analysis determine whether an outage can be cleared or not.

The case building steps typically follows these steps:

- Provide a base network case
- Select outage requests to study
- Import or generate **forecasts** for load and optionally wind generation and solar generation
- Import or run the UCED tool with the forecasts applied to create the **generation schedule**
- Import or run an optimization-based ACPF with flexible limits and controls to determine the **voltage controls schedule**
- For each outage request, perform an ACPF **contingency analysis** to determine feasibility by judging if the ACPF converges and if there are any violations

The same process may be applied to other applications, such as in the planning timeframe, with some modifications of the algorithms and modeling to help expedite the case building process.

3.3.3 Case study Assumptions

3.3.3.1 Assumed capacity mix

The initial target capacity mix for the Synthetic NEM case in this study for each of the regions is described in Table 3. Note that TAS region, which is dc-connected to the rest of the NEM has been ignored. The assumed capacity mix is very renewables heavy in all regions with no conventional thermal generation in the SA region and only 10% in both NSW and VIC regions.

Table 3: Initial target capacity mix

Region	Solar	Wind	OCGT	CCGT	Total
NSW	45%	45%	5%	5%	100%
VIC	45%	45%	5%	5%	100%
QLD	0%	60%	10%	30%	100%
SA	50%	50%	0%	0%	100%
TAS	-				

After running initial commitment with the UCED tool there were shortages, so 24 (20 without the TAS region) battery storage devices were included system to provide support with a total of 15,485 MW of capacity (14,428 MW without the TAS region). The evaluation that was carried out here was to ensure sufficient active power delivery of load across the 24 hour period, while considering the assumed the wind and solar profile. The total generation capacity based on this mix is provided in Table 4. Notice that the target resource mix is somewhat different from the target capacity mix once mapped to generation units.

Table 4: Total capacity mix by type

	NSW	VIC	QLD	SA	TAS	Total w/o TAS
CCGT (MW)	1327	851	6690	0	0	**8868**
OCGT (MW)	1332	810	2250	0	0	**4392**
Wind (MW)	9090	5062	10601	2482	1717	**27235**
Solar (MW)	8744	6459	0	1773	1729	**16976**
Storage (MW)	6056	3377	2786	2209	1057	**14428**
Total w/ Storage (MW)	26549	16559	22328	6464	4503	**71900**
Total w/o Storage (MW)	20494	13182	19542	4254	3446	**57472**

After adding storage and mapping the capacity mix of units to the actual mix the actual resource mix is shown in Table 5.

Table 5: Actual capacity mix

Region	Solar	Wind	OCGT	CCGT	Storage
NSW	33%	34%	5%	5%	23%
VIC	39%	31%	5%	5%	20%
QLD	0%	47%	10%	30%	12%

SA	27%	38%	0%	0%	34%

3.3.3.2 Generator characteristics description

The assumptions for the generator characteristics by generation resource type for thermal generating units are shown in Table 6. This table is based on data gathered in 2022 from AEMO (Integrated System Planning) ISP[1], Aurecon, GHD, and ACIL Allen, and fuel costs are based on 2022 AEMO ISP's step change scenario. Note that only OCGT and CCGT are modelled based on the assumed capacity mix. All coal units, biomass and hydrogen units are not included in the resource mix. The battery storage units are also given 90% efficiency, 0 MW lower limit, and capacities ranging from 236 MW to 1464 MW.

Table 6: Generator unit characteristics

Technology	Heat Rate (GJ/MWh)	Max Ramp Up (MW/min)	Max Ramp Down (MW/min)	Min Up/Down Time (h)	Cold Start-up Notification Time (Hr)	Warm Start-up Notification Time (Hr)	Hot Start-up Notification Time (Hr)	Cold Start-up Costs ($/MW as gen)	Warm Start-up Costs ($/MW as gen)	Hot Start-up Costs ($/MW as gen)
Black Coal (advanced ultra supercritical PC)	8.82	30	30	8	24	4	2	350	120	40
Black Coal (advanced ultra supercritical PC) with CCS	14.32	30	30	8	24	4	2	350	120	40
OCGT (small GT)	10.19	250	250	1	6	1	1	100	100	100
OCGT (large GT)	10.93	250	250	1	6	1	1	100	100	100
CCGT	7.25	22	22	4	15	3	1	25	15	5
CCGT with CCS	8.94	22	22	4	15	3	1	25	15	5
Biomass	13.74	1.2	1.2	No data	24	4	2	210	105	40
Hydrogen turbine (large)	10.93	10	10	No data	No data	No data	No data	No data	No data	No data
Battery Storage	No data	999	999	No data	No data	No data	No data	No data	No data	No data

3.3.3.3 Demand profile

The daily demand profile is based on the 2030 projection of the average time of day profile detailed in the 2023 AEMO ISP report[2]. The profile used for the study is shown in Figure 22. The system is afternoon peaking with a peak of 25,000 MW.

[1] https://aemo.com.au/-/media/files/major-publications/isp/2022/2022-documents/2022-integrated-system-plan-isp.pdf?la=en
[2] https://aemo.com.au/-/media/files/major-publications/isp/2022/2022-documents/2022-integrated-system-plan-isp.pdf?la=en

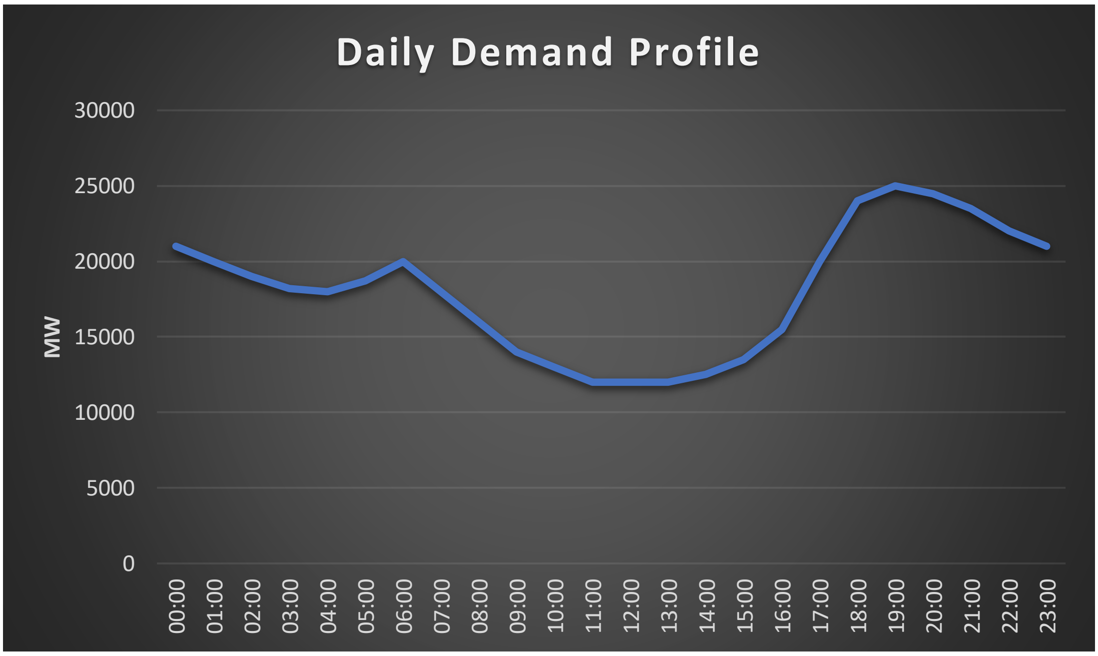

Figure 22: Demand profile of an average day

The total capacity without storage and the additional storage capacity are compared to the peak demand hour (hour: 19:00) is shown below per region in Figure 23.

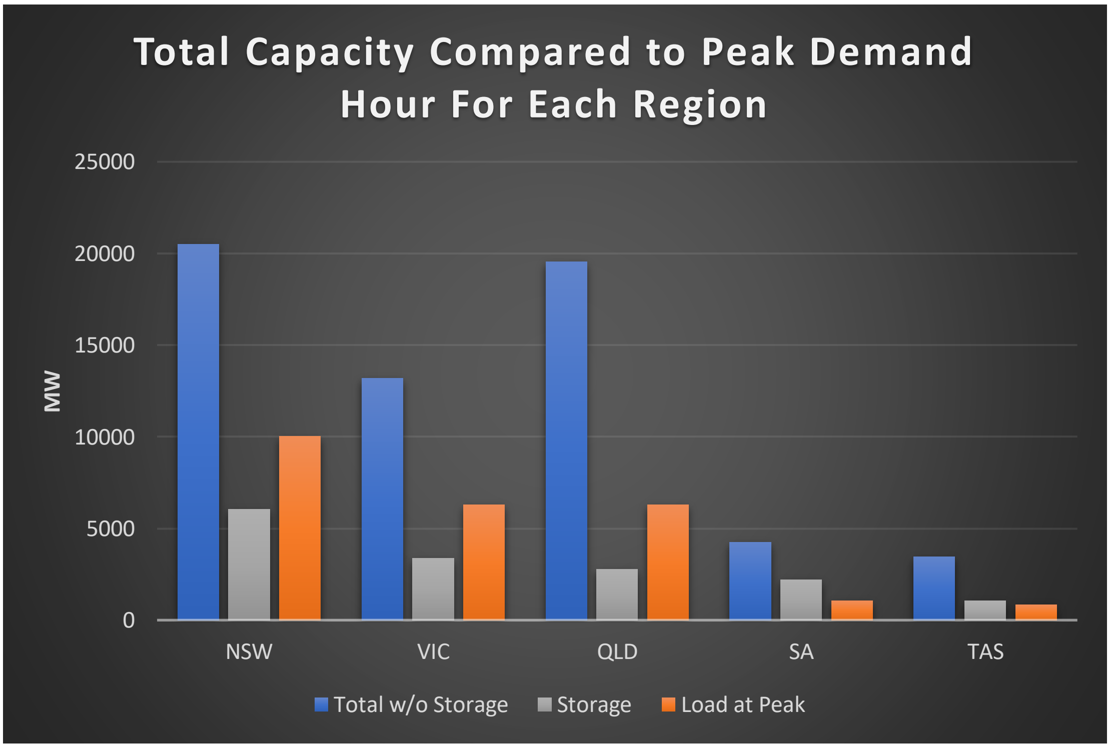

Figure 23: Total capacity, storage capacity, and peak load of the average day

3.3.3.4 Network components

The base case provided had the following number of components for the power flow modelling as tabulated in Table 7. Batteries are modelled as generators.

Table 7: Number of network components

	Full System	Modeled (w/o TAS)

Buses	2453	2218
Shunts	414	397
Lines	1821	1672
2wTransformers	1420	1259
3w Transformers	113	107
Generators	265	229
Loads	3093	2790

3.3.4 Case building process

The model in UCED is a PTDF-based system equivalent, assuming a constant voltage magnitude and neglecting reactive power. To provide a more realistic representative of power system, especially the nonlinearity of power flows, and to conduct the studies on system stability and resilience with contingencies, the full AC power flow analysis is built with GAT using the process described here.

In the UCED results, all shunts are modelled as fixed shunts, and all transformers are fixed transformers, thus the system has limited capability in voltage regulation. To better optimize the system performance, assumptions are needed for the controls in the AC power flow studies.

Assumptions for Voltage Control and Reactive Power Support

- Assumption 1, all shunts are:
    - Converted from fixed to switched shunts
    - Providing voltage regulation on the local bus
    - Continuous in susceptance
    - With estimated max/min susceptance
- Assumption 2, all transformers are:
    - Converted to tap changing transformers
    - Providing voltage regulation on the sending-end bus
- Assumption 3, all load reactive power are made flexible but with limiting penalty from their given initial point using the base case power factor

3.3.4.1 Case building algorithms

Starting from the production cost model result, the following steps are taken to find the AC feasible solution, as the case building process:

1. Perform DC power flow
2. Reset bus voltage magnitudes and relax voltage limits
3. Update shunts and transformer types and limits
4. Assign conventional generators to be re-dispatchable
5. Solve AC optimal power flow problem allowing reactive power violations, and with reactive resources free of regulation
6. Reset voltage settings based on the result of (5) and re-run AC optimal power flow
7. Solve AC optimal power flow problem with reactive power regulation, and/or with shunts and tap changers in locked mode
8. Resolve reactive power violations (optional)
9. Solve AC power flow with Newton-Raphson method

If the problem is still infeasible, additional curtailment on renewable energy, load shedding, or expansion of VAR support may be applied.

Here, ideally the results can also be combined with the reactive power loss minimization algorithm that is available in the VCA tool. Such a merger of the analysis from both tools is expected future work.

3.3.5 Case study results

The Synthetic NEM case with the PSO input data is infeasible in UCED for the 24 hours. A few factors could result in the infeasibility. The primary reason is that the UCED generation data is not adequately mapped to the PSS/E power flow files. An initial mapping of the data has been carried out based on bus numbers, but this is yet to be verified. Further, in the initial base case data, all generators are assumed to be in-service and as a result, minimal information is available regarding the on/off status due to ramping constraints. This unavailability of data makes it more challenging to develop a feasible dispatch. Further, as only 16 out of 265 generation units are conventional, the network has relatively little flexibility. Additional energy storage units have been added, but additional modelling in UCED may be needed to better model storage. Further, UCED aggregates the units to only 5 buses, however the fix on the locations doesn't help with the convergence of AC power flow studies in the following step.

The UCED result is only feasible with load curtailments. With load curtailment, the generation commitment and dispatch results for the 24 hours are shown below in Figure 24. As is easily noted, there are many hours that are particularly MW deficient (the yellow line – generation – does not follow the orange line – load). If load curtailment or redispatch of conventional generators is allowed, some scenarios are AC feasible with the proposed case building algorithm, as shown in Table 8, while the rest of hours failed to be solved.

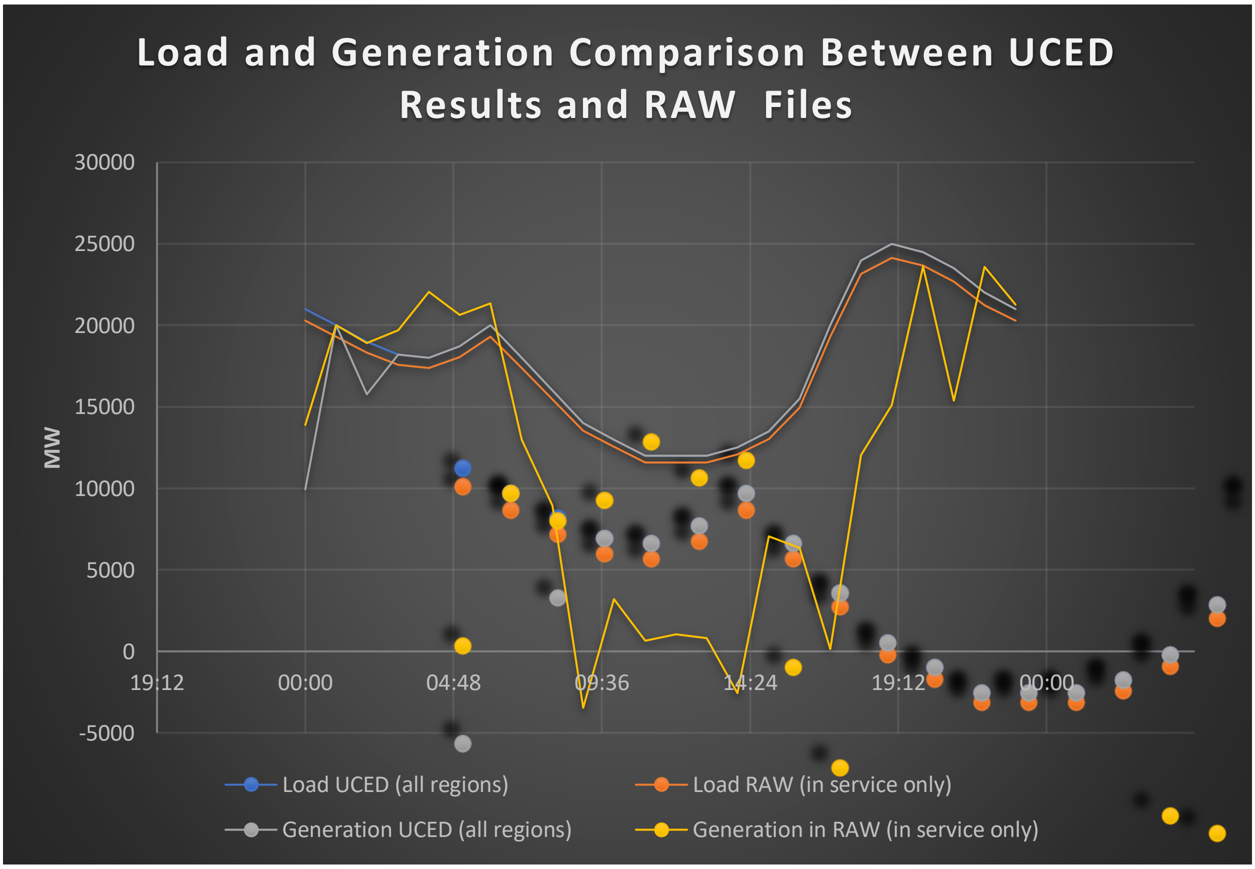

Figure 24: 24 hours of UCED results with load curtailment

Table 8: 24 hours result in tabular form

Hourly Case	AC feasible	Gen MW difference	Shunt MVAR difference
00:00	ACPF (NR) without Q limit	15,282.38 (110.04%)	256,628.93 (4914.12%)
01:00	ACPF (NR) without Q limit	9,381.83 (46.91%)	635,231.49 (12161.07%)
02:00	ACPF (NR) without Q limit	73.58 (0.30%)	2729.36 (0.67%)
03:00	ACPF (NR) without Q limit	6,972.93 (35.38%)	648,447.80 (12414.44%)
04:00	Infeasible problem	-	-
05:00	ACPF (NR) without Q limit	6,842.92 (33.18%)	613,964.18 (11754.26%)
06:00	ACOPF (AugL) with Q limit	7,297.54 (34.19%)	633,065.25 (12119.94%)
07:00	Infeasible problem	-	-

08:00	Infeasible problem	-	-
09:00	Infeasible problem	-	-
10:00	ACPF (NR) without Q limit	29.39 (0.16%)	2,666.65 (0.62%)
11:00	Infeasible problem	-	-
12:00	Infeasible problem	-	-
13:00	Infeasible problem	-	-
14:00	Infeasible problem	-	-
15:00	Infeasible problem	-	-
16:00	Infeasible problem	-	-
17:00	Infeasible problem	-	-
18:00	Infeasible problem	-	-
19:00	Infeasible problem	-	-
20:00	Infeasible problem	-	-
21:00	Infeasible problem	-	-
22:00	ACPF (NR) without Q limit	50.16 (0.19%)	2,722.09 (0.89%)
23:00	ACPF (NR) without Q limit	144.29 (0.54%)	3,995.39 (0.93%)

For many of the solved hours, significant generation redispatch and shunt MVAR support are required for the AC feasible solution. For the hours that are infeasible, the challenges may be due to:

1. **Uniform distribution of the demand**. UCED assumes the constant load distribution factors from the given case and distribute the total load MWs accordingly, whereas the actual loads likely are not uniform at each node during the day.
2. **Estimation on load MVAR consumptions**. The case building process assumes that all loads have constant power factors, which is unlikely as different types of loads will consume different MVARs through the day.
3. **Modelling on the voltage regulation devices such as shunts and transformers**. Although the transformers and shunts are modified from fixed to voltage regulating, the estimation on the regulation limits and initial values may need refinement.

3.3.6 Summary of findings

The UCED PCM combined with the GAT tool to build AC feasible cases is still promising but some issues remain to enable the process to be automated and consistently working for large networks such as the Synthetic NEM. The main issue is the translation of the UCED generation dispatch accurately to the units in the raw file must be fixed. Note that there doesn't seem to be a problem with the translation of the loads. There are also potentially other issues such as the setting the initial dispatch values to more reasonable (non-zero) values, however, they are certainly secondary issues.

The next steps should be to investigate the issue with the translation and ensure that the generation from the UCED is closely matched to the generation in the 24 hour raw files. The GAT case building process with redispatch and voltage control should be tested again and ensured that each hour converges. Once that is complete, any violations should be investigated with changes to controls or with the Voltage Control Area (VCA) tool. The unit commitment (UC)/economic dispatch (ED) uses a DC power flow model. AC optimal power flow (ACOPF) and contingency analysis (CA).

The process here showcases the challenges that may come up in applying the operating point dependent stability evaluation algorithm to large networks with high penetration of inverter resources. Although one can question the need to develop such algorithms to determine operating points, when other well established methods and processes exist, they are nevertheless important because an inverter device requires careful attention on its operating point due to the limited current headroom that may be available.

As more work is yet to be completed on this topic, the transient stability results in the next chapter do not consider an optimal development of commitment and dispatch but rather assumes that every resource is dispatched for every hour of the day, and just that the active power output is scaled based on the load. This assumption is suitable for the current year of this research effort but will have to re-visited in the next phase, if the project continues.

4. Determination of an analytical function to evaluate frequency characteristics of a device

Both grid-following and grid-forming inverters play an important role in the integration of renewable energy resources and battery storage systems into existing power systems. However, the stability and performance of these inverters significantly rely on their output impedance, which is a dynamic and continuously varying parameter influenced by various factors, including grid parameters and inverter operating points (P, Q, V).

This section illustrates first the white box models of IBRs that are employed to illustrate how the variations in the inverter operating point impacts its output impedance. Then, an in-depth analysis of how both grid parameters and inverter operating points affect the inverter output impedance is performed. Afterwards, the application of the inverter output impedance for stability assessment is also discussed. Finally, this section introduces two prediction algorithms that can estimate the inverter output impedance using only a few available datasets. The first technique is a data-driven approach, while the second approach is based on an analytical method. Subsequently, the application of this prediction method is showcased on an example network.

4.1 Development of analytical impedance models for black-box IBR model over many operating points

In this subsection, the admittance models of four kinds of grid-following inverters are sequentially derived. In addition, the correctness of these admittance models are verified using the time-domain step responses and frequency scanning. The obtained theoretical models will be the benchmark for further black-box-based impedance/admittance prediction.

4.1.1 Admittance Modelling of the Current-Controlled Grid-Following Inverters without considering effect of PLL

Figure 25(a) shows the block diagram of a typical LCL-filtered grid-following inverter equipped with the inner current control and synchronous reference frame phase-locked loop (SRF-PLL), of which the block diagrams are shown in Figure 25(b) and Figure 25(c), respectively. The inner current includes the dq-axis decoupling capability and the grid voltage proportional feed-forward with the coefficient β . In addition, the SRF-PLL tracks the grid frequency to provide the reference angle for current injection. The superscript c denotes that the variables are represented in the controller dq reference frame. The circuit and controller parameters of Figure 25 are listed in Table 9. The detailed derivation procedure of admittance model of the current-controlled grid-following inverters without considering PLL effect is shown in Appendix A.

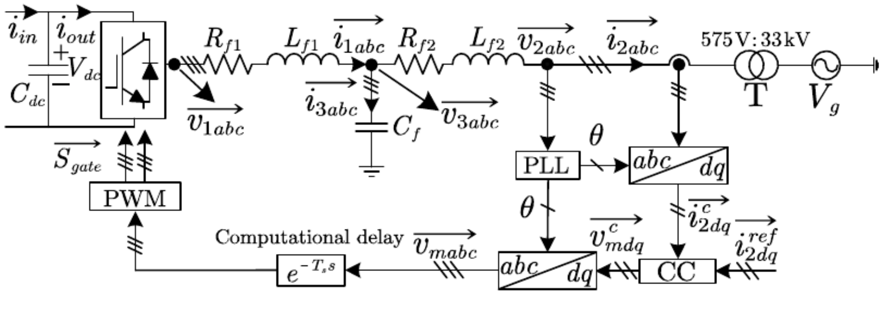

(a)

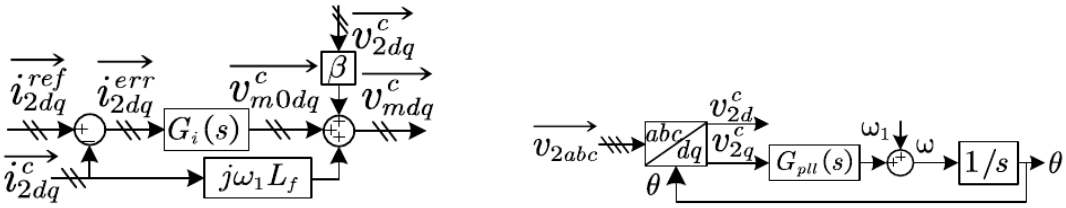

(b) (c)

Figure 25: The block diagrams of (a) the grid-following inverter with inner current control and SRF−PLL, (b) the inner current control, and (c) the SRF-PLL.

Table 9: Circuit and Controller Parameters of the GFLI

Parameter	Value	Parameter	Value
V_{dc}	1150 V	L_{f2}	250 μH
V_g	33 kV	C_f	50 μF
ω_1	100π rad/s	K_{pi}	$1.7391 \times 10^{-4}\ \Omega$
f_s	5.0 kHz	K_{ii}	$0.0348\ \Omega/s$
f_{sw}	5.0 kHz	K_{ppll}	20 rad/(Vs)
R_{f1}	3 mΩ	K_{ipll}	200 rad/(Vs^2)
L_{f1}	250 μH	β	0
R_{f2}	3 mΩ		

Figure 26 shows the time-domain comparison between the Matlab/Simulink benchmark model with the ideal PLL and the linearized 14th-order small-signal model derived in Appendix A for a step up of i_{2d}^{ref} from 3195 A to 3408 A at 10 s and a step up of i_{2q}^{ref} from 0 A to 426 A at 20 s. It can be seen that i_{2d}^{sim} and i_{2q}^{sim} of the simulation model highly agree with i_{2d}^{ssm} and i_{2q}^{ssm} of the derived small-signal model, which validates the correctness of the derived small-signal model in Appendix I-A.

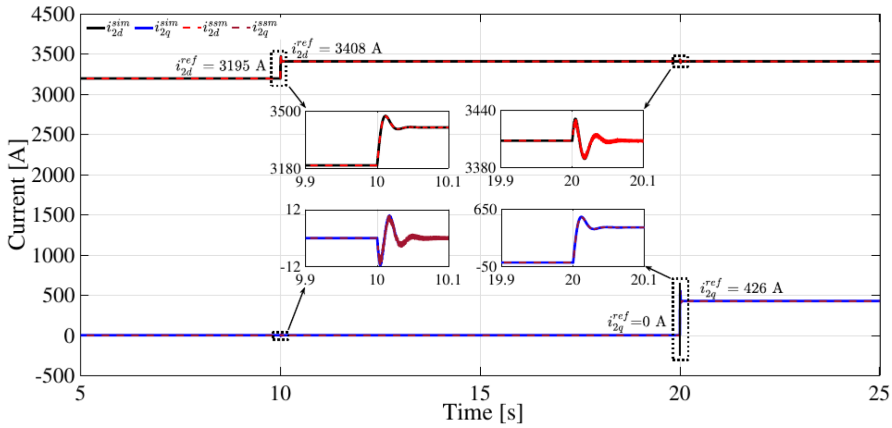

Figure 26: Time-domain verification of the derived state-space model of the current-controlled grid-following inverter.

Figure 27 plots the Bode diagrams of the dd-and qq-axis elements of $Y_{vsc1}$with the current reference point (3195 A, 0 A) and under three current controller configurations (K_{pi}, K_{ii}), i.e., $1.7391 \times 10^{-4}\ \Omega$, $3.4782 \times 10^{-2}\ \Omega/s$), ($8.6955 \times 10^{-4}\ \Omega$, $1.7391 \times 10^{-1}\ \Omega/s$), and ($1.7391 \times 10^{-3}\ \Omega$, $3.4782 \times 10^{-1}\ \Omega/s$). It can also be seen that the two admittance elements are the same, which results from the symmetric structure of the inner current control loop. In addition, the three measured admittance frequency responses (e.g., Y_{vsc1}^{mea1}, Y_{vsc1}^{mea2}, and Y_{vsc1}^{mea3}) agree with the three theoretical admittance frequency responses (e.g., Y_{vsc1}^{theo1}, Y_{vsc1}^{theo2}, and Y_{vsc1}^{theo3} very well, which validates the correctness of the derived input admittance model.

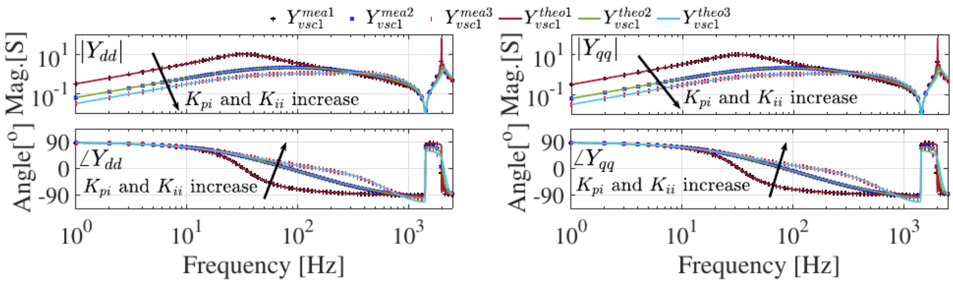

Figure 27: Frequency-domain verification of the derived admittance model of the current-controlled grid-following inverters without considering PLL effect.

4.1.2 Admittance Modelling of the Current-Controlled Grid-Following Inverters with Considering PLL Effect

The detailed derivation procedure of admittance model of the current-controlled grid-following inverters with considering PLL effect is shown in Appendix B. The extensive simulation results show that the grid-following inverters considering PLL effect has the same time-domain transient behaviour as that of the grid-following inverters without considering PLL effect shown in Figure 26, which results from the fact that the grid-following inverter is connected to the ideal voltage source, and the PLL dynamic is inactivated. The time-domain verification of the grid-following inverter considering PLL effect is thus not provided for brevity.

Figure 28(a) plots the Bode diagrams of the dd-and qq-axis elements of Y_{vsc2} with (K_{ppll}, K_{ipll}) as (20 $rad/(Vs)$, 200 $rad/(Vs^2)$) and under three current reference points $(i_{2d}^{ref}, i_{2q}^{ref})$, i.e., (3195 A, 0 A), (1065 A, 0 A), and (3195 A, -2132 A). Furthermore, Figure 28(b) plots the Bode diagrams of the dd-and qq-axis elements of Y_{vsc2} with the current reference point $(i_{2d}^{ref}, i_{2q}^{ref})$as (3195 A, 0 A) and under three PLL controller configurations (K_{ppll}, K_{ipll}), i.e., (20 $rad/(Vs)$, 200 $rad/(Vs)$), (40 $rad/(Vs)$, 800 rad/(Vs^2)), and (60 $rad/(Vs)$, 1800 rad/(Vs^2)). Only the dd- and qq-axis admittance Bode plots are shown for simplicity, since the stability is dominated by them. It can be seen that the measured admittance frequency responses (e.g., Y_{vsc2}^{mea1}-Y_{vsc2}^{mea5}) obtained using the frequency scanning in the Matlab\Simulink software agree with the theoretical admittance frequency responses (e.g., Y_{vsc2}^{theo1}-Y_{vsc2}^{theo5}) very well, which validates the correctness of the derived input admittance model.

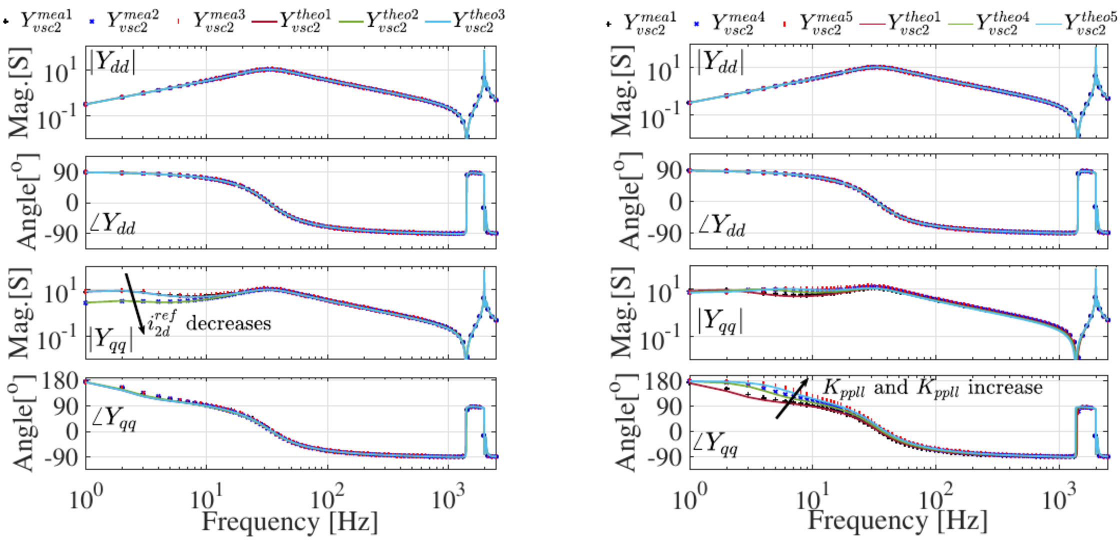

(a) (b)

Figure 28: Frequency-domain verification of the derived small-signal model considering PLL effect by changing (a) current reference point and (b) PLL parameters.

4.1.3 Admittance Modelling of the Power-Controlled Grid-Following Inverters

Figure 29 and Figure 30 show the block diagram of the closed-loop active power control and closed-loop reactive power control, respectively. The derivations of their small-signal models are shown in Appendix C. By combining the small-signal models of the closed-loop active power control, closed-loop reactive power control, and that of the grid-following inverters considering the PLL dynamic, the small-signal model of the power-controlled grid-following inverters can be derived as shown in Appendix C.

(a) (b)

Figure 29: The (a) block diagram and (b) state-space model of the closed-loop active power control.

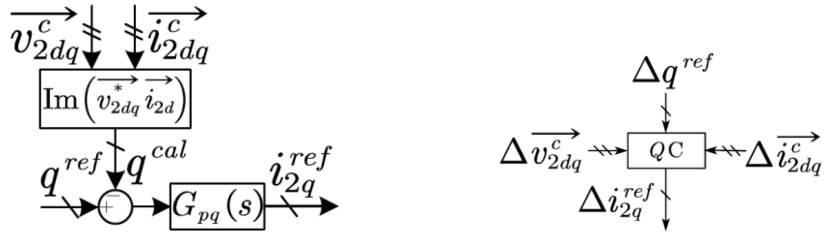

(a) (b)

Figure 30: The (a) block diagram and (b) state-space model of the closed-loop reactive power control.

Figure 31 shows the time-domain comparison between the Matlab/Simulink benchmark model and the linearized 18th-order small-signal model for a step up of p^{ref} from 1.5 MW to 1.6 MW at 10 s and a step up of q^{ref} from 0 MVar to 0.2 MVar at 20 s. It can be seen that i_{2d}^{sim} and i_{2q}^{sim} of the simulation model highly agree with i_{2d}^{ssm} and i_{2q}^{ssm} of the derived small-signal model, which validates the correctness of the derived small-signal model.

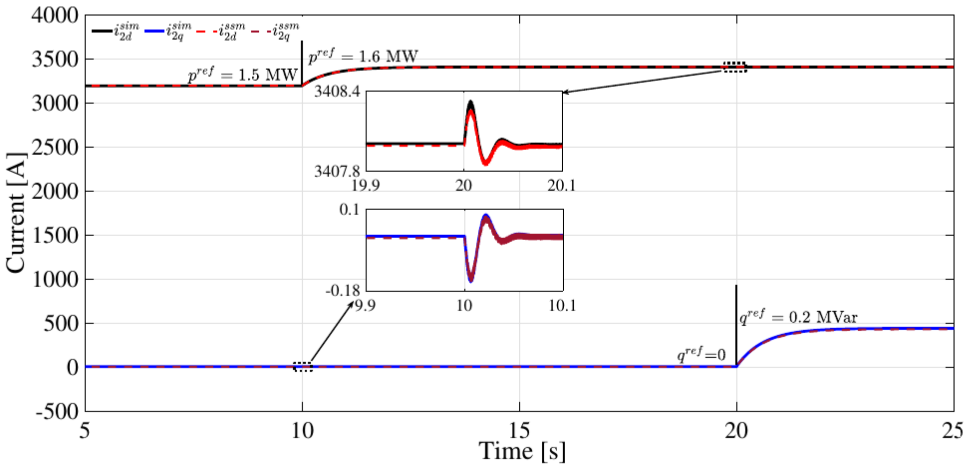

Figure 31: Time-domain verification of the derived state-space model of the power-controlled grid-following inverter.

Figure 32(a) plots the Bode diagrams of the dd-and qq-axis elements of Y_{vsc6} with (K_{ppq}, K_{ipq}) as (1.7391 × 10^{-5} A/W, 3.4782 × 10^{-3} $A/(Ws)$) and under three power reference points (p^{ref}, q^{ref}), i.e., (1.5 MW, 0 MVar), (0.5 MW, 0 Mvar), and (1.5 MW, -1.0 MVar). Furthermore, Figure 32(b) plots the Bode diagrams of the dd-and qq-axis elements of Y_{vsc6} with (p^{ref}, q^{ref}) as (1.5 MW, 0 Mvar) and under three power controller configurations (K_{ppq}, K_{ipq}), i.e., (1.7391 × 10^{-5} A/W, 3.4782 × 10^{-3} $A/(Ws)$), (1.1594 × 10^{-5} A/W, 2.3188 × 10^{-3} $A/(Ws)$), and (8.6955 × 10^{-6} $A/$

W, 1.7391×10^{-3} $A/(Ws)$). It can be seen that the measured admittance frequency responses (e.g., Y_{vsc6}^{mea1}-Y_{vsc6}^{mea5}) agree with the theoretical admittance frequency responses (e.g., Y_{vsc6}^{theo1}-Y_{vsc6}^{theo5}) very well, which validates the correctness of the derived input admittance model.

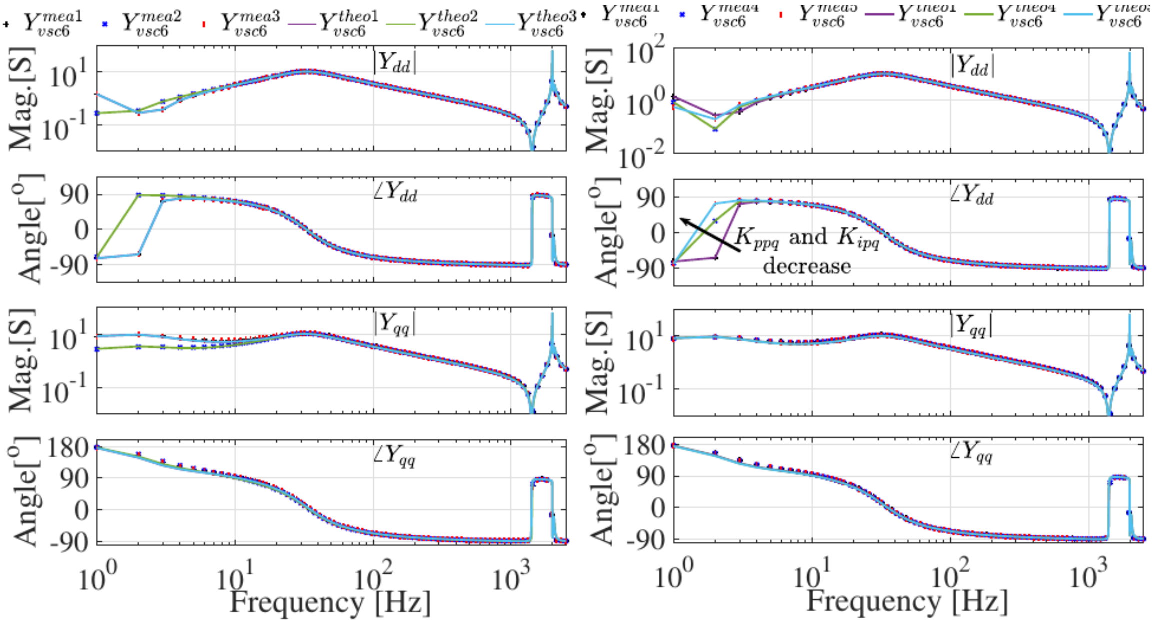

(a) (b)

Figure 32: Frequency-domain verification of the derived small-signal model of the closed-loop power-controlled grid-following inverter by changing (a) power reference point and (b) power controller parameters.

4.1.4 Admittance Modelling of the Voltage-Controlled Grid-Following Inverters

Figure 33 and Figure 34 show the block diagram of the dc-link voltage control and PCC voltage control, respectively. The derivations of their small-signal models are shown in Appendix D. By combining the small-signal models of the dc-link voltage control, PCC voltage control, and that of the grid-following inverters considering the PLL dynamic, the small-signal model of the voltage-controlled grid-following inverters can be derived as shown in Appendix D.

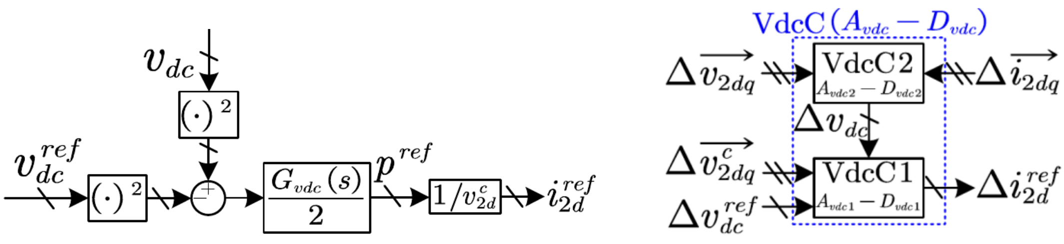

(a) (b)

Figure 33: The (a) block diagram and (b) small-signal model of the dc-link voltage control.

(a) (b)

Figure 34: The (a) block diagram and (b) small-signal model of the PCC voltage control.

4.2 Impacts of grid impedance on PCC voltage profile

Various grid parameters, such as V_{pcc}, δ_{pcc} , SCR, and X_g/R_g, have a significant impact on the inverter output impedance profile. For instance, in a strong grid, the sensitivity of voltage to change in current injection is low, whereas for a weak grid with high grid impedance, the sensitivity is high. To quantify the changes in V_{pcc} and δ_{pcc}, the power equations are used to derive mathematical expressions for these parameters as functions of the inverter operating point and the grid parameters. Thereafter, steady-state analysis is carried out, as explained below. The power flow from the inverter, which connects the PCC to the grid, is mathematically expressed in (1) for the two-bus system shown in Figure 35.

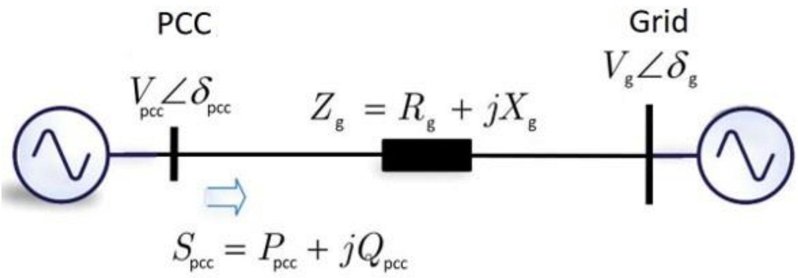

Figure 35: Two bus system

$$S_{pcc} = V_{pcc}e^{\delta_{pcc}}(I_{pcc}e^{\delta_{i-pcc}})^* \tag{1}$$

Where S_{pcc} is the apparent power, V_{pcc} is the magnitude of the PCC voltage, Ipcc is the magnitude of the PCC current, and δ_{pcc} and $\delta_{i-pcc}$are the angles for the voltage and current at the PCC.

From Equation (1), the voltage magnitude and angle at the PCC can be expressed as a function of the grid parameters and the inverter operating point.

$$V_{pcc} = \sqrt{\frac{(-V_g{}^2 - 2\alpha) \pm \sqrt{(-V_g{}^2 - 2\alpha)^2 - 4(\alpha^2 + \beta^2)}}{2}} \tag{2}$$

$$\delta_{pcc} = sin^{-1}(\frac{P_{pcc}X_g - Q_{pcc}R_g}{V_{pcc}V_g}) \tag{3}$$

In which:

$$\alpha = P_{pcc}R_g + Q_{pcc}X_g;\ \beta = P_{pcc}X_g + Q_{pcc}R_g \tag{4}$$

A comprehensive study on the operation of grid-connected inverters under different conditions is conducted. The objective of this study is to investigate the variation of the voltage magnitude and angle at the Point of Common Coupling (PCC) under different grid strengths (strong and weak) and types (inductive and resistive). The steady-state analysis is being conducted under two scenarios: fixed inverter operating point at nominal power and variations in the inverter operating point. Multiple tests are being performed to assess the impact of grid type and strength on the PCC voltage magnitude and angle.

In Figure 36, the comparison between V_{pcc} and δ_{pcc} is shown for three sets in a strong grid with SCR=10, where X_g/R_g is equal to 7, 3, and 1. The results show that V_{pcc} falls within the range of 0.93 p.u. and 1.08 p.u. The Australian standards specify voltage limits of +10% and -6%. Moreover, δ_{pcc} varies between -0.5 and 5 degrees for X_g/R_g=7 and between -2.2 and 5.6 degrees for X_g/R_g =1.

Likewise, in Figure 37, the comparison between V_{pcc} and δ_{pcc} is presented for three sets in a weak grid with SCR=3, with X_g/R_g ratios identical to those in the previous scenario. The results clearly show that V_{pcc} varies significantly, exceeding both the upper and lower voltage limits. The study also revealed that the angle of the PCC voltage varied significantly in weak grids, particularly those with inductive properties. For instance, δ_{pcc} varied remarkably to around 25 degrees for X_g/R_g=7.

For each case study shown in Figure 36 and Figure 37, it is clear that changing the inverter operating points has a significant impact on the PCC voltage magnitude and angle. The results indicate that, for a particular grid strength and type, variations in the active and reactive power outputs of the inverter have a significant effect on the PCC voltage magnitude and angle. For instance, Figure 37 illustrates the correlation between the PCC voltage magnitude and angle and different operating points for a weak grid scenario with the SCR= 3 and X_g/R_g= 7.

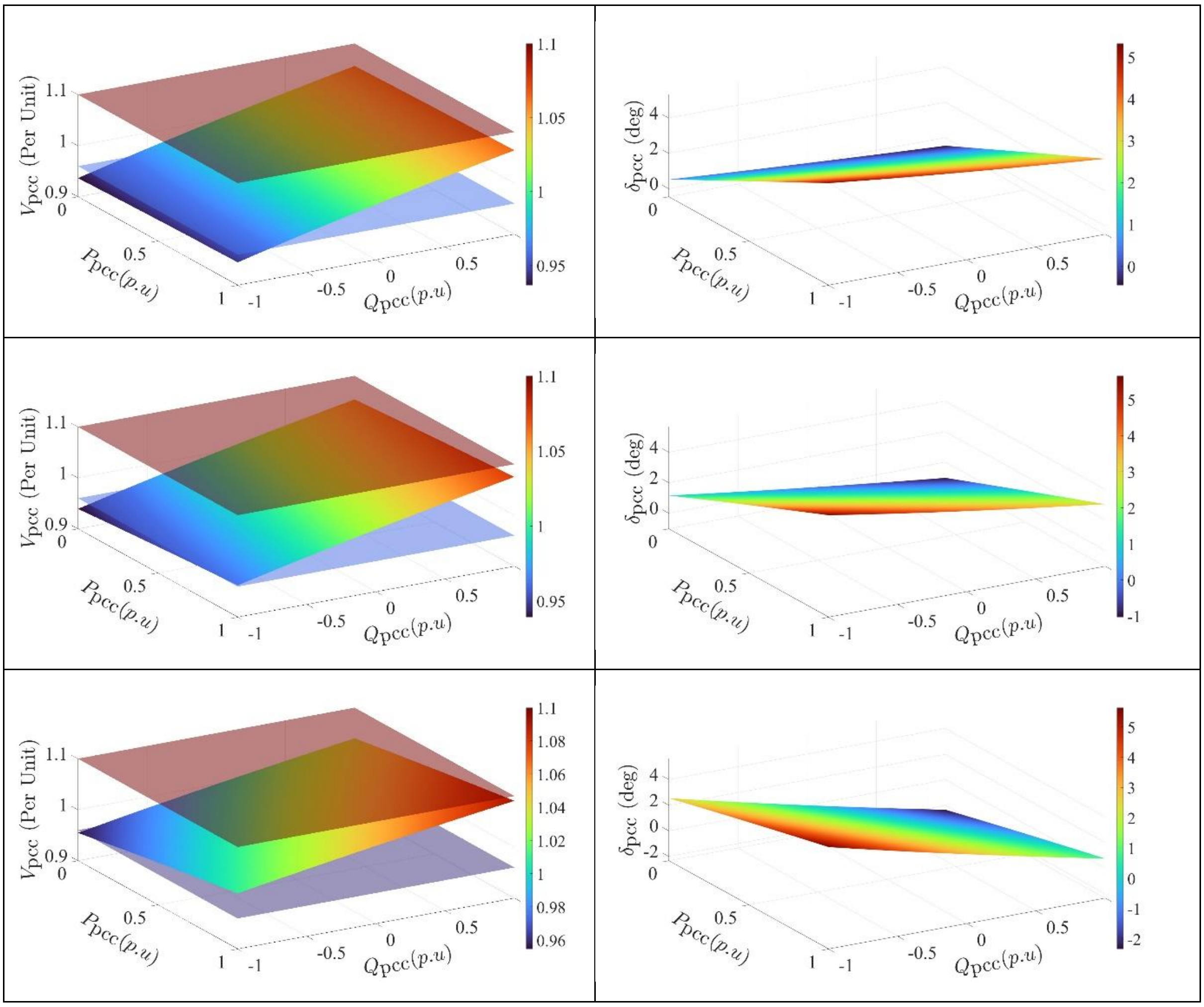

Figure 36: PCC voltage magnitude and angle when the inverter operating points is varied from 0 to 1 p.u. for active power and -1 to 1 p.u. for reactive power in a strong grid condition with SCR=10: (top) X_g/R_g=7, (middle) X_g/R_g=3, (bottom) X_g/R_g=1.

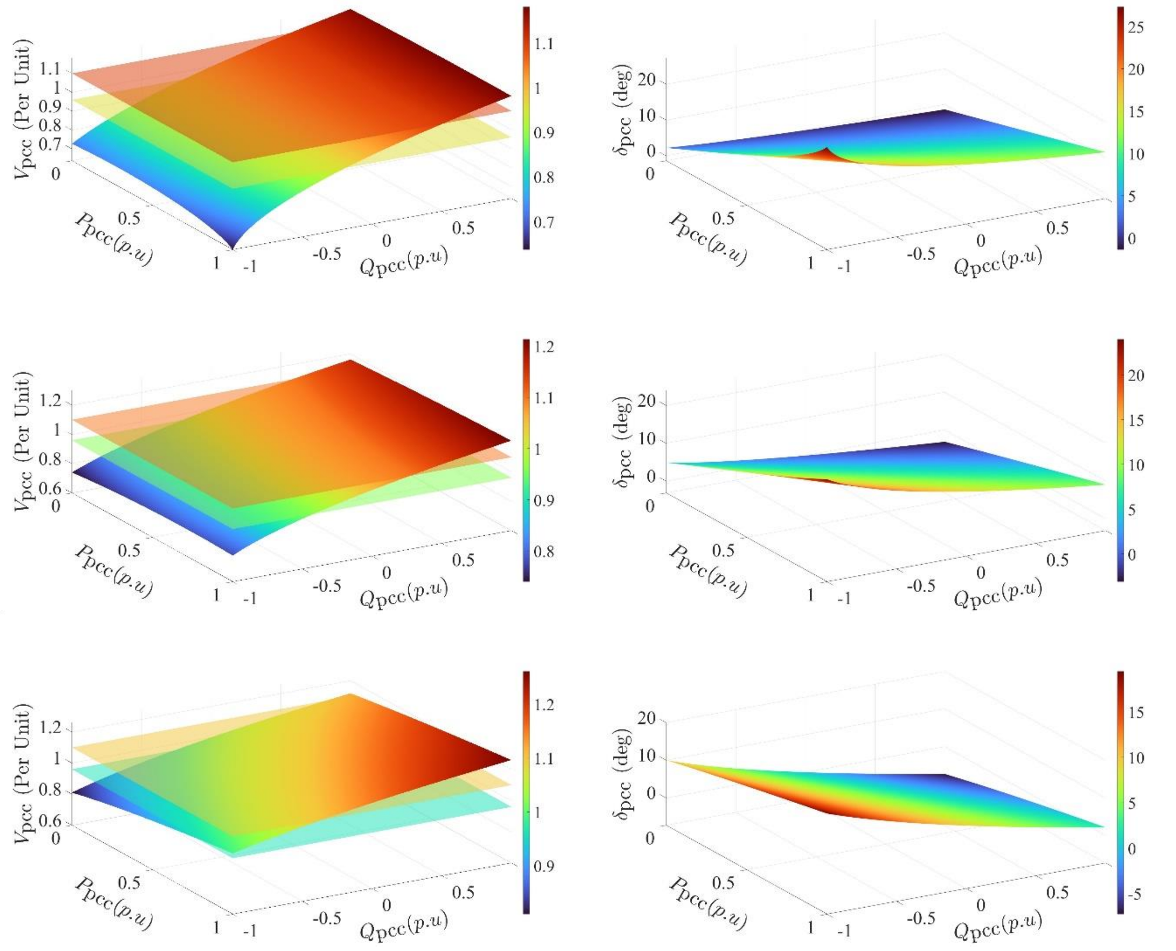

Figure 37: PCC voltage magnitude and angle when the inverter operating points is varied from 0 to 1 p.u. for active power and -1 to 1 p.u. for reactive power in a weak grid condition with SCR=3: (top) X_g/R_g=7, (middle) X_g/R_g=3, (bottom) X_g/R_g=1.

4.3 Impact of the IBRs operating point on its frequency domain characteristics and stability

In the previous section, the impact of the grid parameters on the PCC voltage was studied. This section evaluates the impacts of the variations of the inverter operating point on its output impedance in the dq reference frame. The study deploys the derived white box small-signal model of the grid-connected inverter with outer active-reactive power control using, presented previously in Section 4.1. The inverter performance was evaluated in both the frequency and time domain to assess conditions that could lead to instability. The conditions tested included variations in power reference commands and grid strength. The frequency domain analysis was performed using the Generalized Nyquist Criterion (GNC) to predict instability, and the Bode plot was used to identify low-frequency oscillations and calculate stability margins.

The inverter's output impedances were derived in the synchronous (dq) reference frame from the white box state-space model. A thorough analysis was conducted to investigate the effect of variations in the inverter operating point (P_{ref}, Q_{ref}) on the trajectory of its dq impedances. In the first test, P_{ref} was changed from 0.25 to 1 p.u. while keeping Q_{ref} at zero. In the second test, P_{ref} was set to its nominal value (1 p.u.) and Q_{ref} was varied from 0 to 1 p.u.

The results from the first and second tests are depicted in Figure 38 and Figure 39, respectively. It is evident that changes in both P_{ref} and Q_{ref} have an impact on the impedance trajectory in the low-frequency range. The magnitude of the coupling dq impedances is very small in the low-frequency range when only active power is injected (Q_{ref} =0). Figure 38 shows the inverter output impedance in the dq reference frame as P_{ref} varies from 0.25 to 1 p.u. It is noticeable that under extremely weak grid conditions, the inverter is prone to instability due to limited stability margins at low frequency range. When the phase margin exceeds 180 degrees, the IBR becomes unstable. Furthermore, Figure 39(d) shows that increasing the injection of reactive power will improve the phase of the inverter impedance at the q-axis, thus enhancing the stability margins of the inverters.

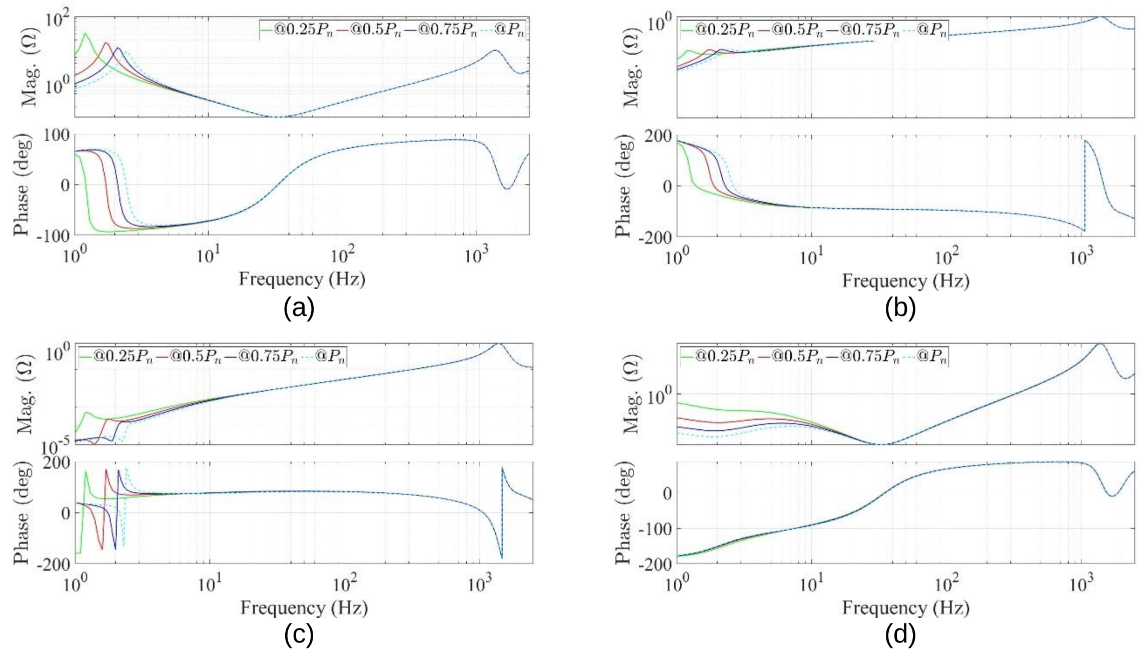

Figure 38: Impacts of the variations of the Inverter operating point P_{ref} (when $Q_{ref} = 0$) on: (a) Z_{dd} , (b) Z_{dq} (c) Z_{qd} , and (d) Z_{qq}

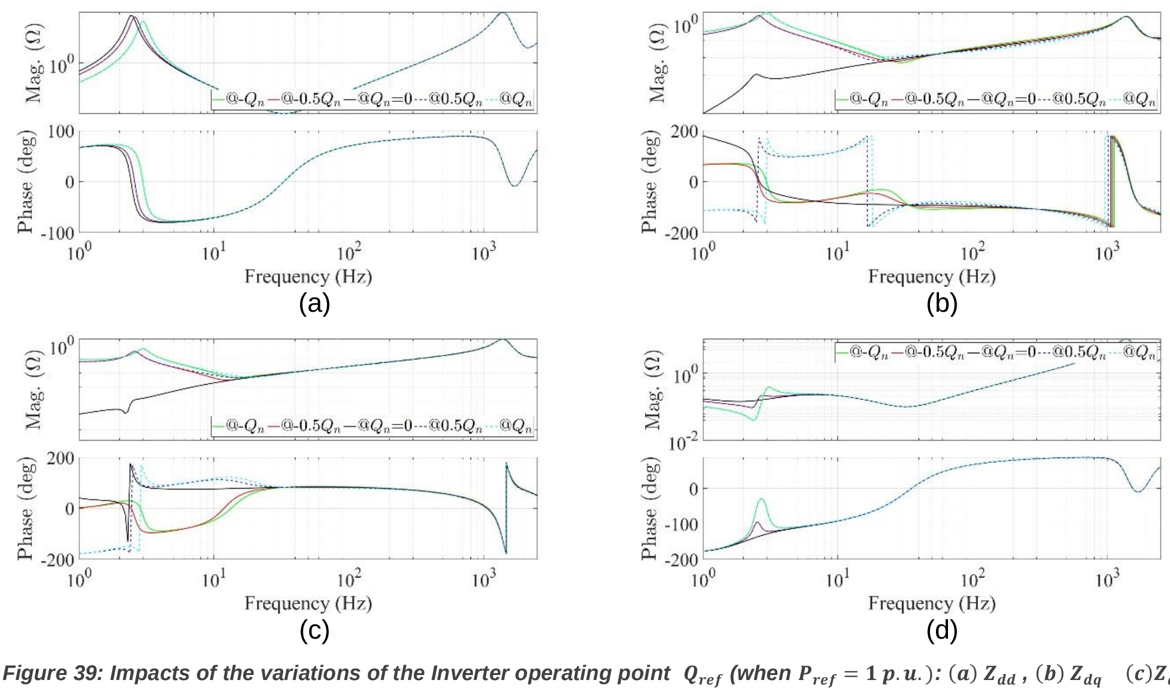

Figure 39: Impacts of the variations of the Inverter operating point Q_{ref} (when $P_{ref} = 1\ p.u.$): (a) Z_{dd} , (b) Z_{dq} (c) Z_{qd} , and (d) Z_{qq}

Figure 40 illustrates the stability analysis based on the GNC in the q-axis using impedance for all three grid conditions (strong, weak, and very weak). The Nyquist plots do not encircle the critical point (-1, 0), implying that the inverter operation will be stable in strong and weak grids. However, the inverter will be unstable when connected to a very weak grid. This frequency domain finding is further supported by the EMT modeling of the power-controlled GFLI in the time domain, as shown in Figure 41. The results reveal that the inverter is stable only in strong and weak grids (Cases#1 and #2), but unstable in the very weak grid (Case#3).

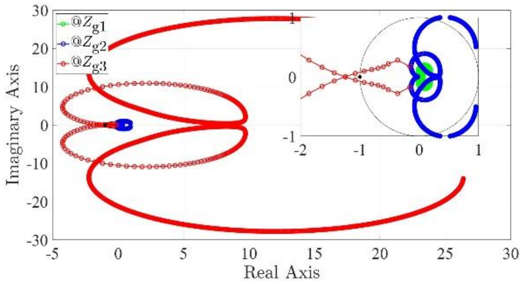

Figure 40: Frequency domain analysis using Nyquist plot at the q-axis showing the impact of grid strength on the GFLI operation

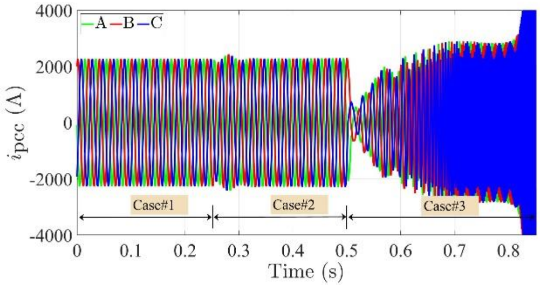

Figure 41: Time domain verification of the impact of grid strength on the GFLI operation

4.4 Inverter Output Admittance/Impedance Estimation at Arbitrary Operating Point Based on A Few Available Admittance Data Points

4.4.1 Impedance Estimation of IBRs Based on Data-Driven Method

In recent years, data-driven modelling has emerged as a powerful technique for modelling complex systems, particularly those that exhibit time-varying behaviour. Considering the various control configurations of IBRs and the infinite operating points that present a unique set of challenges, data-driven modelling can provide insights without the need to derive analytical models. By leveraging large datasets and advanced machine learning algorithms, data-driven models can capture the dynamic behaviour of time-varying characteristics of the IBRs, from $Z_{dd}$to Z_{qq}. This section introduces the use of a data-driven modeling technique called Gaussian Process Regression (GPR) to predict the IBRs' output impedances at any operating point vector (P, Q, Vpcc) based on the trained GPR model.

Using GPR as a data driven modelling approach offers several advantages. The non-parametric nature of this approach allows for great adaptability across various datasets. By utilizing kernel functions, it can accurately estimate values even when dealing with limited data samples. Additionally, the use of a Bayesian framework ensures that results are robust and reliable, accounting for both estimation error and sampling errors. As a preferred method for prediction tasks, this approach offers a representation of uncertainty and is highly adaptable, making it an ideal choice for a wide range of applications [29] [30].

Considering the training dataset S, which comprises N observations represented by (xi, yi), where xi and yi are 1xN input and output vectors, respectively. To predict the output for a new set of input covariates, the GPR model is utilized as follows:

$$y = h(x)^T \beta + f(x) \tag{4.1}$$

In which

$$f(x) \sim GP(0, k(x, x')) \tag{4.2}$$

The function h(x) represents the basis function for the covariates, while β is the vector of coefficients for the basis function. The latent function, denoted by f(x), has a Gaussian process with a zero mean and an identical distribution. The covariance function k(x,x') is used to describe the similarity between the observed data.
To predict the output at any given instance using the GPR model, the training process is performed first. After the GPR model is trained, the predicted output y can be obtained using the following equation:

$$P(y_i | f(x_i), x_i) \sim N(y_i | h(x_i)^T \beta + f(x_i), \sigma^2) \tag{4.3}$$

The GPR model incorporates a noise variance, denoted by σ^2, and a standard deviation, denoted by σ.

To take advantage of GPR's ability to work well with small data sets, the GPR model is trained using only 30 data sets in this work. The inverter operating points (P, Q, V) are used as inputs, while the inverter output impedances (Zdd, Zdq, Zqd, Zqq) are used as outputs. Figure 42, Figure 43, Figure 44 show the predicted output impedances of a current-controlled grid following inverter, a power-controlled grid following inverter, and a virtual synchronous generator-based grid forming inverter, respectively. Additionally, the predicted impedances in the dq reference frame for the arbitrary operation point [Pref = 0.51 p.u, Qref = 0 p.u, Vpcc= 1 p.u] are compared with the true values obtained from the analytical models.
Overall, the data-driven impedance prediction algorithm provides accurate predictions for the grid following and forming inverters, as shown in the figures. However, it is clear from figures that the predicted impedance does not always match well with the analytical solution in certain cases. This can be attributed to two primary reasons. Firstly, the high impedance dynamic of this type of controller, known as outer power control, at low frequencies makes it highly sensitive to changes in the operating point. Secondly, since only 30 operating points are used for training, the accuracy of the prediction algorithm can be improved by expanding the training data set.

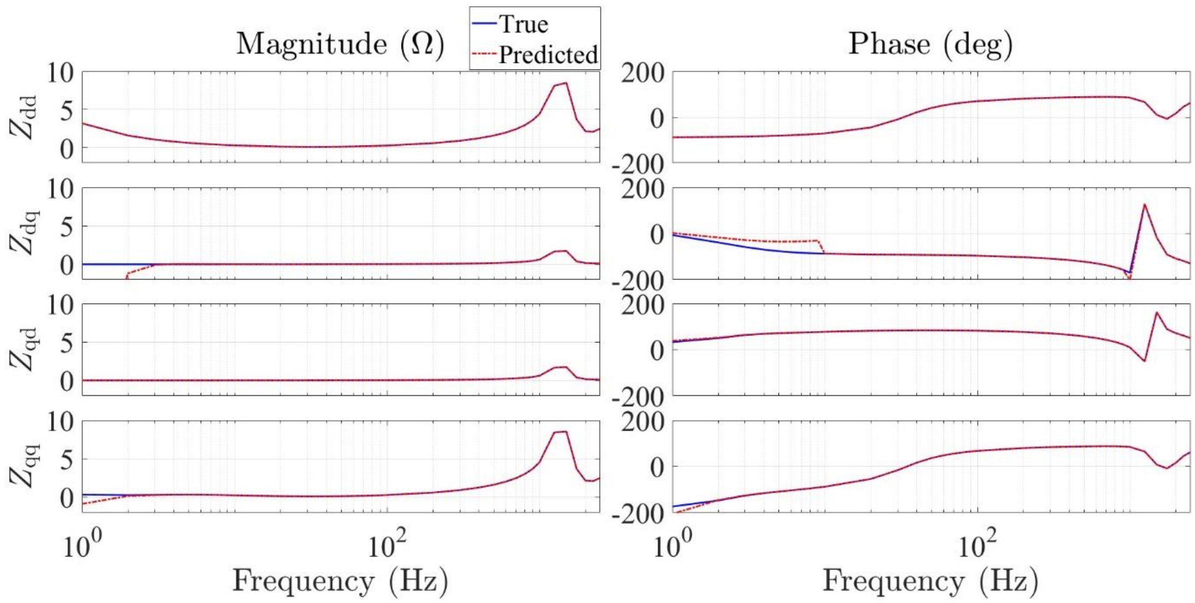

Figure 42: The prediction results for the output impedance of a current-controlled grid-following inverter using a data-driven approach. The results correspond to an arbitrary operating point with P_{ref} = 0.51 p.u, Q_{ref} = 0, and V_{pcc}= 1.p.u.

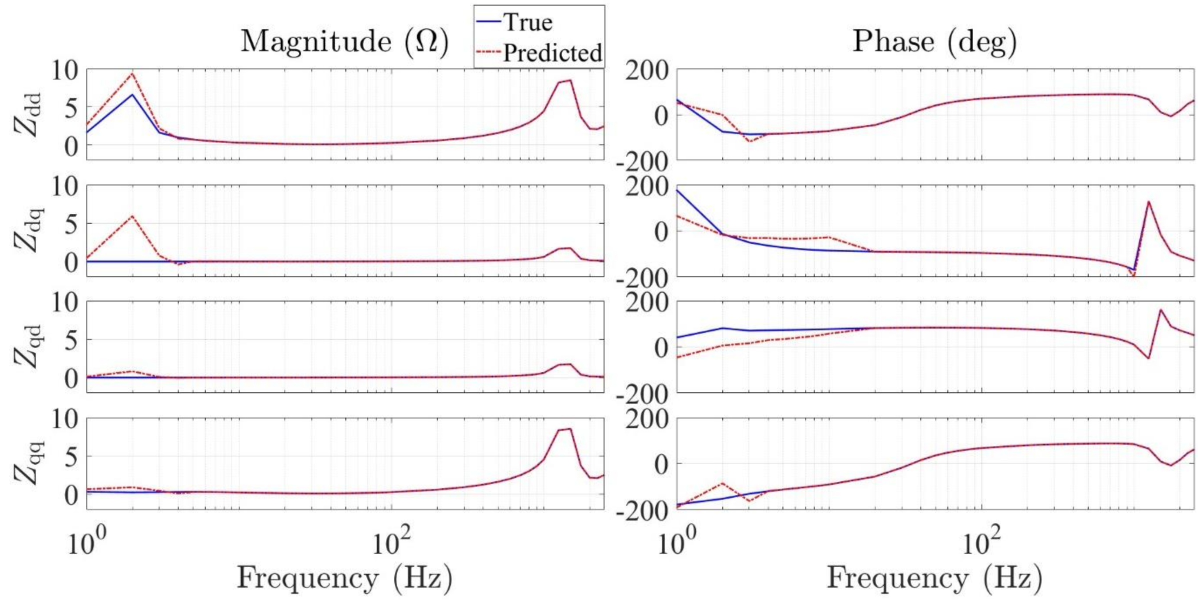

Figure 43: The prediction results for the output impedance of a power-controlled grid-following inverter using a data-driven approach. The results correspond to an arbitrary operating point with P_{ref} = 0.51 p.u, Q_{ref} = 0, and V_{pcc}= 1.p.u.

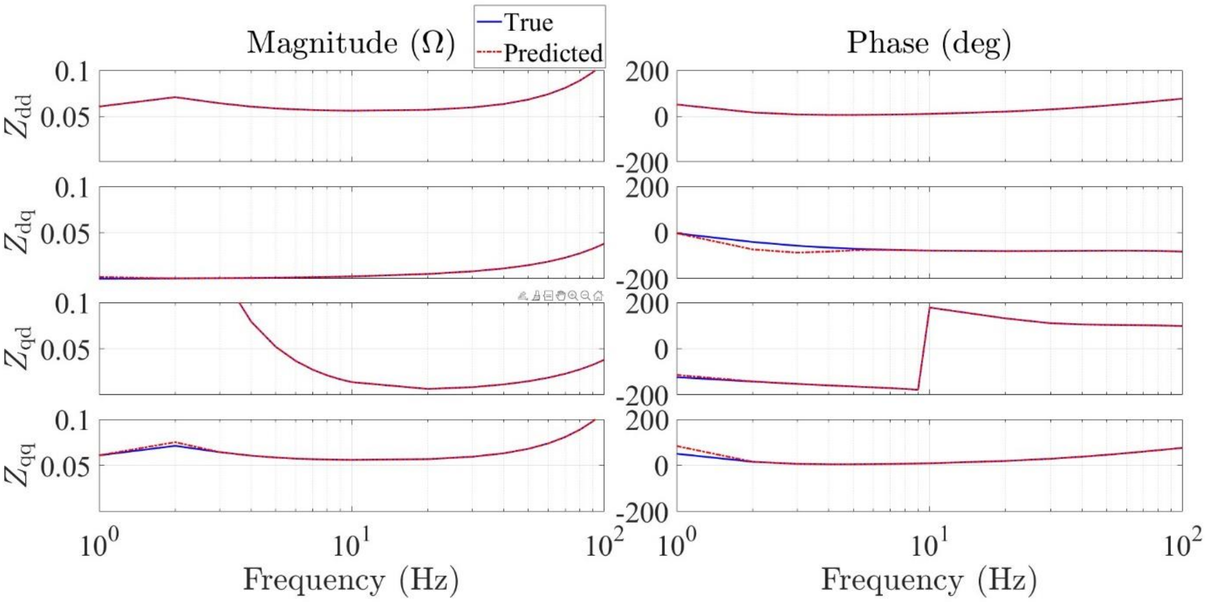

Figure 44: The prediction results for the output impedance of a VSG-based grid-forming inverter using a data-driven approach. The results correspond to an arbitrary operating point with P_{ref} = 0.51 p.u, Q_{ref} = 0, and V_{pcc}= 1.p.u.

4.4.2 Admittance Estimation Based on Analytical Models

Based on the analytical admittance models derived in Section 4.1, the admittance of the grid-following inverters at arbitrary operating points can be estimated based on a few available admittance data points. The admittance estimation is inspired by [31], where detailed algorithm derivation and implementation can be found.

To verify the admittance estimation method, the admittance data at 1 Hz intervals for arbitrary operating point is estimated. Since the qq-axis admittance is most important for PLL-based grid-following inverters' stability, it is taken as an example. Seven qq-axis 1-Hz admittance data of current-, voltage-, and power-controlled grid-following inverters are calculated using the derived white-box models in Section 4.1 and listed at the top of Table 2. V_d, I_d, and I_q are limited within [0.9,1.1], [0,1.0], and [-1.0,1.0] p.u., respectively, constrained by 1.0 p.u. power capacity. The qq-axis 1-Hz admittance data at four operating points @1-@4 are estimated and listed at the middle of Table 10, which agree with the theoretical admittance data listed at the bottom of Table 10. Figure 45(a)/(b),

Figure 46(a)/(b), and Figure 47(a)/(b) further show that 2-, 5-, 10-, 40-, and 100-Hz qq/dd-axis admittance data at the four operating points are successfully predicted for the current-, voltage-, and power-controlled grid-following inverter, respectively.

Table 10: Implementation Results on the QQ-Axis 1-Hz Admittance Data

(V_d, I_d, I_q) (p.u.)	#1 GFLI1	#2 GFLI	#3 GFLI	#4 GFMI
Seven available qq-axis 1-Hz admittance data				
$(0.92, 0.1, 0.6)$	$1.08\angle 183.80$	$1.25\angle 174.92$	$1.26\angle 177.91$	$4.13\angle -107.67$
$(0.93, 0.2, 0.5)$	$2.07\angle 181.86$	$2.43\angle 173.45$	$2.45\angle 176.32$	$5.10\angle -112.30$
$(0.95, 0.3, -0.4)$	$3.01\angle 181.20$	$3.52\angle 173.12$	$3.57\angle 175.96$	$7.18\angle 75.33$
$(0.97, 0.4, -0.3)$	$3.90\angle 180.87$	$4.57\angle 173.04$	$4.62\angle 175.86$	$9.46\angle 67.22$
$(1.03, 0.5, 0.2)$	$4.58\angle 180.70$	$5.31\angle 173.41$	$5.37\angle 176.23$	$9.07\angle -101.35$
$(1.05, 0.7, -0.2)$	$6.26\angle 180.44$	$7.25\angle 173.39$	$7.34\angle 176.20$	$12.88\angle 58.31$
$(1.08, 0.9, 0.1)$	$7.81\angle 180.31$	$9.00\angle 173.51$	$9.11\angle 176.32$	$12.19\angle -89.65$
Four predicted qq-axis 1-Hz admittance data				
@1$(1.00, 0.3, 0.3)$	$2.86\angle 181.28$	$3.32\angle 173.59$	$3.35\angle 176.44$	$6.98\angle -105.34$
@2$(1.10, 0.3, 0.3)$	$2.61\angle 181.43$	$2.96\angle 174.40$	$2.99\angle 177.25$	$6.51\angle -106.52$
@3$(1.00, 0.6, 0.3)$	$5.64\angle 180.52$	$6.59\angle 173.04$	$6.67\angle 175.85$	$8.27\angle -117.21$
@4$(1.00, 0.3, 0.6)$	$2.86\angle 181.28$	$3.32\angle 173.59$	$3.35\angle 176.44$	$4.81\angle -125.10$
Four theoretical qq-axis 1-Hz admittance data at the predicted operating points				
@1$(1.00, 0.3, 0.3)$	$2.86\angle 181.28$	$3.32\angle 173.59$	$3.35\angle 176.44$	$6.98\angle -105.34$
@2$(1.10, 0.3, 0.3)$	$2.61\angle 181.43$	$2.96\angle 174.40$	$2.99\angle 177.25$	$6.51\angle -106.52$
@3$(1.00, 0.6, 0.3)$	$5.64\angle 180.52$	$6.59\angle 173.04$	$6.67\angle 175.85$	$8.27\angle -117.21$
@4$(1.00, 0.3, 0.6)$	$2.86\angle 181.28$	$3.32\angle 173.59$	$3.35\angle 176.44$	$4.81\angle -125.10$

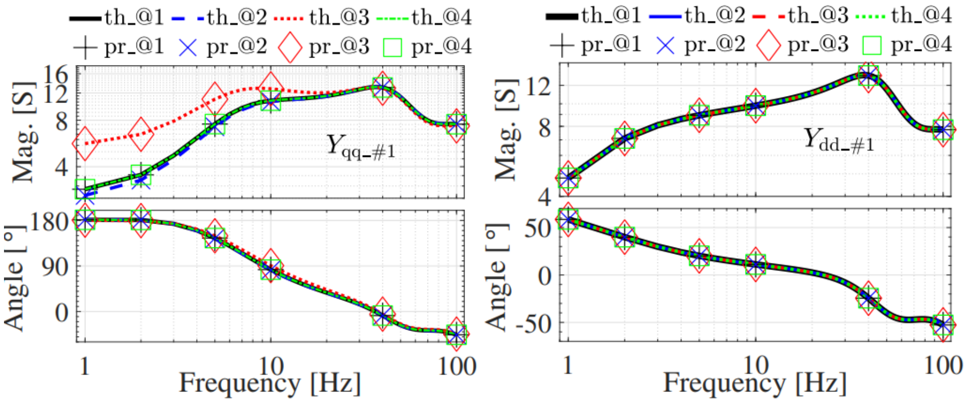

(a) (b)

Figure 45: Estimation of (a) qq- and (b) dd-axis admittance of current-controlled grid-following inverter with considering PLL effects.

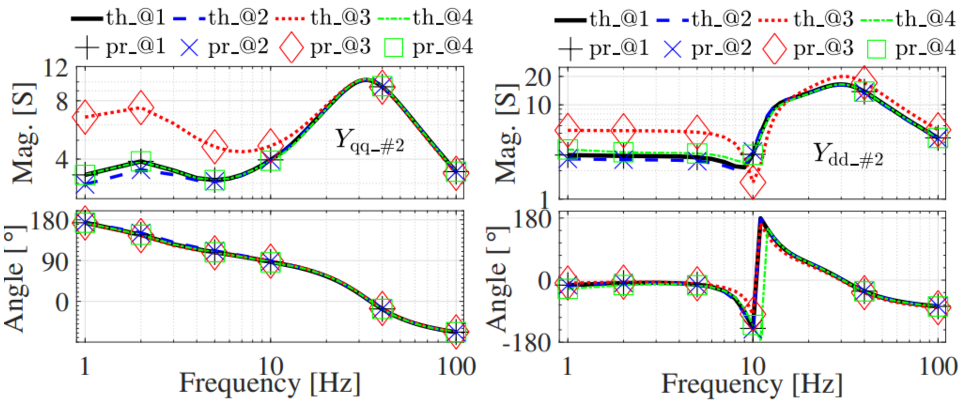

(a) (b)

Figure 46: Estimation of (a) qq- and (b) dd-axis admittance of voltage-controlled grid-following inverter.

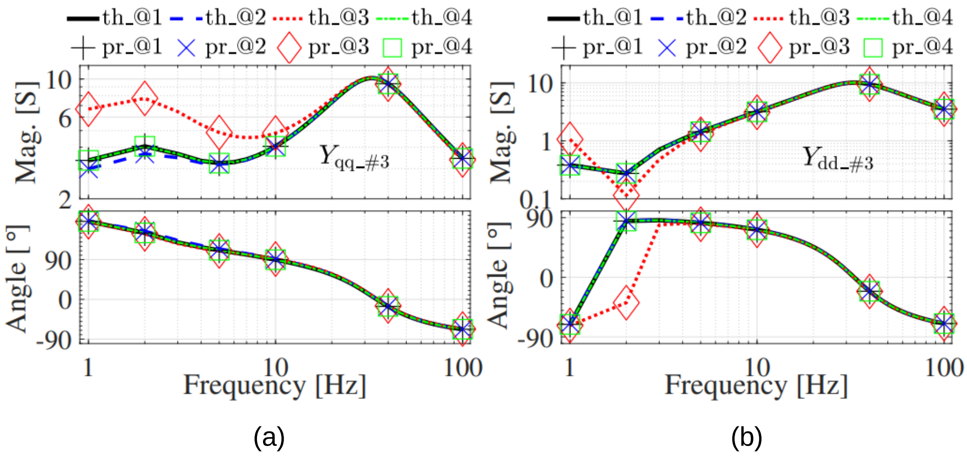

Figure 47: Estimation of (a) qq- and (b) dd-axis admittance of power-controlled grid-following inverter.

5. Application of the Vector Fitting Algorithm on the Estimated Admittance of the IBR for Eigenvalue Analysis

State-space model-based eigenvalues analysis method has been widely used to analyse stability issue of power electronics-dominated power systems. One important advantage of it is to perform participation factor analysis, so oscillation source can be identified. However, the derivation procedure of state-space is complicated for large-scale power systems. Furthermore, it's not easy to obtain system state-space model due to unknown internal structure and parameters. An incremental state space modelling method of power electronics-fed power system based on measured components impedance matrices on local dq frames is proposed here. Terminal impedance frequency responses of all components are first measured at few select operating points by frequency scanning method on local dq frames. Then, the impedance at any particular operating is predicted using the approaches presented in the previous chapter. Subsequently, state-space models of all components are fitted according to the predicted dq impedance matrices by a matrix fitting algorithm. Finally, state-space model series operator and parallel operator are used to aggregate the fitted components state-space models in a recursive way. Simulation results show that the proposed incremental state space modelling method does not need to know components' internal information. In addition, dynamics of all components can be preserved in the established system state-space model, while the information is lost in the existing dq impedance matrices aggregation method.

5.1 Proposed Incremental State Space Modelling Method

Figure 48 shows control diagram of a voltage source converter connected to a capacitive grid, Z_{dq} should be transferred from l reference frame to k reference frame. The dq impedance matrix of the voltage source converter in the two reference frames can be linked by

$$\mathrm{Z}_{\mathrm{dq}}^{\mathrm{k}} = \mathrm{R}_{\mathrm{dq}}(\theta)\mathrm{Z}_{\{\mathrm{dq}}{}^{\mathrm{l}}\mathrm{R}_{\mathrm{dq}}^{-1}(\theta) \tag{5.1}$$

where $\mathrm{R}_{\mathrm{dq}}(\theta) = [\cos\theta, \sin\theta; -\sin\theta, \cos\theta]$ is rotation matrix, and θ is angle difference of voltages between node l and node k as shown in Figure 48.

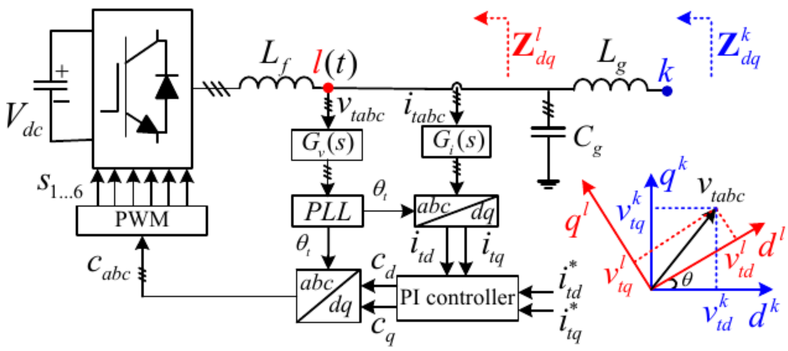

Figure 48: The control diagram of a L-filtered VSC with current control loop and PLL.

Although the conventional serial and parallel dq impedance matrices aggregation as shown in Figure 49 can be used to implement impedance-based stability analysis, individual component dynamic is lost in the aggregation procedure. The combination of state-space model of different components can maintain individual component dynamics in the finally-established system state-space model, so contribution of each component to instability phenomena can be calculated. In this project, the state-space model's series operator ⊕ and parallel operator ⊙ are proposed, and details of the proposed incremental state space modelling method are given, which can be found in Appendix E - G.

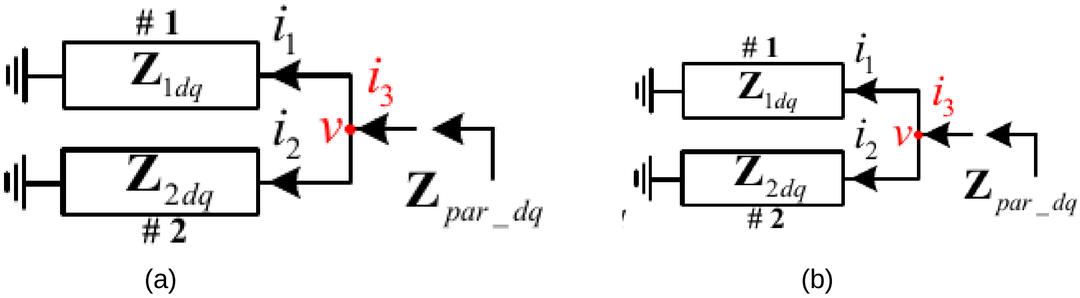

Figure 49: Two basic components connection cases. (a) Series connection case; (b) Parallel connection case.

Figure 50 shows implementation procedure of the proposed incremental state space modelling method, which includes two steps.

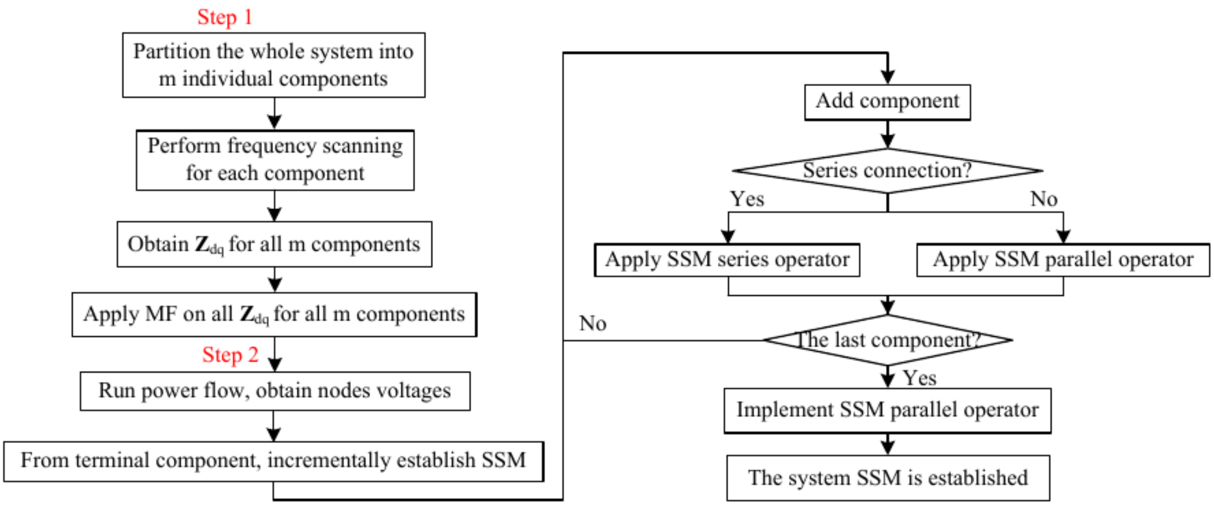

Figure 50: Flowchart of the proposed incremental state space modelling method. MF and SSM denote the matrix fitting and state-space mode, respectively.

Step 1 is to extract individual state-space models from terminal impedance frequency responses on local dq frames by matrix fitting algorithm. The overall system is first partitioned into m individual components. Then, frequency scanning is performed for each component. Discrete impedance frequency response of each component on local dq frame during concerned frequency range can be extracted. Further, the state-space model matrices can be generated by applying matrix fitting algorithm on these discrete impedance frequency responses.

Step 2 is to establish state-space model of the overall system using the proposed state-space model operators $\oplus$ and $\odot$. Simulation is first run to obtain all nodes voltages by power flow. Then, components are combined together by using proposed series and parallel operators in a recursive way. The last component is regarded as connected with the rest part in parallel, so the state-space model parallel operator $\odot$ is used in the last step.

5.2 Implementation procedure of proposed modelling method

Four voltage source converter under the control structure shown in Figure 48 are used in Figure 51. Specifically, VSCs #1 and #2 are with LCL filters, and VSCs #3 and #4 are with L filters, respectively. In addition, grid side filter inductor L_{f2} and filter capacitor C_f are only used for VSCs #1 and #2.

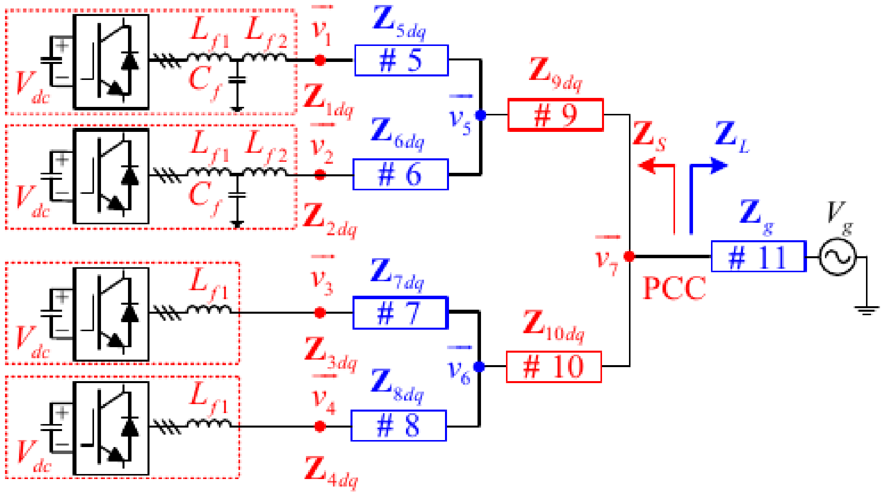

Figure 51: Four VSCs-based studied power system.

In Figure 47, the admittance estimation on the power-controlled grid-following inverter which is studied in the multi-paralleled inverter system is shown to be accurate. The admittance estimation algorithm is thus applied on the four VSCs in Figure 51. Figure 52 shows frequency characteristics of the estimated dq impedance matrix Z_{dq_mea} and theoretically-derived dq impedance matrix Z_{dq_the} for VSCs #1 and #2. Similarly, the estimated and theoretically-derived results for VSCs #3 and #4 are shown in Figure 53. It can be seen from Figure 52 and Figure 53 that dq impedance frequency characteristics for both LCL-type VSC and L-type VSC have been identified.

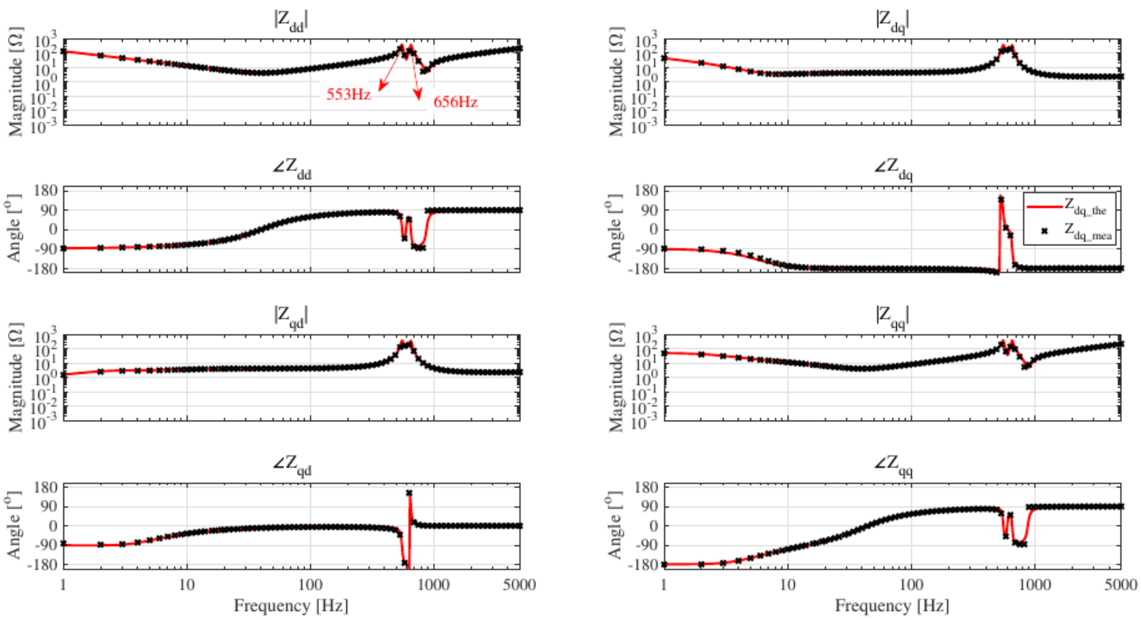

Figure 52: Bode diagrams of Z_{dq_mea} and Z_{dq_the} of VSCs #1 and #2.

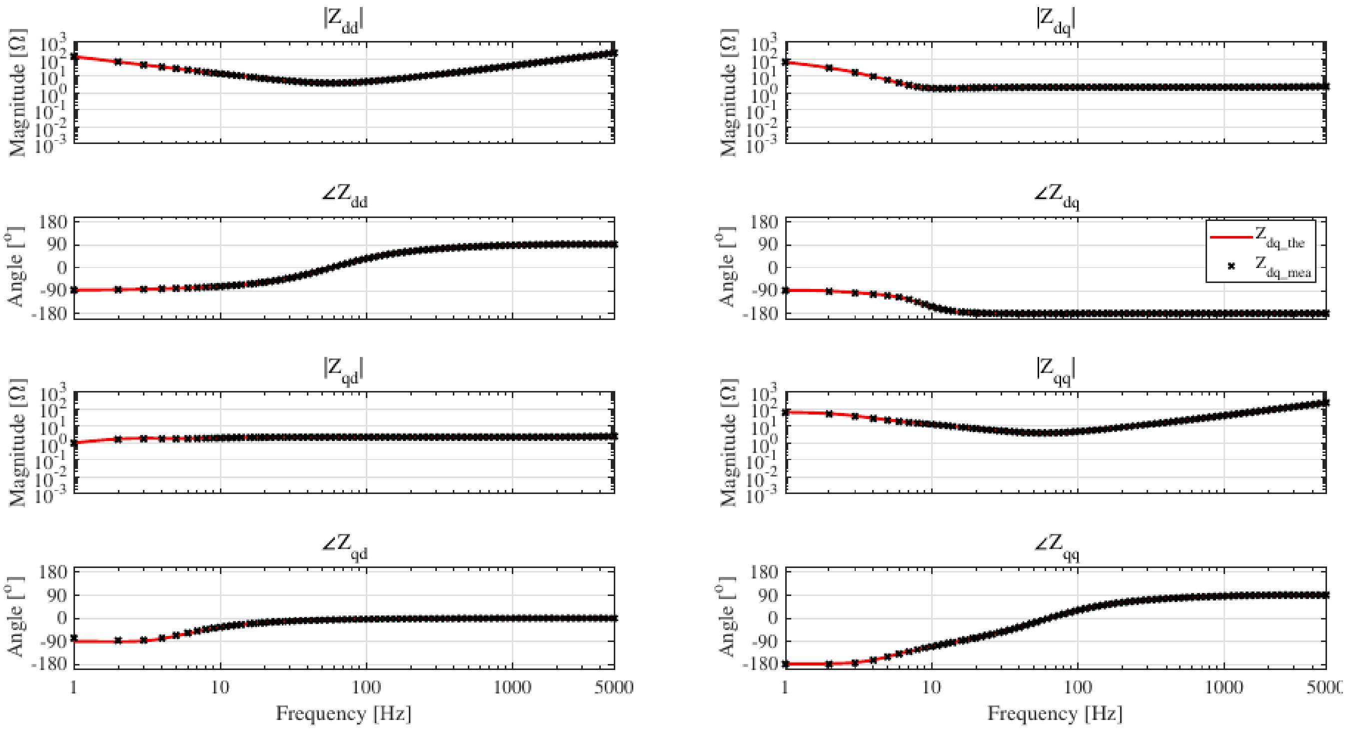

Figure 53: Bode diagrams of Z_{dq_mea} and Z_{dq_the} of VSCs #3 and #4.

The estimated impedance frequency responses for both kinds of VSCs are then fitted by matrix fitting algorithm. The eigenvalues of the fitted 10-order state-space models for four VSCs are listed in Table 11. As for VSCs #1 and #2, it can be seen from Figure 52 and Table 11 that, the imaginary part of these extracted eigenvalues agree with the magnitude peaks of the impedance-frequency curves, i.e., 554.0661Hz is close to 553Hz, and 654.3337 Hz is close to 656Hz. As for VSCs #3 and #4, the fitted frequency 346.7350Hz has a high damping coefficient, which means that no magnitude peak will appear in its Bode diagram. It agrees with the Bode diagram shown in Figure 53. These fitted state-space models of all VSCs will be used to establish system state-space model by the proposed state space modelling method.

Table 11: Eigenvalues of the Fitted 10-Order State-Space Models of Four VSCs Using Matrix Fitting Algorithm.

VSCs #1 and #2	Frequency [Hz]	VSCs #3 and #4	Frequency [Hz]
-0.0031		-0.0135	
-33.8222		-3.1474	
-7.1911e+04		-12.8606	
-1.1576e+05		-30.5599	
-15.9002±11.4563i	1.8233	-14.4804 ±11.3011i	1.7986
-7.3817e+01 ± 3.4813e+03i	554.0661	-1.9357e+04 ± 2.1786e+03i	346.7350
-7.1833e+01 ± 4.1113e+03i	654.3337	-9.4684e+03 ± 1.3812e+05i	21982

In addition, Z_{S_mea} and Z_{L_mea} can be obtained by directly performing frequency scanning at PCC. The Bode diagrams of Z_{S_mea} and Z_{L_mea} are shown as the black and red crossed curves in Figure 54. Z_{sys_mea} is defined as $Z_{S\_mea}//Z_{L\_mea}$ and the Bode diagram is shown as the green crossed curve in Figure 54. It can be seen that the dq impedance matrix of both source and load parts can be obtained by frequency scanning method.

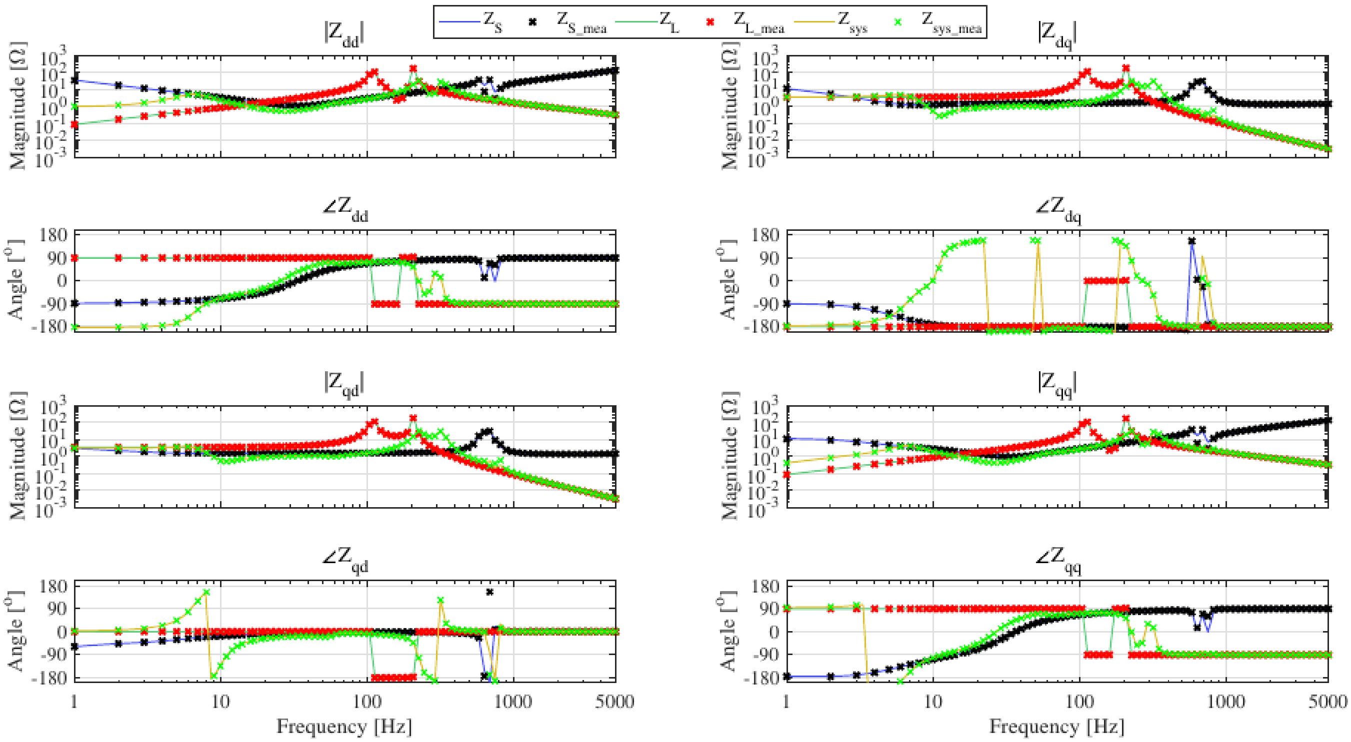

Figure 54: Bode diagrams of Z_{S_mea} and Z_{L_mea} and Z_{sys_mea} obtained by directly performing frequency scanning at PCC (Z_{S_mea}/Z_{L_mea} is the dq impedance matrix of source/load part obtained by directly performing frequency scanning at PCC. Z_{sys_mea} is defined as $Z_{S\_mea}//Z_{L\_mea}$. Z_S, Z_L and Z_{sys} are corresponding theoretically-derived curves).

Matrix fitting algorithm can be used to extract system state-space model from Z_{sys_mea}, and the eigenvalues of the established system state-space model are plotted in Figure 55. The eigenvalues of the established system state-space model using the proposed method are also plotted in Figure 55. It can be seen that, both system state space modelling methods obtain almost the same eigenvalues. In addition, these eigenvalues also agree with the magnitude peaks of Z_{sys_mea}. It shows that the proposed state space modelling method can obtain the same stability analysis conclusion as the impedance-based stability criterion and the apparent impedance analysis method. It should be noted that, compared with the other two methods, the system state-space model derivation process using the proposed method can preserve individual components dynamics, thus participation factors of all components can be calculated.

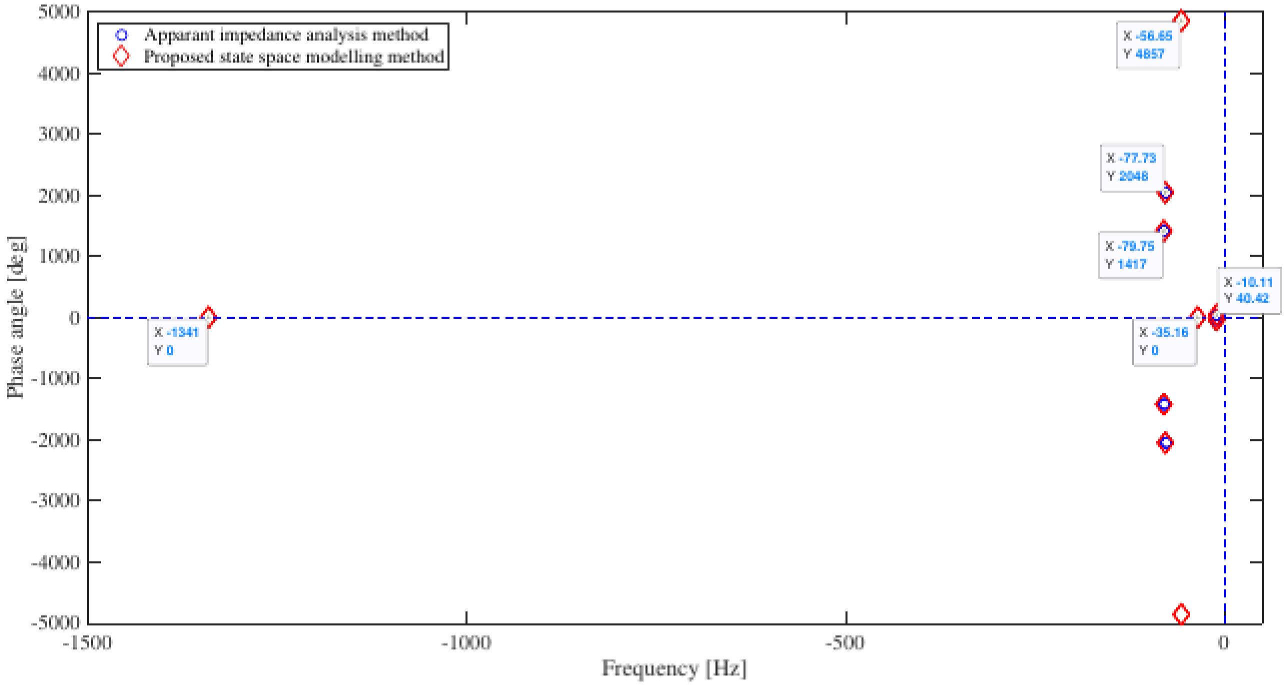

Figure 55: System eigenvalues obtained by the ``apparent impedance'' analysis method and the incremental state space modelling method proposed in this project

This research presents an incremental state space modelling method of power systems based on measured components impedance matrices on local dq frames. State-space models of all components are first extracted from terminal impedance frequency responses on local dq frames by matrix fitting algorithm. Series operator and parallel operator are proposed to combine state-space models of different components in a recursive way. Simulation results show that the proposed state space modelling method can obtain the critical eigenvalues for stability analysis.

6. Transient stability dynamic analysis on Synthetic NEM

The previous chapters define the methods to obtain an estimation of the impedance characteristics for each IBR device connected to a network and also propose a method to evaluate the stability factors for an interconnected network. While an ideal next step would be to apply the method to a network as large as the Synthetic NEM, there are still few computational challenges to be resolved, such as ability to construct, parameterize, and invert large mathematical matrices that would be required for this analysis. These computation challenges do not present themselves in a small network. As a result, the application of the impedance estimation method and its corresponding stability evaluation process on a large network such as the Synthetic NEM is earmarked for the next stage of this project.

Instead, from a time domain perspective, it will now be seen how the operating point through a day can impact the stability and additionally, how use of metrics such as remaining MVA can be used as an initial screen to develop stability improvement plans in the network. For dynamic analysis the first step is the preparation of a dynamic data file (dyr) which contains the models of generators, both synchronous and IBRs. Currently there are no dynamic load models in the system making the system loads all static loads. For synchronous generators, the models used are: GENROU for generator, ESAC4A for exciter, and TGOV1 for the governor. These are all standard library models available in Siemens PTI PSS®E. For renewable generators, the models used are REGCCU1 for generator and REECCU1 for modeling the excitation system which are again generic models. REECCU1 is a standard library model available in Siemens PTI PSS®E, but REGCCU1 is a generic model which is expected to be available as standard library model in version 35 of Siemens PTI PSS®E. In order to use this model in version 33 or version 34 of the software, a Dynamic Linked Library (DLL) is available from EPRI [32] and has been used in this study. This IBR model has been shown to numerically robust for low short circuit scenarios and has even been able to showcase the presence of instability with high percentage of IBRs [24] [23]. For these IBRs, plant controller models have not been used as it is assumed that the small signal interactions under study would be within the dead bands of plant controllers. Also, the IBRs have been set to control their local terminal voltage to help improve the stability of the network [17].

There is another model that has also been used for few IBRs in the network, namely a user-written grid-forming model GNRGFM. This model is also available from EPRI as a DLL and be used to study systems with large percentage of IBRs, up to 100%. This model provides a system planner the ability to study the impact of grid forming controls on the power system. The dynamic data files with parameters are provided in the Appendix L. Note that when grid forming IBR are added to the network, for each IBR POI, a bus with a step-down transformer is added where the controller is implemented.

The existing power flow case was reduced to remove buses pertaining to the Tasmania island state. Then existing generators were checked so that MVA>Pmax>=Pgen and appropriate Qmax and Qmin values are used. Resultant case has 2096 buses, 170 generators, 1547 loads ~30GW. Although the buses related to the Tasmania island state were removed, the injection of power from the Tasmania to mainland HVDC link was still represented by a generator at the mainland point of connection.

For analyzing the stability of the system over various hours, dynamic simulations are performed with a load trip. This disturbance resulted in system dynamics which was studied, and stability of various operating points was observed. Figure 56 shows the voltages at two buses in the system over the 24 consecutive hours starting from Hour 00 to Hour 23, as the system operating point changes due to variation of load from one hour to the next hour. For each subplot, at time = 4sec, a disturbance is applied by means of tripping one of the loads at bus 979 (~ 24MW) and based on resulting system voltage behavior, stability is determined. If the voltages settle after the load trip event, that hour/operating point can be deemed as stable whereas for oscillatory behavior, that hour/operating point can be deemed as unstable.

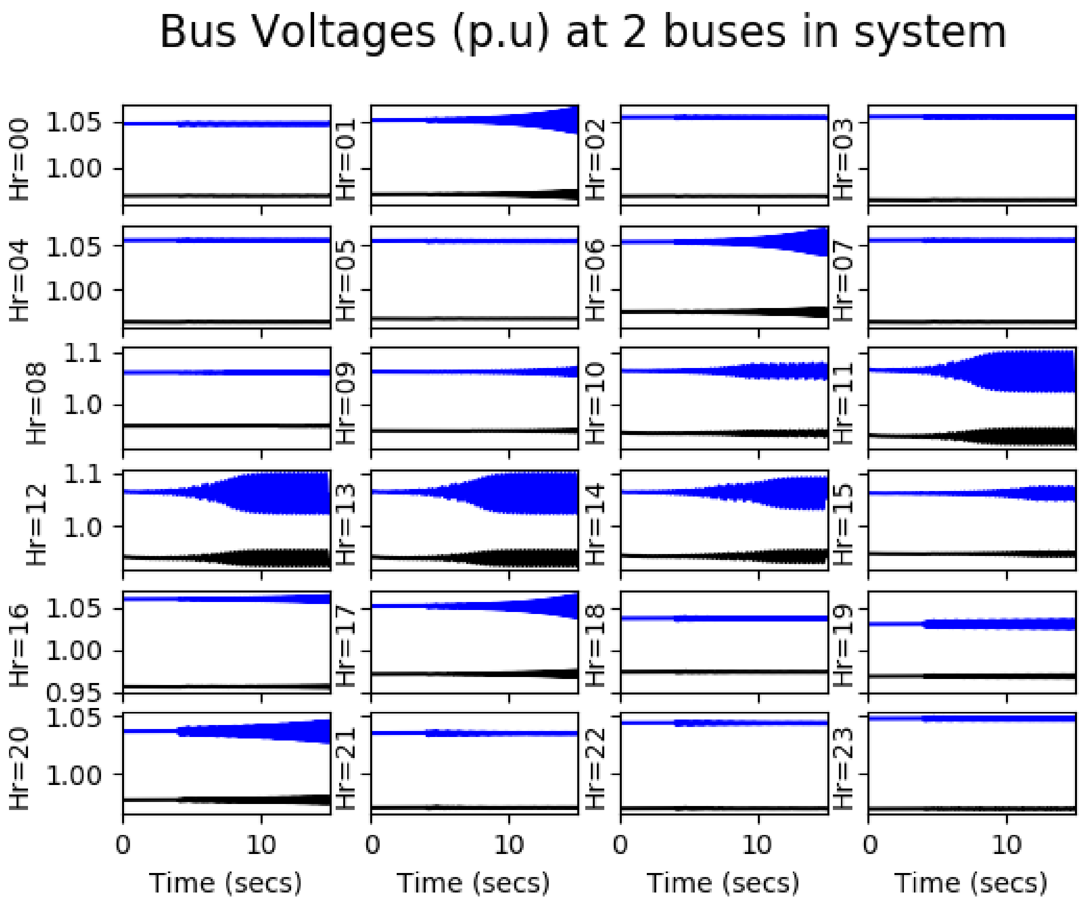

Figure 56: Simulations results with REGCC and REECC models representing the IBRs

From analysis of available MVA using EPRI's GSAT tool, it was found that for a SCR threshold of 3.0pu, there were 35 IBRs with available MVA negative. Table 12 below lists the generators with negative available MVA and actual value. The MVA available (negative quantity) is an input to the Grid Forming Control models used for these generators.

Table 12: Negative Available MVA at generators

Bus	MVA available	Bus	MVA available
18	-27.803	1640	-91.3825
20	-82.7511	1663	-929.681
21	-80.1556	1683	-139.367
64	-9.55591	1684	-368.928
65	-10.3544	1685	-401.247
66	-4.79279	1686	-358.293
67	-19.8826	1690	-98.9878
654	-22.6721	1691	-89.4674
655	-180.611	1692	-100.233
688	-116.916	1693	-409.637
689	-242.501	1694	-407.433
698	-20.5833	1695	-397.395
708	-50.3167	1696	-154.651
710	-12.6986	1706	-130.83
986	-165.426	1708	-8.52141

1437	-73.2501	1709	-113.459
1438	-0.53535	1710	-7.63137
1636	-19.7799		

Negative available MVA is an indication that these generators will be problematic and hence flagged down as candidates for replacing their controls with Grid Forming Controls modeled using the GNRGFM model. Replacing these 35 IBRs with GFM controls results in an improved response from system stability perspective as shown in Figure 57. Comparing with Figure 56, it is evident that the oscillatory behavior noted during several hours in the non Grid Forming Controls case are mitigated in the Grid Forming Controls case. This indicates that GSAT was able to correctly identify the generators which have an adverse impact on stability.

For ease of comparison between the two different controls and their impact on system stability Figure 58 is provided with system responses provided only for two hours, corresponding to light load and peak load.

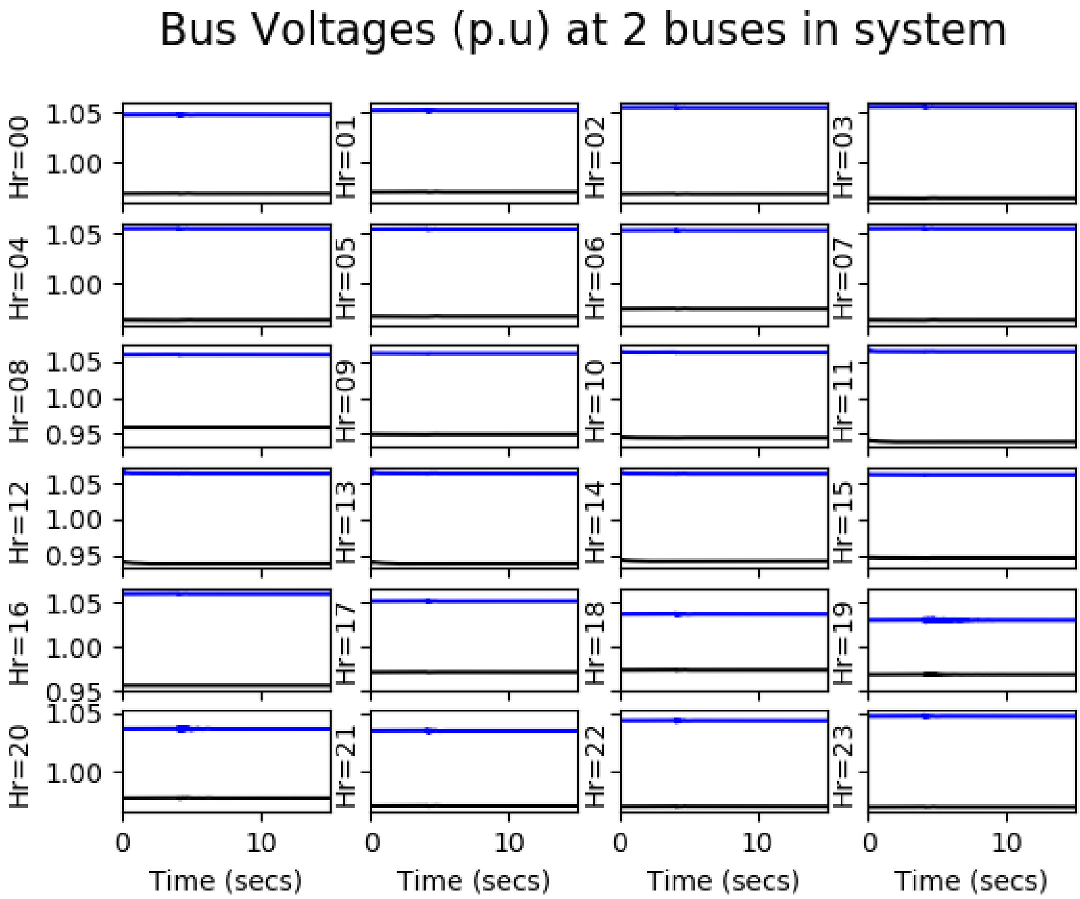

Figure 57: Simulation results with grid forming models replacing 35 IBRs with negative available MVA

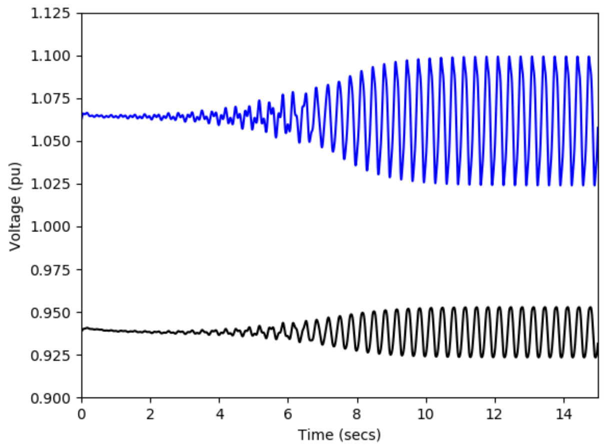

Hour 11 (light load) with GFL controls

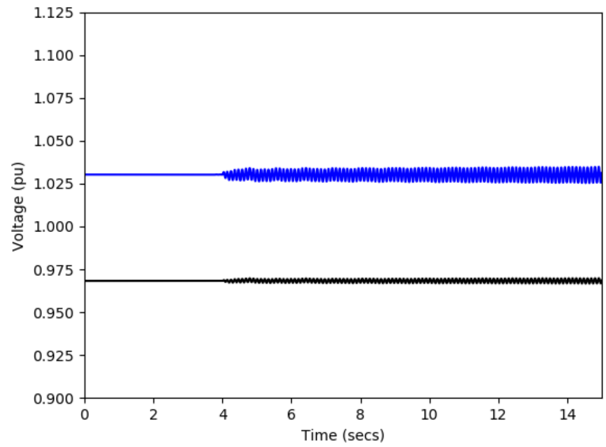

Hour 19 (peak load) with GFL controls

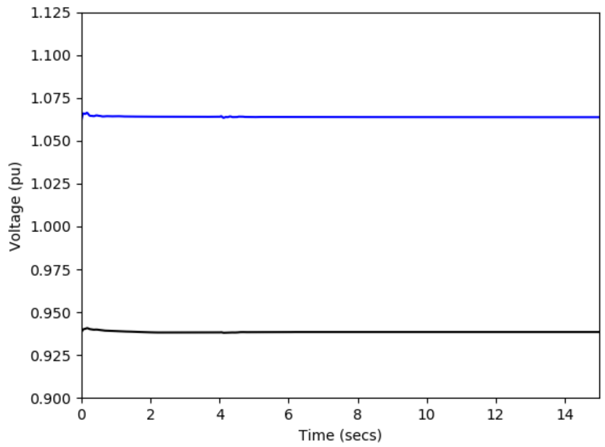

Hour 11 (light load) with GFM controls

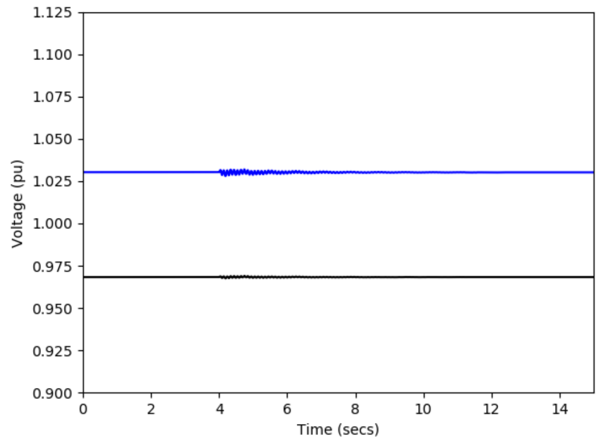

Hour 19 (peak load) with GFM controls

Figure 58: Comparison between light load and peak load system conditions with and without GFM controls

Figure 59 shows the location of the buses, all the generators overlaid on the Australian map. Please note that the latitude longitude locations of the buses are approximate since the system is a synthetic NEM network. Also shown in the figure are the locations of all the IBR generators on the Mainland and the IBR generators for which controls were replaced with GFM controls for improving stability of the overall system.

The analysis conducted here showcases the presence of instability in a time domain simulation at multiple hours of the day. Although an indication of this situation was provided from the remaining available MVA evaluation, it could only be verified by time domain simulation. An interim step of verification can however be the impedance and stability prediction at arbitrary operating points. While a proof of concept of use of this approach has been shown on a test system, future stages of this project can tackle the application of the concept on a network as large as the NEM.

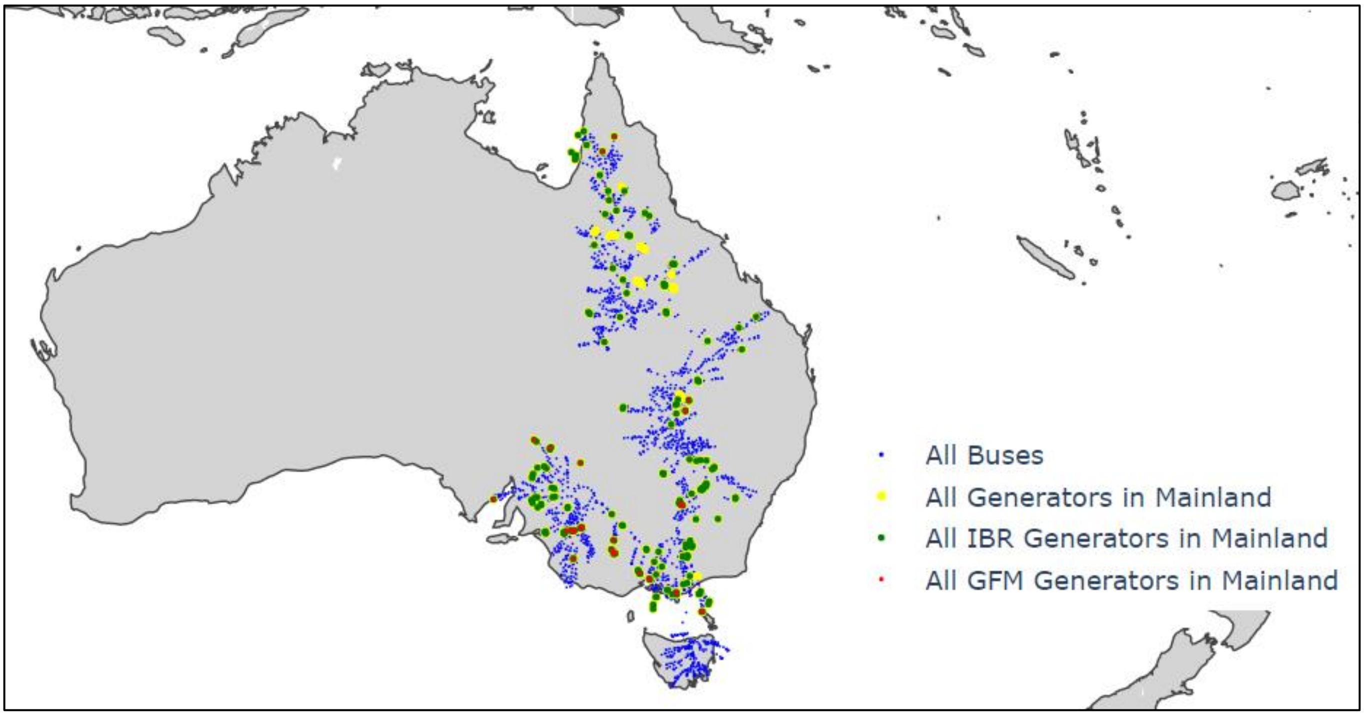

Figure 59: System map showing the locations with IBRs both before and after replacement some IBRs with GFM controls

7. Inferences obtained from analysis

Analysis of stability of a large system such as the NEM involves several steps. Figure 60 shows this sequence of processes, each step providing inputs in terms of data and insights to the next.

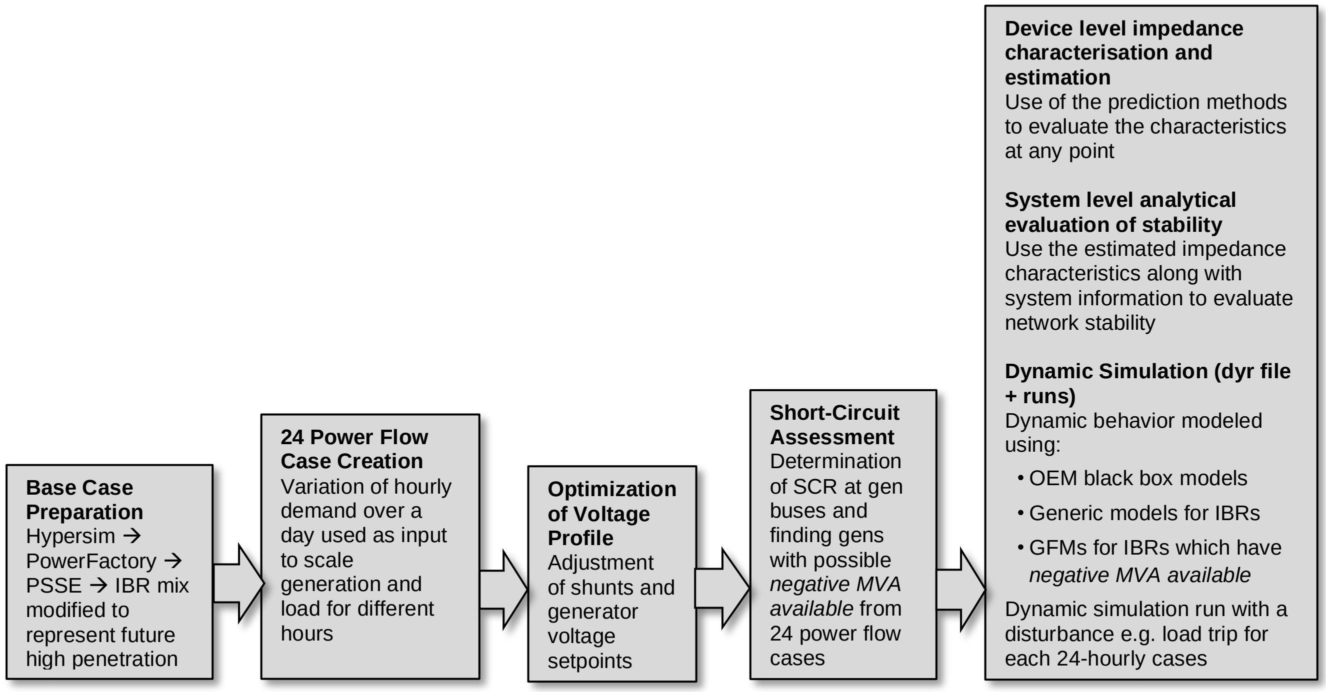

Figure 60: Stability analysis process flow

Some important insights are as follows:

- The power flow cases used for analysing stability over various operating points should be carefully prepared. Since these cases usually model future grid conditions, these would include decommissioning thermal units, replacing with IBR devices and batteries, and possible addition of new transmission lines. Real and reactive power limits, and MVA rating limits on all generators should be checked carefully. Finally with several significant changes being made to a base case, convergence of the case can sometimes pose challenges. Additional complications can arise due to different data formats involved where power flow case data is converted from one power system software to another.
- Optimizing voltages by adjusting generator reactive power outputs and shunts and transformer taps is also a key step, since generator redispatch to meet varying load profile by itself might not be effective in an optimal voltage distribution. In extreme cases, there might be generators exchanging reactive power. Also, the evolution of system voltage profile provides insights about the stability evolution between operating points as well.
- System short circuit evaluation is the most important step in flagging down problematic IBR generators, identified using metrics such as negative available MVA. The negative MVA metric can be used to identify locations for GFM resources
- These various outer power or voltage control loops can affect the near-zero-frequency, low-frequency, or high-frequency *dq*-domain admittance characteristics. In addition, it is found that the *qq*-axis admittance model of the current-controlled-IBR is not affected by the reactive current injection, whereas the *dq*-domain impedance model of the power-controlled-IBR is affected by the reactive power injection. The outer dc-link voltage control induces both high-frequency and low-frequency non-passive frequency regions for the *dd*-axis admittance element.
- Using methods such as the proposed prediction of impedance at multiple operating points, it can potentially be possible to reduce the time frame needed to evaluate the stability of a large network. However, more work is required on this task. To evaluate the training data for impedance prediction, an EMT model of the IBR device is required. If there are challenges in getting the IBR model to initialize or

achieve a steady state, then it may not be possible to obtain the training data, and hence it may not be possible to estimate the impedance at any operating point. This would subsequently impact the evaluation of the system wide stability.

- Finally, for various operating conditions, dynamic simulation run with a disturbance can ascertain stability of a particular operating condition. This process, however, involves preparing a dynamic data file incorporating dynamic models of the system generators, loads etc with proper parameterization to reflect controls etc. In a large system, some of these dynamic models might be proprietary user-written models provided by OEMs and various vendors, with or without much insight into their inner control loops and pose challenges due to various versions, compilers etc in which they were prepared.
- Grid forming models were found to have a much more stable dynamic response as compared to grid-following models.

.

8. Conclusion and future work

Analysing stability of large system such as the NEM involving thousands of buses, hundreds of generators, and loads, incorporating a large amount of power-electronic based IBR resources is an involved process, that needs careful step-by-step approach even when evaluating at a certain snapshot reflecting a particular operating point. With evolving grid conditions, such as even the diurnal load variation, the system operating point changes and it is a cumbersome process to perform the entire stability analysis for every operating point. In this work, an attempt has been made to understand how stability evolves over various system conditions by applying an analytical model, without having to run dynamic simulations for every operating condition to check for stability.

Two admittance prediction methods for the black-boxed IBR was proposed. This method was shown to be simple, efficient, and capable of estimating the admittance frequency responses at any arbitrary operating points by using minimal amount of input data, thereby avoiding repeated and time-consuming admittance measurements. Due to time constrains, it was only possible to test these methods out on small systems. In the subsequent stages of this project, the potential of this admittance prediction method in large practical IBR-based modern power systems and other related applications can be explored. Additionally, further refinements can be made to improve this method's accuracy and robustness, particularly under nonnegligible practical measurement error conditions.

The prediction of the admittances at any operating point can be combined with a state space evaluation method for stability analysis. Compared with the existing dq impedance matrices aggregation method, the proposed state-space modelling method can maintain individual dynamics by using the proposed state-space model series operator and parallel operator. Compared with conventional state space modelling method, internal structure and parameters are not required in modelling procedure. It should be noted that it is not possible for the proposed state space modelling method to determine any further details because the state variables have no physical meaning. For example, it is not possible to identify whether the oscillation mode is a controller mode or it is associated with the electrical system of the device.

Once the analytical stability of the network can be determined using the prediction of the impedance at an operating point and the state space representation, it can be verified using time domain results. In this work effort, the impact of operating point on the stability of a system such as the NEM has been shown. At different hours of the day, one can have different levels of stability depending on the P and Q output of the inverters.

Further, in this project, a proof of concept has been showcased to show the ability of developing prediction based algorithms to evaluate the stability of a network at any arbitrary operating points. This approach can significantly reduce the computation time of stability evaluation and as a result, have potential application in real time operations. However, before going towards application in real time operations, from a conceptual point of view, there are few more questions to be addressed such as:

- Is there a general number of operating points at which the training models can be developed?
- Are there any rules and guidelines to be followed when developing the training data?
- At which P, Q, V point would these general operating points be evaluated at?
- How does the operation at current limit affect the evaluation of stability?
- Can the required matrix computations needed for a large system such as the NEM be accomplished in an efficient manner?

It is expected that these questions would be addressed in next stage of this research effort. In addition to this as the topic of determining analytical functions of stability for blackbox models is a new research area, real-time tools should be developed to assess the stability margins of grid-connected inverters by considering not only the normal operations of the power system but the abnormal operations (e.g., during faults and unbalanced events) of the electricity grids. More precisely, future funding opportunities could aim towards addressing the following concepts:

- Determination of region of convergence of an operating point
- Modularization of the analytical stability functions that allow for easy system reconfiguration
- Development of tools that can automate the developed process
- Distinguishing between small signal and large signal stability challenges
- Development of a process to update the analytical functions if the blackbox models undergo a change due to firmware updates in the actual product in the field
- Evaluation of compatibility of derived analytical stability functions with existing commercial simulation tools

9. References

[1] Electric Power Research Institute, "CSIRO Australian Research for the GPST: Topic 2 - Stability Tools and Methods," CSIRO, 2021.

[2] P. Kundur, Power System Stability and Control, McGraw Hill, 1994.

[3] S. Shah and L. Parsa, "Impedance Modeling of Three-Phase Voltage Source Converters in DQ, Sequence, and Phasor Domains," *IEEE Transactions on Energy Conversion,* vol. 32, no. 3, pp. 1139-1150, 2017.

[4] A. Rygg, M. Molinas, C. Zhang and X. Cai, "A Modified Sequence-Domain Impedance Definition and Its Equivalence to the dq-Domain Impedance Definition for the Stability Analysis of AC Power Electronic Systems," *IEEE Journal of Emerging and Selected Topics in Power Electronics,* vol. 4, no. 4, pp. 1383-1396, 2016.

[5] R. Luhtala, H. Alenius, T. Messo and T. Roinila, "Online Frequency Response Measurements of Grid-Connected Systems in Presence of Grid Harmonics and Unbalance," *IEEE Transactions on Power Electronics,* vol. 35, no. 4, pp. 3343-3347, 2020.

[6] M. Sumner, B. Palethorpe, D. W. P. Thomas, P. Zanchetta and M. C. Di Piazza, "A technique for power supply harmonic impedance using a controlled voltage disturbance," *IEEE Transactions on Power Electronics,* vol. 17, no. 2, pp. 207-215, 2002.

[7] N. Mohammed, M. Ciobotaru and G. Town, "Fundamental grid impedance estimation using grid-connected inverters: A comparison of two frequency-based estimation techniques," *IET Power Electronics,* vol. 13, no. 13, pp. 2730-2741, 2020.

[8] L. Fan and Z. Miao, "Admittance-Based Stability Analysis: Bode Plots, Nyquist Diagrams or Eigenvalue Analysis?," *IEEE Transactions on Power Systems,* vol. 35, no. 4, pp. 3312-3315, 2020.

[9] J. Sun, "Impedance-Based Stability Criterion for Grid-Connected Inverters," *IEEE Transactions on Power Electronics,* vol. 26, no. 11, pp. 3075-3078, 2011.

[10] B. Gustavsen and A. Semlyen, "Rational approximation of frequency domain responses by vector fitting," *IEEE Transactions on Power Delivery,* vol. 14, no. 3, pp. 1052-1061, 1999.

[11] S. Thakar and D. Ramasubramanian, "Intricacies of formulating measurement-based small signal models of inverter based resources," in *1th Bulk Power Systems Dynamics and Control Symposium (IREP 2022)*, Banff, Canada, 2022.

[12] D. Ramasubramanian, W. Baker and S. Thakar, "Grid Forming Inverters for Increase in Inverter Based Resource Percentage," Electric Power Research Institute (EPRI), Palo Alto, CA, 2002020786, 2021.

[13] Australian Energy Market Operator, "Power System Model Guidelines," Australian Energy Market Operator, Melbourne, 2018.

[14] L. Arnedo, D. Boroyevich, R. Burgos and F. Wang, "Polytopic black-box modeling of dc-dc converters," in *2008 IEEE Power Electronics Specialists Conference*, Rhodes, Greece, 2008.

[15] G. Angelis, "System analysis, modelling and control with polytopic linear models, Ph.D. Thesis," Technische Universiteit Eindhoven, Eindhoven, 2001.

[16] A. Frances, R. Asensi and J. Uceda, "Blackbox polytopic model with dynamic weighting functions for dc-dc converters," *IEEE Access,* vol. 7, pp. 160263-160273, 2019.

[17] D. Ramasubramanian, W. Baker, J. Matevosyan, S. Pant and S. Achilles, "Asking for Fast Terminal Voltage Control in Grid Following Plants Could Provide Benefits of Grid Forming Behavior," *IET Generation, Transmission & Distribution,* vol. 17, pp. 411-426, 2023.

[18] *Powerfactory file "nem_2300_not_SA.pfd" received from Tom Philpott, University of Wollongong, on July 13, 2022,* 2022.

[19] Australian Energy Market Operator, "2022 Integrated System Plan," Australian Energy Market Operator, Melbourne, 2022.

[20] Electric Power Research Institute, "Grid Strength Assessment Tool," Electric Power Research Institute, Palo Alto, CA. 3002024263, 2022.

[21] Working Group B4.62, "Connection of wind farms to weak AC networks," CIGRE, 2016.

[22] W. Wang, G. M. Huang, D. Ramasubramanian and E. Farantatos, “Transient stability analysis and stability margin evaluation of phase-locked loop synchronised converter-based generators,” *IET Generation, Transmission, & Distribution,* vol. 14, no. 22, pp. 5000-5010, 2020.

[23] D. Ramasubramanian, X. Wang, S. Goyal, M. Dewadasa, Y. Li, R. J. O'Keefe and P. F. Mayer, “Parameterization of generic positive sequence models to represent behavior of inverter based resources in low short circuit scenarios,” *Electric Power Systems Research,* vol. 213, no. 108616, 2022.

[24] D. Ramasubramanian, W. Wang, P. Pourbeik, E. Farantatos, A. Gaikwad, S. Soni and V. Chadliev, “Positive sequence voltage source converter mathematical model for use in low short circuit systems,” *IET Generation, Transmission & Distribution,* vol. 14, no. 1, pp. 87-97, 2019.

[25] Electric Power Research Institute, “Voltage Control Areas (VCA) Studio,” Electric Power Research Institute, Palo Alto, CA, 3002025866, 2022.

[26] T. Ibrahim, S. Guggilam, A. Del Rosso and M. Patel, “Voltage and Reactive Power Optimization with VCA Studio Software,” Electric Power Research Institute, Palo Alto, CA, 3002024427, 2022.

[27] D. Ramasubramanian, E. Farantatos, O. Ajala, S. Dhople and B. Johnson, “A Universal Grid-forming Inverter Model and Simulation-based Characterization Across Timescales,” in *56th Hawaii International Conference on System Sciences (HICSS)*, Maui, 2023.

[28] Electric Power Research Institute, “FESTIV DA Op Mode,” Electric Power Research Institute, Palo Alto, CA, 3002023444, 2022.

[29] M. Seeger, “Gaussian processes for machine learning,” *International journal of neural systems,* vol. 14, no. 02, pp. 69-106, 2004.

[30] C. E. Rasmussen, *Gaussian processes in machine learning,* Canberra: In Advanced Lectures on Machine Learning: ML Summer Schools, 2003.

[31] W. Liu, X. Xie, J. Shair and X. Li, "A nearly decoupled admittance model for grid-tied VSCs under variable operating conditions," *IEEE Trans. Power Electron.,,* vol. 35, no. 9, pp. 9380-9389, 2020.

[32] Electric Power Research Institute, “REGC_C Implementation in PSS/E (REGC_C (PSS/E)) v1.2,” Electric Power Research Institute, Palo Alto, CA. 3002020781, 2021.

10. Appendix

A separate document is provided containing the following appendices:

A. Admittance Modelling of the Current-Controlled Grid-Following Inverters without Considering PLL Effect
B. Admittance Modelling of the Current-Controlled Grid-Following Inverters with Considering PLL Effect
C. Admittance Modelling of the Power-Controlled Grid-Following Inverters
D. Admittance Modelling of the Voltage-Controlled Grid-Following Inverters
E. Proposed Incremental State Space Modelling Method - One Existing Solution to Align Local dq Frames and Aggregate dq Impedance Matrices
F. Proposed Incremental State Space Modelling Method - Basis of VF and MF
G. Proposed Incremental State Space Modelling Method - Details of the Proposed Incremental State Space Modelling Method
H. The State-Space Model of the Current-Controlled Grid-Following Inverter without Considering PLL Effect
I. The State-Space Model of the Current-Controlled Grid-Following Inverter Considering PLL Effect
J. The State-Space Model of the Power-Controlled Grid-Following Inverter
K. The State-Space Model of the Voltage-Controlled Grid-Following Inverter
L. Dynamic Data file for Siemens PTI PSS® E simulations on Synthetic NEM